Chapter 3

AEOLIAN PROCESSES IN PROCTOR CRATER ON MARS: 1. SEDIMENTARY HISTORY AS ANALYZED FROM MULTIPLE DATA SETS

Lori K. Fenton

Division of Geological and Planetary Sciences, California Institute of Technology, Pasadena, California

A. Wesley Ward

Astrogeology Team, United States Geological Survey, Flagstaff, Arizona

Joshua L. Bandfield

Department of Geology, Arizona State University, Tempe, Arizona

Abstract. The sedimentary history of Proctor Crater is described especially with regards to aeolian processes. Proctor Crater is a 150 km diameter crater in Noachis Terra, within the southern highlands of Mars. The analysis leading to the sedimentary history incorporates several data sets including imagery, elevation, composition, and thermal inertia, mostly from the Mars Global Surveyor mission. The resulting stratigraphy reveals that the sedimentary history of Proctor Crater has involved a complex interaction of accumulating and eroding sedimentation. Aeolian features spanning much of the history of the crater interior dominate its surface, including large erosional pits, stratified beds of aeolian sediment, sand dunes, erosional and depositional streaks, dust devil tracks, and small bright bedforms that are probably granule ripples. Long ago, up to 450 m of layered sediment filled the crater basin, now exposed in eroded pits on the crater floor. These sediments are probably part of an ancient global deposit of aeolian volcaniclastic material. Since then an enormous quantity of this material has been

eroded from the top layers of the strata, perhaps as much as 50 m. Small bright duneforms lie stratigraphically beneath the large dark dunefield. Relative to the large dark dunes, the bright bedforms are immobile, although in places their orientations are clearly influenced by the presence of the larger dunes. Their abundance in the crater and their lack of compositional and thermal distinctiveness relative to the crater floor suggests that these features were produced locally from the eroding basin fill. Dust devil tracks form during the spring and summer, following a west-southwesterly wind. Early in the spring the dust devils are largely restricted to dark patches of sand because they absorb more heat than the surrounding terrain. As the summer approaches, dust devil tracks become more plentiful and spread to the rest of the crater floor, indicating that the entire region acquires an annual deposit of dust that is revealed by seasonal dust devils. The dark dunes contain few dust devil tracks, suggesting that accumulated dust is swept away directly by saltation, rather than by the passage of dust devils. Spectral deconvolution indicates that the dark dunes are composed almost entirely of basalt. The average thermal inertia calculated from TES bolometric temperatures is $277 \pm 17\,J\,m^{-2}\,s^{-0.5}\,K^{-1}$, leading to an effective grain size of $740 \pm 170\,\mu m$, which is consistent with coarse sand and within the range expected for Martian sand. The coarse basaltic sand that composes the large dunefield originated from outside the crater, saltating in from the southwest. The provenance of this sand is undetermined, but it entered the region in a single event and accumulated in many of the craters of Noachis Terra. Most of the transport pathway that delivered this sand to the dunefield has since been eroded away or buried. The sand was transported to the right-center of the crater floor, where beneath the present-day dunes a 50 m high mound of sand has accumulated. Dune slipfaces indicate a wind regime consisting of three opposing winds, of which the dominant still blows from the west-southwest, the same wind that originally transported dark sand into the crater. Some of these wind

directions are correlated with the orientations of dust devil tracks and bright bedforms. The combination of a tall mound of sand and three opposing winds is consistent with a convergent wind regime, which produces the large reversing transverse and star dunes that dominate the dunefield. The dark dunes have both active slipfaces and seemingly inactive slipfaces, suggesting that the dunes vary spatially in their relative activity. Nevertheless, the aeolian activity that has dominated the history of Proctor Crater still continues today.

1. Introduction

Mars has long been known as a place dominated by aeolian processes [*e.g., de Vaucouleurs*, 1954]. Evidence for the action of wind on the surface ranges from the local-scale features discovered at each lander site to the planet-encircling dust storms that occasionally inundate the entire globe. Therefore the study of material transport and landscape evolution on Mars is not complete until aeolian processes are fully understood. Of the many different types of aeolian features, dunes are unique in that their morphology provides information on the complexity of the wind regime in which they reside and the direction of net transport of a specific range of particle sizes. Thus the study of Martian sand dunes can broaden the understanding of the near-surface wind circulation patterns and the erosion, deposition, and transport of sand on the surface. In addition, knowledge of the terrain in the vicinity of a dunefield is necessary to understand how dunes relate and react to their environment. This work incorporates a number of data sets from the Mars Global Surveyor mission to produce a stratigraphic record of the dunes and underlying terrain in Proctor Crater, one of several craters in Noachis Terra containing a large dark dunefield.

The first dunes identified on Mars were found in Mariner 9 images of Proctor Crater [*McCauley et al.,* 1972; *Sagan et al.,* 1972]. Further work following this discovery quickly established the important role of aeolian processes in the

modification of the Martian surface [*Smith,* 1972; *Cutts and Smith*, 1973; *Arvidson,* 1974]. Since then, the dunefields of Noachis Terra (formerly known as the Hellespontus dunefields), and especially the dunes of Proctor Crater, have become the type location for the study of dark dunes on Mars. *McCauley et al.* [1972] and *Cutts and Smith* [1973] took a close look at the Proctor dunes, noting the NNW-striking ridges with a spacing of 1–2 km in the center of the dunefield. *Cutts and Smith* [1973] concluded that the dunes are located in an area where the effective sand-saltating winds are balanced, with possible dominant winds from the southwest. *Breed* [1977] compared the spacing and widths of the Proctor dunes to terrestrial crescentic dunes, finding that the Martian dunes are dimensionally similar to dunes in several terrestrial dunefields. *Thomas* [1984] found that the color variations of Proctor Crater dunes, streaks, and plains are similar to but simpler than crater splotches with associated streaks in other areas on Mars. *Lancaster and Greeley* [1987] took a close look at the Noachis Terra dunefields and discovered pyramid-shaped dunes and multiple slipfaces, indicative of dunes produced by a multidirectional wind regime. However, since their discovery, the dunes of Proctor Crater have generally been classified as large transverse and barchan dunes.

Thermal studies have also focused on the Noachian dunefields [*Christensen,* 1983; *Edgett and Christensen,* 1991; *Edgett and Christensen,* 1994; *Herkenhoff and Vasavada*, 1999]. Because dunefields consist of a large quantity of well-sorted unconsolidated particulate material, thermal inertia measurements over such areas provide an ideal condition in which to calculate effective mean grain sizes. Furthermore, such a well-constrained situation is useful for calibrating new thermal inertia techniques. The dunes of Proctor Crater have been targeted several times, producing a thermal inertia consistent with sand.

In this work, the classification of dune morphology follows the terms defined by *Breed and Grow* [1979]. Crescentic or barchan dunes are crescent-shaped features created by unidirectional winds, with the "horns" of the dune pointing downwind. Transverse dunes, like barchan dunes, form slipfaces that are orthogonal to the dominant sand-transporting winds, but occur where more sand is available, and may be considered coalesced barchans [*Wasson and Hyde*, 1983]. Linear or longitudinal dunes are elongate features with slipfaces on either side of the peak, generally indicative of bi-directional winds, and they are aligned generally parallel to the direction of the resultant wind. Star dunes are large piles of sand that accumulate in a multidirectional wind regime (*i.e.,* where winds converge), often displaying overlapping slipfaces that create a star-like shape in plan view. Reversing transverse dunes occur where seasonally shifting winds oriented close to 180° apart change the slipface direction from one side of the dune to the other, so that the dunes appear as transverse dunes at any given time but may seasonally switch slipface directions. More detailed descriptions and examples are discussed in *Breed and Grow* [1979].

The provenance of dune sand in the Noachis area of Mars is largely unresolved. *Christensen* [1983] proposed that the intracrater dunefields on Mars were formed by entrapment of dark material in the topographic lows of craters. *Breed et al.* [1979] explored the reasons why crescentic dunes appear to be so much more abundant than linear dunes on Mars. They considered that linear (longitudinal) dunes represent areas of active sand transport, whereas crescentic dunes represent areas of low or no current sand transport. They concluded that most crescentic dunes, like the ones in Proctor Crater, represent the final accumulation site of sand, and that any linear dunes that might have transported large quantities of sand have since been eroded away. They also propose that many Martian dunes are similar to terrestrial dunes located in closed basins, and that they may have taken millions of years or more to accumulate, like their terrestrial

counterparts. While also considering the sand sources discussed above, *Thomas* [1984] suggests that intracrater dunes may have been formed from the aeolian reworking of eroded crater floor deposits, evidenced by the many large pits visible in craters with dunes and the lack of obvious transport pathways outside the craters. Earlier, *Thomas* [1982] proposed that the intracrater dune sand may have been supplied from eroding layered deposits near the south pole. Clearly a more detailed study of sand deposits is necessary to determine the origin of the intracrater dune materials.

This work is the first of two papers describing aeolian processes in Proctor Crater. The second paper (hereafter called Paper 2) discusses the results of mesoscale atmospheric modeling of the winds over the Proctor Crater dunes and relates dune morphology to regional winds and transport systems. In this work, a graphical information system (GIS) is built and used to correlate aeolian features with data products from the Viking Orbiters and Mars Global Surveyor. The GIS incorporates images, albedo, thermal inertia, composition, elevation, and (discussed in Paper 2) wind orientation and stress to provide a tool that aids in understanding how aeolian processes affect the surface of Mars. In Section 2, the method and materials used in building the GIS are described. In Section 3 Proctor Crater is described both from a regional standpoint and at a detailed view to provide a context for the dunefield. The dark dunefield is illustrated in Section 4, with an emphasis on morphology. The composition of the dunes and crater floor are covered in Section 5. Section 6 describes the thermal inertia of the region, including the identification of a trend across the dunes. Finally, in Section 7, a stratigraphic history of the crater interior is proposed, based on the analysis done with the GIS.

2. Method

A number of data sets were incorporated into a Geographic Information System (GIS) in order to study Proctor Crater. A GIS is a thematic mapping system that allows data to be displayed graphically while being stored as a spreadsheet or a database. This is a tremendously powerful tool that can be applied to conduct studies of an area using spatial data. The main advantage of a GIS is that it involves spatial coregistration of any number of data sets, each of which can be displayed separately or in conjunction with other data sets. For example, images of varying resolutions, digital elevation models (DEM's), and any spatial data points can all be combined into a single database and displayed in whole or in part over one another. This allows for identification of spatial and temporal variations, correlations of many different parameters, and statistical calculations of and between different data sets. All of these measurements can in turn be displayed as an overlay on top of any other coregistered data set (*i.e.,* surface slopes steeper than a certain value plotted over a base image). In addition, feature orientations, lengths, areas, and volumes can be measured and plotted over any previously coregistered data set. A GIS is an accumulation of all available data into one database that then allows for further numerical investigation.

The software used was ArcView GIS Version 3.1, created by ESRI (Environmental Systems Research Institute), to build a GIS of Proctor Crater. Our base map is a 250 m/pix MOC WA (Mars Orbiter Camera Wide Angle) image mosaic that has been processed, corrected for gain and radiometric variations, and mapped into a sinusoidal projection using Integrated Software for Imagers and Spectrometers (ISIS) developed by the U. S. Geological Survey. We added in a digital elevation model (DEM) that we constructed from MOLA (Mars Orbiter Laser Altimeter) elevation points at a horizontal resolution of 400 m/pix using Generic Mapping Tools (GMT) software. Inaccuracies in

camera pointing information led to spatial offsets in the positioning information of the WA mosaic, and so we used the MOLA DEM as a reference to adjust the position of the WA mosaic in the GIS by hand. All available MOC NA (Mars Orbiter Camera Narrow Angle) images were processed and projected to match the WA mosaic using ISIS software, and each image was added to the Proctor Crater GIS as a separate layer (theme) and at full resolution. Similar camera pointing errors led to hand positioning of each NA image on the WA mosaic. On top of these images we plotted a number of data sets derived from TES (Thermal Emission Spectrometer). These include bolometric thermal inertia [*Mellon et al.,* 2000], compositional endmember concentrations [*Bandfield et al.,* 2000], daytime and nighttime bolometric temperatures, and bolometric albedo. Also included were all available Viking Orbiter images of Proctor Crater, although the resolution of these proved to be no better than the MOC WA images.

Once the data were assimilated into the GIS, a number of parameters were mapped or measured using data from the Aerobraking through Mapping mission phases. Data from the Extended mission phase have since been added to the GIS and have been inspected for consistency with the previous measurements. Among the features mapped over each NA image in Proctor Crater are dune slipface brinks and orientations, dust devil tracks and orientations, bright duneform location and orientation, boulder density, small craters, and the locations of NA images. This additional information allows for a new assessment of dune morphology, sediment volume, and wind regime using all available information. The results of each of these measurements are described below. It should be noted that this discussion contains a set of conclusions drawn by the author based on the analysis of this GIS. However, this work has greatly benefited by the involvement of several researchers to properly describe and utilize the various data sets listed above.

3. Study Area

3.1 Large-scale Overview

3.1.1 Regional Context. Proctor Crater (see Fig. 3.1a) is one of several large impact basins in Noachis Terra, located in the ancient cratered terrain of the southern highlands of Mars. Located at 47º S, 30º E (330º W), it is one of many craters west of Hellas Planitia (see inset) that contains a prominent, dark dunefield. *Peterson* [1977] mapped the crater floor and the surrounding plains as "plains material," interpreting this unit as unconsolidated sediment deposits that in some areas may be underlain by flood lavas. Proctor Crater itself is roughly 150 km across, and the dark dunefield within extends to ~65 km from southwest to northeast and ~35 km from southeast to northwest. The seasonal polar cap reaches northward beyond Proctor crater, covering the entire crater floor and walls with CO_2 frost during the winter. Proctor Crater is well within the limit of the seasonal frost, which extends to 40º S [*James et al.,* 1992].

3.1.2 Prominent Features. Figure 3.1b shows a digital elevation map (DEM) of the crater, combined with a shaded relief map, at a resolution of 400 m/pix. The DEM was constructed from individual MOLA elevations using the Generic Mapping Tools (GMT). Several features that are barely visible in the MOC Wide Angle mosaic are emphasized in the shaded relief map, which been stretched nonlinearly in color to emphasize relief within Proctor Crater (note color bar in Fig. 3.1b). The crater floor is a fairly flat expanse, smooth at the 400 m resolution of the DEM. It is punctuated by two pits, the larger of which is located on the western side of the crater interior, covers one tenth of the crater floor, and is up to a kilometer deep. The interior of the large pit, here called the "western pit," is rugged and contains several large craters. The smaller pit, called the "central pit," is located in the northern central region of the crater floor, has a much smoother floor, and is roughly 100 m deep. Several 10–20 km diameter craters in the
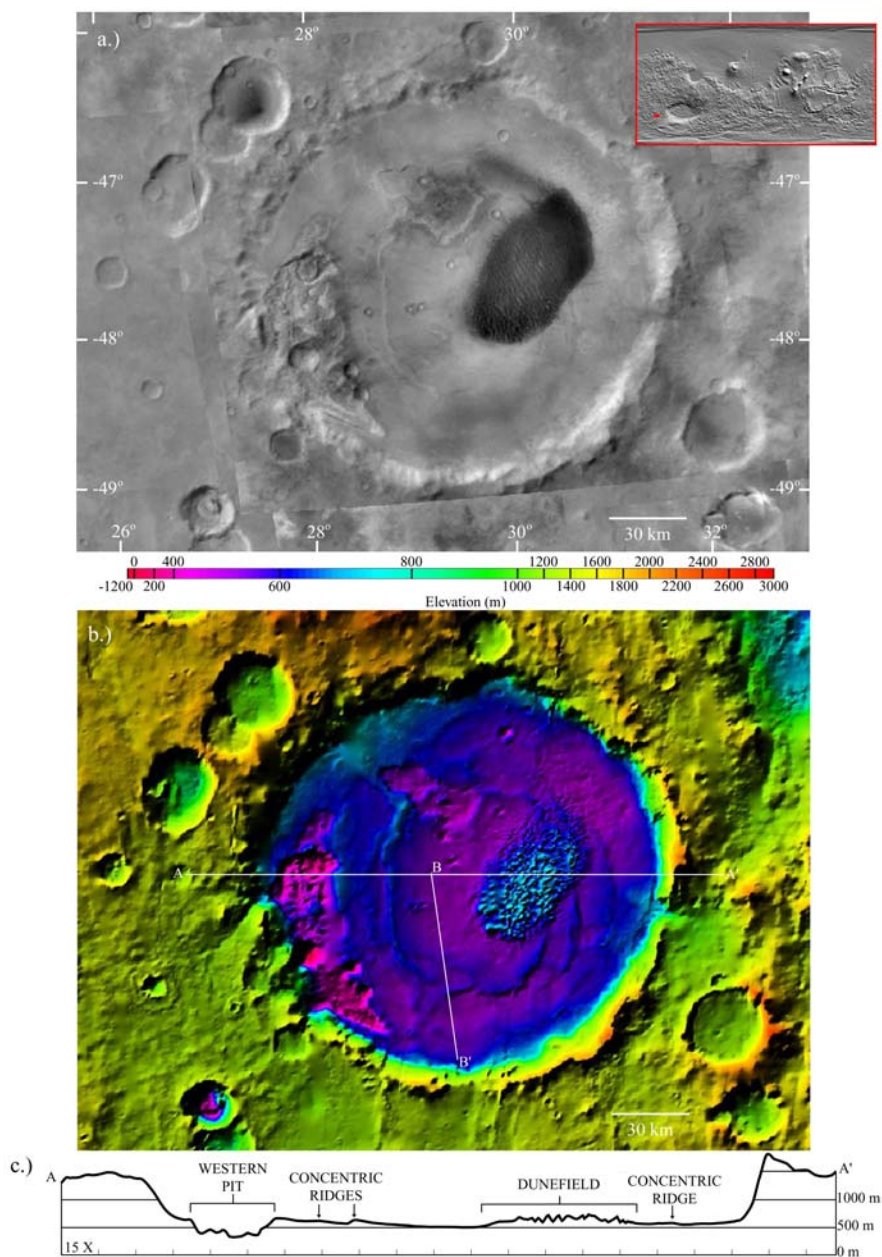
Fig. 3.1. a.) MOC Wide Angle mosaic of the study area, Proctor Crater, at a resolution of 250 m/pix. Proctor Crater is located at 47° S, 30° E (330° W), and it is approximately 150 km across. The small red-bordered inset is a global shaded relief map from MOLA with the study area highlighted in red. b.) MOLA DEM of Proctor Crater at a resolution of 400 m/pix. The elevation scale is stretched nonlinearly to emphasize topography on the relatively flat crater floor (see color bar). Profiles AA' and BB' are shown in Fig. 3.1c and 3.2, respectively c.) Profile AA' across Proctor Crater, with a vertical exaggeration of 15 x. Note that in this and all subsequent images, north is always oriented up.

western pit suggest that the process that eroded the pit may have been triggered by impacts that disrupted the surface, perhaps fracturing and weakening nearby terrain, leaving it susceptible to erosion. However, such craters are not present in the central pit, suggesting that such disruptions are not necessary to initiate pit formation. Figure 3.1b also shows the large dunefield rising above the flat surface as a series of ridges unresolved at the scale of the DEM. There is also a set of ~50 m high ridges ringing the center of the crater at roughly half its diameter (shown in dark violet in Fig. 3.1b, at ~600 m), called the "concentric ridges." *Malin and Edgett* [2001] identify part of a concentric ridge in Proctor Crater (see their Fig. 57), confirming that it is more than just a dust devil track. These ridges are visible as dark rings in MOC Wide Angle images in Fig. 3.1a. Possible origins of these concentric ridges are discussed below.

Figure 3.1c shows a profile crossing the crater, the location of which marked on the map as A–A' in Figure 3.1b. The western pit is a large, rough negative feature that cuts sharply into the crater floor materials. The dunefield appears as a poorly resolved accumulation of material superimposed on the crater floor. Also visible are the concentric ridges, which appear as subtle positive features that are steeper on the slopes facing the crater walls. The remainder of the crater floor is a smooth, fairly featureless plain at the resolution of the DEM.

3.1.3 Basin Fill. It is possible to use crater depth versus diameter measurements to estimate the amount of basin fill within Proctor Crater. Statistics based on MOLA DEM's by *Garvin et al.* [2000] have provided a depth vs. diameter relationship for pristine craters of various sizes. For a crater with a diameter (D) larger than 100 km, the original depth (d) is estimated at

$$d = 1.27D^{0.12} \tag{1}$$

Thus the estimated unmodified depth of Proctor Crater is 2.31 km. The highest remaining elevation of its now largely degraded rim is 2360 m, placing the original crater floor at a lower limit of 50 m. The current crater floor elevation is roughly 500 m, implying that at most a net value of 450 m of material has accumulated in Proctor Crater since its formation. As discussed below, MOC Narrow Angle images show strata exposed in the walls of the western and central pits, suggesting that this basin fill is part of the same sedimentary units described by *Malin and Edgett* [2000a].

3.1.4 Concentric Ridges. The concentric ridges are a rather enigmatic feature in the floor of Proctor Crater. Such rings in a filled basin are unusual, and thus their origin must be considered carefully. Three possible origins for these structures are considered: that they are eroded outcrops of resistant layers, that they are remnant tops of Proctor Crater's peak ring, and that they are wrinkle ridges that formed after the crater accumulated its sediments.

Malin and Edgett [2000a] found that sedimentary layers interior to a crater tend to conform to the shape of the crater wall. If the sediments filling Proctor Crater accumulated over the entire crater floor at once (*i.e.,* regional versus local deposition) then the strata will be bowl-shaped, like that of a tectonically deformed basin, following the contours of the original crater floor. Any relatively resistant layers will form a ring concentric to the crater's center upon erosion, similar to the ridges on the floor of Proctor Crater. In addition, the presence of steeper slopes facing towards the crater walls (see Fig. 3.1c) is consistent with upturned and exposed layers. Such strata should be traceable around the entire crater floor if not otherwise buried. If this interpretation is correct, then at least 50 m of material, the height of the ridges, has been eroded from the original surface of the crater sediments. The only process operating on Mars that could strip this amount of material without leaving behind telltale erosional markers is

aeolian deflation. If this hypothesis is correct, then these resistant strata indicate that a tremendous amount of material has been removed from Proctor Crater by wind action alone. Such a volume of material is nearly five times that of the dark dunefield, which is discussed below in Section 4.3.

The second interpretation requires the assumption that the ridges are part of the original structure of the crater that has been buried by sedimentation and perhaps subsequently exhumed. Peak ring craters are complex craters with diameters between approximately 50 and 300 km [*Pike and Spudis,* 1987]. These craters are large enough to have peak rings rather than just central peaks; hence, they are called peak ring craters whereas the craters with single central peaks are called central peak craters. According to *Wood and Head* [1976], peak ring diameters on Mars are half that of the crater diameter. The average diameter of the concentric ridges on the floor of Proctor Crater is ~80 km, which is roughly half the diameter of the crater (150 km), which is the correct dimension for a peak ring.

As of yet, there are no statistics from MOLA topography on the heights of peak rings [*Garvin et al.* 2000; 2002]. According to *Hale and Grieve* [1982], the heights of lunar central peaks (h_{cp}) follow a predictable trend related to the crater diameter (*D*) for craters less than 51–80 km wide. At larger crater diameters, the central peak heights asymptotically tail off to a height of 2–3 km until the crater diameter at which peak ring craters begin to form. They report that Schrödinger Crater, with a diameter of ~300 km, has a peak ring with a height of 2–3 km, which appears to follow the roll-off in height reached on the curve by central peaks. As shown by *Pike and Spudis* [1987], the difference between crater dimensions and critical diameter values between the Moon and Mars is quite significant, and thus a direct comparison cannot be made. It is not known at what diameter such a roll-off in central peak heights might occur for Martian craters, or even if it occurs at all. However, assuming that peak ring heights follow the same trend as

central peak heights, and using the trend calculated by *Garvin et al.* [2002] for central peak heights of Martian craters,

$$h_{cp} = 0.04D^{0.51}, \tag{2}$$

where h_{cp} is the central peak height and D is the crater diameter, the first-order estimate of Proctor Crater's peak ring height is 520 m. If the concentric ridges stand ~50 m above the ~450 m of sediments on the Proctor Crater floor, then the resulting total height of 500 m is close to that calculated using Equation 2. Thus crater statistics so far cannot rule out that the concentric ridges are eroded remnants of former peak rings, now embayed by hundreds of meters of sediments.

The third proposed origin of the concentric ridges, that they are wrinkle ridges, is perhaps the most unusual of the three. Wrinkle ridges are long, linear or arcuate features of positive relief, often associated with an elevation offset from one side to the other, and most commonly thought to be formed by tectonic compression [*e.g., Plescia and Golombek,* 1986; *Watters,* 1988; *Golombek et al.,* 1991]. On Mars, wrinkle ridges form in a wide variety of geologic terrains, and appear to be located and oriented largely by large impact basins such as Chryse [*Chicarro et al.,* 1985]. The rings in the floor of Proctor Crater superficially resemble wrinkle ridges in areas, particularly in the southwestern quarter (see Fig. 3.1a). Recent analysis of MOLA topography of wrinkle ridge systems in various regions of Mars show a series of successive offsets, indicating deep tectonic faults, possibly reaching through the planet's crust [*Golombek et al.,* 2001]. Circular features interpreted as wrinkle ridges have been identified in a few places, and they have been proposed to be formed by buckling of emplaced material above the rims of buried craters [*Sharpton and Head,* 1988]. In Noachis Terra, *Mangold et al.* [1998] found curved ridges within craters that are part of larger wrinkle ridges that

extend far beyond the crater rim. They argue that deep faults cannot create such arcuate features that are clearly influenced by the structure of the craters they are within, but that instead these ridges must be produced by thrust faults on shallow décollement surfaces. Wrinkle ridges appearing within basin fill, following the shape of a crater rim, and unconnected to outside tectonic features, such as shown by the concentric ridges of Proctor Crater, are not likely to be produced by a deep tectonic thrust. Therefore if the concentric ridges are in fact a wrinkle ridge system, they must be produced by compression at shallow depths as proposed by *Mangold et al.* [1998]. Compression in Proctor Crater could have been produced by subsidence of the basin fill, perhaps by a regional removal of ground water or by cooling of ponded lava. It may be that the weight of 450 m of accumulated sediments alone could have produced a gradual settling of material, perhaps by compaction of the aeolian basin fill. Such subsidence would necessarily have been spatially uniform to produce a thrust fault consistently concentric to the crater walls.

Figure 3.2 shows a MOLA traverse from one of the Narrow Angle images that passes across two concentric ridges (marked as B–B' in Figure 3.1b). Wrinkle ridges tend to show one or more of the following morphological features: a broad rise that extends for several kilometers and peaks at the ridge, a superposed hill that is a few kilometers long and upon which the ridge is situated, and crenulated peaks showing the well-known "wrinkles" of the ridges. Although there is no obvious broad rise present in Fig. 3.2, the two peaks of the ridges are situated on what appears morphologically similar to a superposed hill, following the examples from *Golombek et al.* [1991]. There is no measurable offset, and although offsets are typical of wrinkle ridges, the lack of one here does not preclude this feature from being a wrinkle ridge. The width of the "superposed hill" is 28 km, and if the two peaks are considered two separate wrinkle ridges, then one may consider that the width of the "superposed hill" for each ridge is 14 km. The total relief is

75 m in the case of the inner (northern) ridge and 100 m in the case of the outer (southern) ridge. Given these dimensions, these features do not fit well into the statistical relationships for Martian wrinkle ridges found by *Golombek et al.* [1991], although this relationship is based on measurements of wrinkle ridges in Lunae Planum. The dimensions of the wrinkle ridges of Lunae Planum, which are among those considered by *Golombek et al.* [2001] to be evidence for tectonic faulting that penetrates the Martian crust, may not be representative of all Martian wrinkle ridges, particularly those produced by faulting along shallow décollement surfaces. Based on morphology alone, it is difficult to conclude confidently that these features are indeed wrinkle ridges.

Given the highly eroded state of the concentric ridges, it is difficult to decide on which of these three hypotheses is most likely. It is possible that they are created
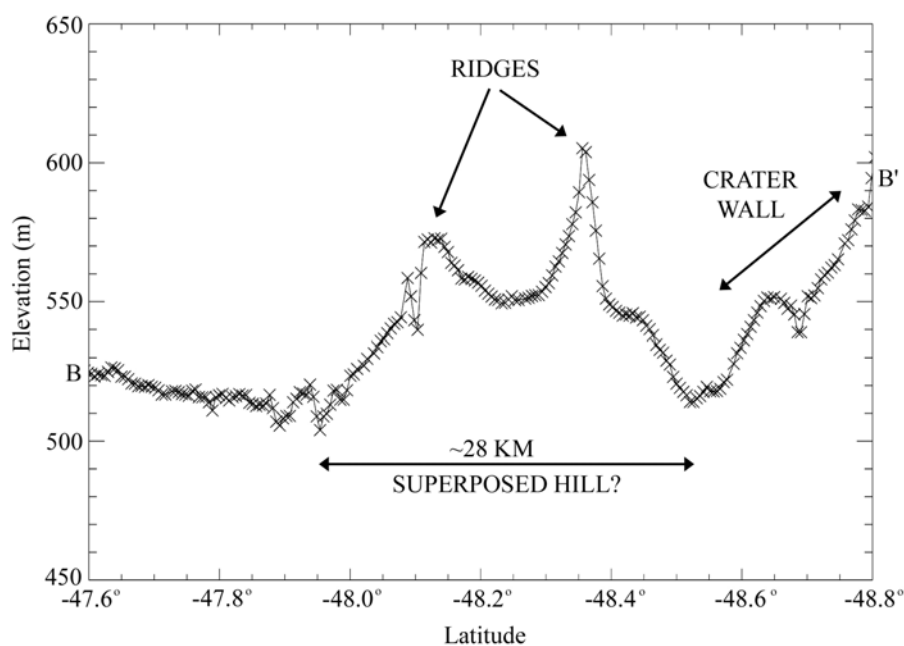

Figure 3.2. Profile BB' (shown in Fig. 3.1b on the MOLA DEM) across two concentric ridges.

by a combination of the above processes. For example, if they are wrinkle ridges, then they may have formed over buried peak rings, in the same way that wrinkle ridge systems have formed over buried crater rims in other areas on Mars. Unless a new development in one of these areas of study precludes one or more of these hypotheses, more information is required to determine what process produced the concentric ridges.

3.2 Overview at MOC Narrow Angle Resolution

High-resolution MOC NA images provide unprecedented detail of the Martian surface that is often surprising when compared with the lower resolution view. *Malin and Edgett* [2001] found that surfaces on Mars appearing to be rugged at hectometer scales typical of Viking, Mariner 9, and MOC WA, are generally smooth at MOC NA resolutions. They show that the converse is true as well. Thus, a full description of Proctor Crater must include both the high- and low-resolution views. Here, some examples of the various types of terrain on the Proctor Crater floor are shown to emphasize the diversity of surface features in the study area. Further sections in this work discuss many of these features in more detail.

Figure 3.3 shows several high-resolution views of the floor of Proctor Crater. Many characteristics of the surface become evident at this scale. Much of the floor is strewn with boulders ranging in size up to 20 m and down to the limit of resolution at 5 m (Fig. 3.3a, b). In Figure 3.3a, the larger boulders have shadows visible at the MOC NA resolution, indicating that they are blocky, positive features on the landscape. Figure 3.3a also shows drifts of dark sand (see arrows) that partially bury some of the boulders, indicating that the boulders are older than the sand drifts, and that the boulders are taller than the sand drifts are deep. There is little evidence for extensive fluvial or glacial activity in the crater, and the Proctor Crater walls are generally too far from most of the crater floor to have
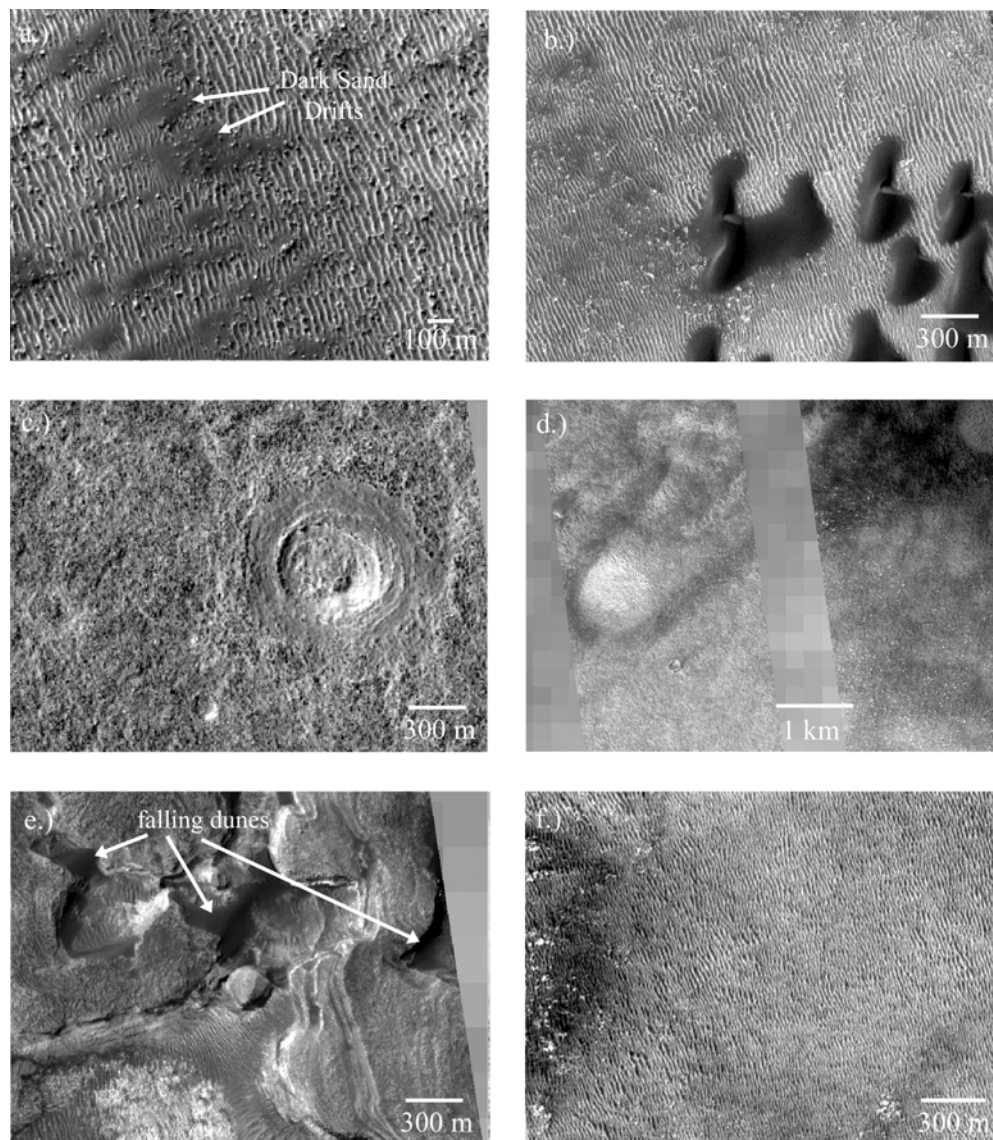
Fig. 3.3. Examples of MOC Narrow Angle images on the Proctor Crater floor. a.) Boulders and sand drifts (MOC NA M2301221), b.) boulders, dark barchans and bright duneforms (MOC NA M0303088), c.) degraded craters on the Proctor Crater floor (MOC NA M0201510), d.) dark erosional wind streaks (MOC NA M0201510, M0306827), e.) strata of basin fill and dark falling dunes in the western pit (MOC NA M0300338), f.) uniform coverage of bright duneforms (MOC NA M0306827).

produced these boulders from mass wasting. Thus, these boulders were most likely emplaced by impact events on the Proctor Crater floor. Boulders produced
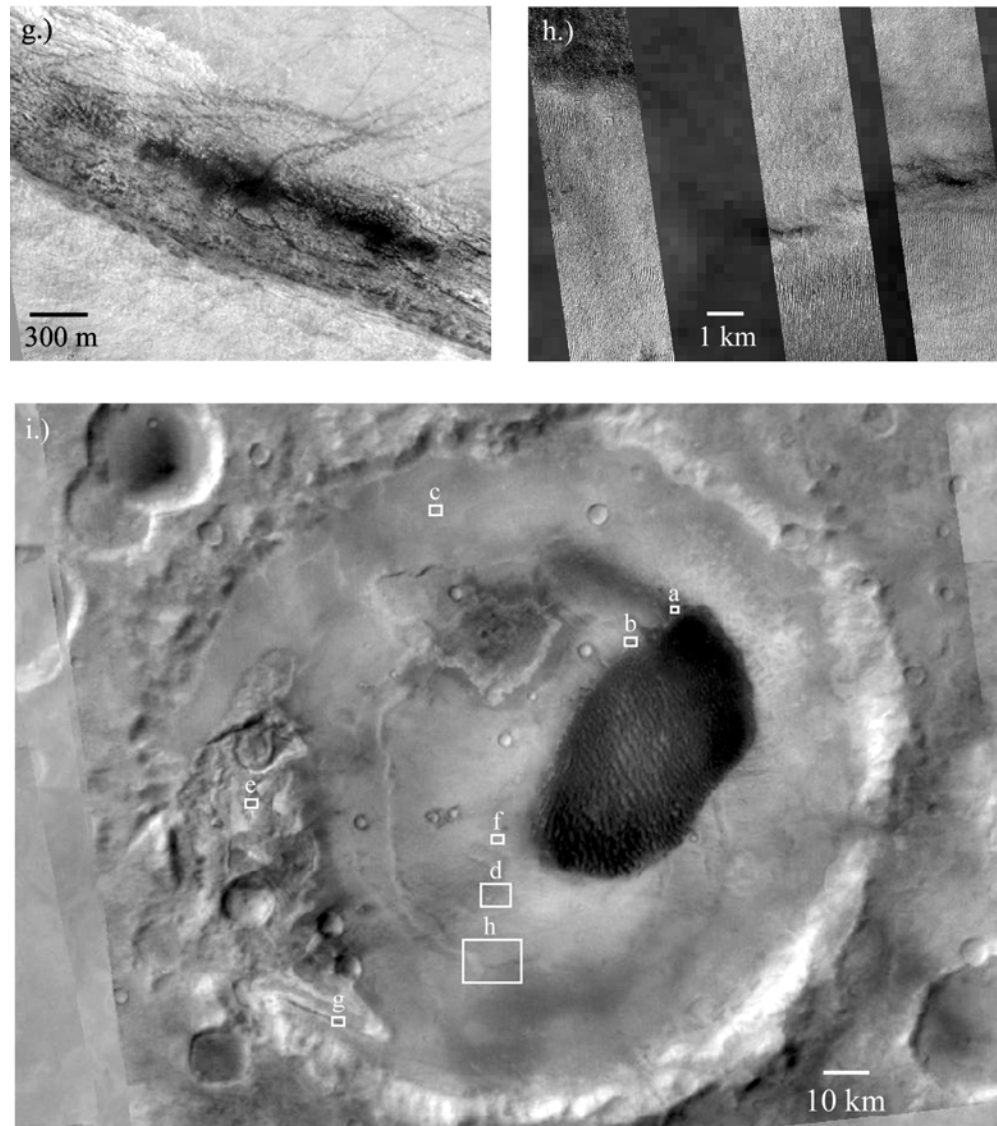
Fig. 3.3. (cont.) g.) dark sand trapped against a northeast-facing hill slope, spawning dust devils as revealed by dark tracks (MOC NA M1103806), h.) mosaic of three MOC Narrow Angle frames over part of a concentric ridge (MOC NA M0201510, M0301614, M0306827), i.) and Wide Angle context for frames a through h.

by crater formation indicate that the surface is consolidated enough to produce coherent blocks that do not shatter or crumble upon landing. *Malin and Edgett* [2000a] state that crater ejecta blankets extend out to one crater radius, far less

than what is necessary to explain the ubiquitous boulder fields on the crater floor given the paucity of small craters present both on the floor of and outside the crater. Thus these boulders could not all have come from outside Proctor Crater. Their high abundance on the floor of Proctor Crater must indicate some process by which boulders accumulate relative to other features, and is considered below with regards to the numerous eroded craters on the crater floor. Close views of the dark dunes at the perimeter of the dunefield reveal slipfaces and stoss slopes typical of barchans (Fig. 3.3b). The presence of barchans at the edge of the dunefield indicates that the dunes, when last moved, were left in a state of disequilibrium with their environment. This could mean that the dunefield has yet to reach its final resting location. A more likely conclusion is that the dunefield is mostly in a state of equilibrium, and that these barchans at the edges of the dunefield reflect small variations in relative wind strengths over the course of several centuries or perhaps millennia. Such barchans are typical of dunefield perimeters on Earth, and they tend to be more mobile than the larger interior dunes because they contain less material. Thus they reflect more recent winds.

Beneath the barchans in Fig. 3.3b are smaller, brighter aeolian features, here referred to as "bright duneforms" or "bright bedforms." These smaller bedforms have been identified in many different terrains on Mars [*Malin and Edgett*, 2001], and in addition they are widespread across the floor of Proctor Crater. Where they coexist with large dark dunes, they consistently lie stratigraphically beneath the larger dunes [*Malin and Edgett*, 2001]. The small bedforms have an appearance more consistent with ripples than with dunes, leading to the proposal that they are large granule ripples [*Zimbleman and Wilson,* 2002]. The superposition relationship and the difference in distribution across the crater floor indicates that the bright duneform and dark dune materials are different populations of aeolian material, and that they were clearly laid down at different times.

There are many small craters in varied states of erosion on the floor of Proctor Crater (Fig. 3.3c). It is tempting to conclude that the subdued appearance of these craters is caused by burial alone, but the ubiquitous boulder fields on the crater floor suggest the situation is more complex. Dust or sand mantles that bury craters should also bury boulders unless there is a constant supply of boulders. The lack of fresh craters indicates that the supply rate of boulders is very low. Thus, the crater floor has undergone extensive erosion and perhaps minor mantling, leaving behind boulders as finer material is blown away, and leading to the highly degraded state of craters observed today. Only deflation by the wind is capable of removing so much material so uniformly across the flat crater floor. Except for the accumulated dunes and bright duneforms, the Proctor Crater floor is currently a landscape dominated by aeolian erosion.

Figure 3.3d shows an area to the southwest of the main dark dunefield, showing dark wind streaks draped downwind of a small crater and a larger relatively bright topographic low that may be a highly degraded crater. Dark streaks such as these may be caused by either the deposition of dark material, such as the dark sand that comprises the dunefield, or by the preferential erosion of relatively bright material, such as the bright duneforms. The streaks are aligned with southwest winds, much like the dark dunes, indicating that the streaks must be aeolian in origin [*Cutts and Smith,* 1973]. The small bright bedforms in this area are oriented roughly transverse to this wind. A greater concentration of boulders within the dark streaks relative to the immediate vicinity is consistent with preferential erosion, and so we consider the dark streaks in this area to be caused by erosional stripping of a relatively bright material over a darker, bouldered surface, as opposed to deposition of dark sand.

A close view of the large western pit (Fig. 3.3e) shows that the crater floor is composed of layered material that appears to be the same sedimentary strata

described by *Malin and Edgett* [2000a]. Some surfaces appear rough and may be exhumed volcanic flows, although any source of lava from within Proctor Crater has since been buried by successive infill of sediments. The layers exposed in the pit may comprise all or part of the ~450 m of crater fill. To first order the strata appear to be horizontal beds, indicating that little deformation or faulting has taken place. In the pits the basin fill material has undergone erosion, very likely by wind action, to expose these strata. This erosion occurred after a period of cratering on the surface of the layered unit, but prior to the passage of dark sand through the area. Superimposed on the erosional surface are small ripple-like bedforms and larger accumulations of dark sand. The dark sand is mostly piled against cliffs facing north and east, although some sand stretches across the valleys to reach the opposing wall. These bedforms are "falling dunes," or sand trapped in the lee of topographic highs by prevailing winds from the southwest. Studies of climbing dunes, falling dunes, sand sheets, and dunefields in the terrestrial deserts such as the Mojave of North America [*Zimbleman et al.,* 1995] and the Sahara [*Wilson,* 1971; *Mainguet and Cossus,* 1980] has led to an understanding of sand transport pathways from the original sand source to the final sand sink. For the first time, satellite imagery of Mars is of high enough resolution to allow a similarly detailed pursuit on another planet. These images show that many areas in the large western pit of Proctor Crater have dark falling dunes, indicating that the sand in the large dark dunefield in the center of the crater has traveled from at least as far away as the western pit, and probably from beyond, as the westernmost edges of the western pit also have accumulations of dark sand. The eastern edge of the western pit is not steep enough to inhibit sand from moving up onto the central crater floor.

Small bright bedforms cover much of the crater floor, in addition to lying stratigraphically beneath the large dark dunefield (see Figs. 3.3a, 3.3b, 3.3f, and 3.3h). In several areas they dominate the landscape, obscuring underlying

features. In other areas they appear somewhat eroded. In a few areas they are not apparent at all, and it is unclear whether they have completely eroded away or if they never formed in the first place. Figure 3.3f shows one area where the crater floor is uniformly covered by bright duneforms. In this location, these features have a wavelength of ~20 m, and their pattern is broken only by the occasional large boulder. The nearly ubiquitous distribution of bright duneforms across the crater floor with no obvious transport pathways (*i.e.,* no climbing or falling dunes) suggests that these features were probably formed from local materials, such as eroding basin sediments. Bright duneforms and their origin are discussed in detail in Section 3.4.

Dust devil tracks are common features on the floor of Proctor Crater in spring and summer images (see Fig. 3.3g). These tracks are of the typical sort described by *Malin and Edgett* [2001]. They are always dark, most likely indicating the removal of bright dust from a relatively darker substrate. The tracks cross over almost all terrains including the dunefield, and they are commonly ten to fifty meters in width. These are the "long dark filaments" first described by *Cutts and Smith* [1973], although they did not attribute them to dust devils. *Grant and Schultz* [1987] mapped these features in a portion of the Proctor Crater floor in both Mariner 9 and Viking images, noting that they appear in midsummer and disappear in the fall, and that from one year to another their positions change. These tracks almost certainly provide information on the orientations of winds of moderate strength. Weaker winds would not have the strength to move dust devils downwind [*Metzger*, 1999], and very strong winds remove kinetic energy from the boundary layer, preventing dust devils from forming. Dust devils are discussed in detail in the next section (Section 3.3).

In addition to dust devil tracks, Figure 3.3g shows another example of layered material exposures at the southern end of the western pit. In this image the lower

left corner is high ground. The layers are visible in a steep wall that crosses the frame from the upper left to the lower right. The upper right corner is low ground, and largely covered in bright dust that has been removed in places by dust devils. The dark splotches on the hillside are interpreted as accumulations of dark sand that has been transported into the region from the southwest (lower left), much like the falling dunes of Figure 3.3e. Some of the dust devil tracks appear to originate in the dark sand, and then to move downwind to the ENE. The surface heating over dark sand will be greater than that over bright dust, and so it is probably easier for dust devils to form over dark sandy surfaces than elsewhere. Further discussions below of dust devils in the vicinity of the dark dunefield support this conclusion. The dust devil tracks also appear darker over the low ground than the high ground, suggesting that more dark sand may be piled up in the bottom of the western pit than is visible in the images, because these deposits are obscured by the accumulation of bright dust.

Figure 3.3h is a mosaic of MOC Wide Angle and Narrow Angle images that shows a close view of one of the concentric ridges that rings the crater floor. Little of the original structure is obvious at this scale. Small bright duneforms are ubiquitous in this image, although they become larger and sharper immediately south of the concentric ridge. To the north of the ridge, dark patches indicate small accumulations of dark material [*Malin and Edgett,* 2001], probably the same dark sand that comprises the dark dunefield and the falling dunes in the western pit. Both the bright duneforms and the dark sand deposits postdate the emplacement of the ridge; however, the different areas and modes of deposition reflect different conditions under which these features formed. The single deposit of dark sand, trapped downwind of the ridge, suggests that this is a remnant of material that previously swept through the region, originating elsewhere. However the commonness of the bright duneforms indicates that the materials

forming these features has not moved on downwind, and in fact they may have formed in place.

Examination of small-scale features at the resolution of MOC Narrow Angle images reveals a great deal regarding the nature of the Martian surface. The floor of Proctor Crater has undergone extensive modification by the wind. There are indications of accumulation of sediments from beyond the crater rim as well as the reworking of material composing the strata of the basin fill. Aeolian features range from the vast western pit, probably formed by wind deflation, to the tenuous and temporary dust devil tracks that lightly scour the surface. The sedimentary history of the Proctor Crater floor is clearly a rich and complex chronology of aeolian deposition and erosion.

3.3 Temporal Features

3.3.1. Dust Devil Tracks. Of the twenty-six MOC NA images taken of Proctor Crater before the end of the mapping mission, nine contain features that we interpret as dust devil tracks. Like the features described by *Malin and Edgett* [2001], these tracks are long and thin, up to at least a few kilometers long and ten to fifty meters wide. *Grant and Schultz* [1987] mapped a number of similar features on the floor of Proctor Crater, attributing them to "tornado-like tracks." Dust devils are local vortices produced in unstable atmospheric conditions. The Martian surface, which warms up significantly more than the overlying atmosphere, is an ideal place for the forming of dust devils, particularly during the summer when surface heating is at its peak.

All the dust devil tracks in Proctor Crater are dark features, indicating that the dust devils removed a relatively bright material from the surface as they passed by. The tracks cross dark sand, bright duneforms, and seemingly bare surfaces. Although there are tracks on dark sand sheets at the edge of the dunefield, most

dark dunes are free of these features, even in images where the tracks are dense just off the edge of the dunefield. This suggests that if dust devils do pass over dark dunes, there is little bright dust present on the surface of the sand to be removed by a passing dust devil. With two exceptions (described below), the tracks are found in images ranging in season from $L_s = 223-354°$, or from mid spring through late summer. This is the same time of year that they were observed by *Grant and Schultz* [1987] in Mariner 9 and Viking Orbiter images. Seasonal CO_2 frost begins to appear partway through autumn, and remains on shady slopes until late winter. Thus, dust devils appear to form and create erosive tracks during the warmest time of year when surface heating is at a maximum and frost is absent.

Malin and Edgett [2001] describe one feature on the Proctor Crater floor that has the appearance of a dust devil track from a Viking frame, but in a MOC Narrow Angle image is revealed to be the same feature that has been termed a concentric ridge in this work (see Section 3.1). However, part of this feature (marked by arrows in Fig. 57 of *Malin and Edgett* [2001]) is not visible in all MOC Wide Angle images of Proctor Crater (*e.g.,* Fig. 3.1a). The eastern half of the feature is in fact the ridge described by *Malin and Edgett* [2001] and above in Section 3.1. But this ridge, as shown by the MOLA DEM in Fig. 3.1b, does not continue westward like the feature shown by *Malin and Edgett* [2001], but instead curves northward, concentric to the crater rim. Therefore the western half of the feature is probably a dust devil track of the type described by *Grant and Schultz* [1987]. Indeed, it is aligned with most of the other tracks observed both in this work (described below) and by *Grant and Schultz* [1987]. The fact that the western half of the feature is not visible in all MOC Wide Angle images simply reflects the transience of dust devil tracks. This partial misinterpretation is a demonstration of the need for a more complete spatial coverage of high-resolution images as well as careful consideration of all information available.

To determine the daytime wind regime during the summer, the orientations of the most prominent dust devil tracks were measured using an application in Arcview. Fig. 3.4 shows a rose diagram (*i.e.,* a histogram on a polar plot) of the mean orientation of 196 measured dust devil tracks. Because determining the upwind versus downwind direction is impossible from observing most dust devil tracks, all directions shown have been restricted to 0° to 180°. Tracks oriented at 0° or 180° are oriented north-south, and tracks measured at 90° are oriented east-west. One modal direction is evident in Fig. 3.4, with a spread from 60° – 100°, or
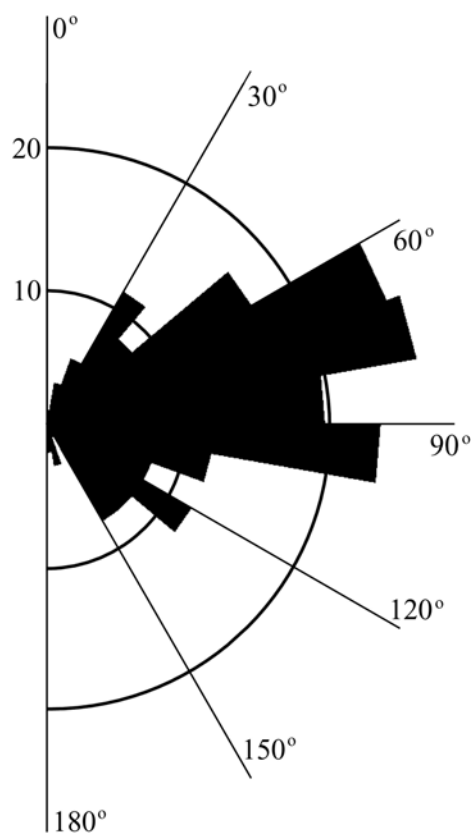

Figure 3.4. Rose diagram of dust devil track orientations. Orientations of 0° or 180° indicate a north-south alignment while an orientation of 90° indicates an east-west alignment. Because of an upwind versus downwind measurement ambiguity, all orientations are restricted to an orientation of 0°–180°. Note the two concentrations of orientations at 60–80° and 90–100°.

generally ENE–WSW. This is the same main orientation of dust devil tracks mapped by *Grant and Schultz* [1987] in both Mariner 9 and Viking Orbiter images. Because of the dust devil tracks appearing to initiate on the sand patch shown in Fig. 3.3g, these dust devil tracks are considered to be formed by winds from the WSW. This direction corresponds to the dune orientations observed by *Cutts and Smith* [1973], as well as those measured in this work, as discussed below in Section 4.2.

The orientation measurements of dunes and dust devil tracks have several implications. The persistence of dust devil track orientations from one mission to another indicates that daytime summer winds are very consistent in direction. Because the dunes in Proctor Crater are so large, they have a much longer memory, and thus reflect the prevailing winds over at least several decades, and possibly over the last million years. The correspondence of dust devil tracks to dune slipface directions indicates that these wind directions have been very typical of this area in the summer for quite a while. Furthermore, dunes require winds above the saltation threshold to shape them, but dust devils may move under lighter winds (*Metzger* [1999] estimates that ~5 m/s winds will move dust devils), and so this alignment indicates that both strong and moderate winds blow in this direction. The correlation of these wind features to modeled surface winds is the topic of Paper 2, although the current wind regime of the crater floor as shown by aeolian features is summarized in this work.

Figure 3.5 shows several examples of dust devil tracks in Proctor Crater. Figure 3.5a shows the locations of each example. Figure 3.5b shows several dust devil tracks that are quite apparent when crossing over a featureless surface, but appear only faintly over a nearby outcrop. The outcrop is likely composed of bedrock of relatively high albedo, covered by little to no dark sand that could be revealed by a passing dust devil. On the other hand, the surrounding terrain is a
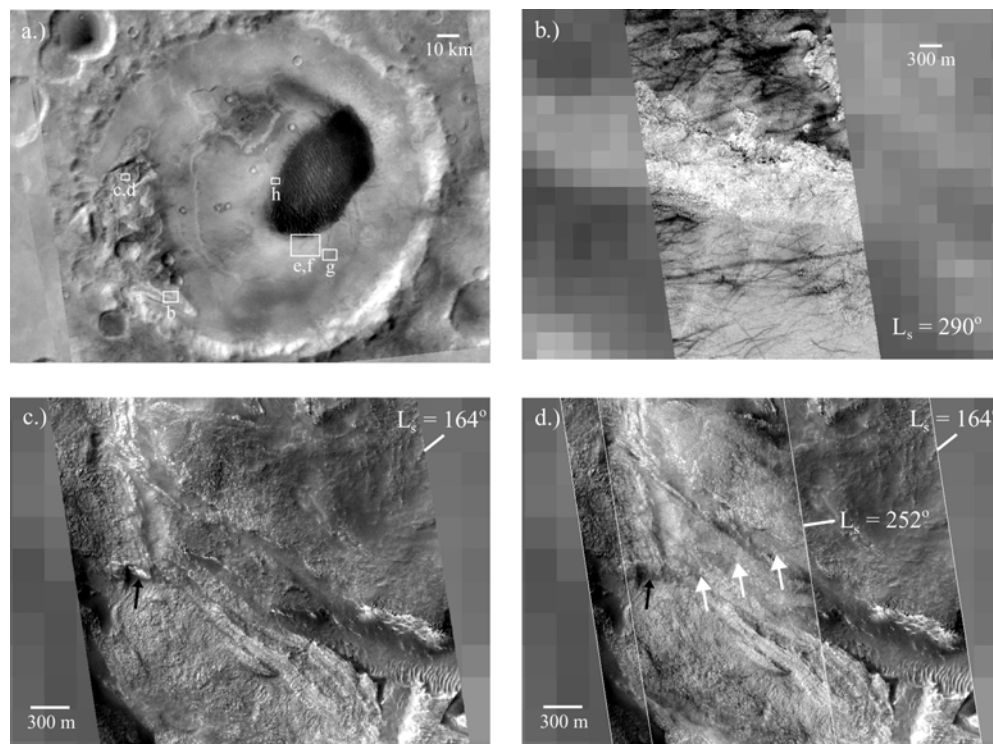
Figure 3.5 Dust devil tracks on the Proctor Crater floor. a.) Context for frames b through h. b.) Tracks crossing featureless plain but not across a bright outcrop (MOC NA M1103806). c.) and d.) are overlapping images in the late winter and late spring, demonstrating the appearance of a dust devil track (MOC NA M0300338, M0906250).

relatively flat area that is likely covered in dark sand overlain by a thin bright layer of dust. Thus the two surfaces produce very different dust devil tracks. If dust devils continue to erode the overlying layer of bright dust on the flatter surface, then it is likely that the albedo and thermal emission spectra will vary accordingly with season.

There are two examples of MOC NA frames that overlap, allowing for a study of dust devil development through the spring and summer. Figures 3.5c and 3.5d show an example from inside the western pit. In Figure 3.5c, an image from late winter, there are no signs of dust devil tracks. In Figure 3.5d, there is one faint
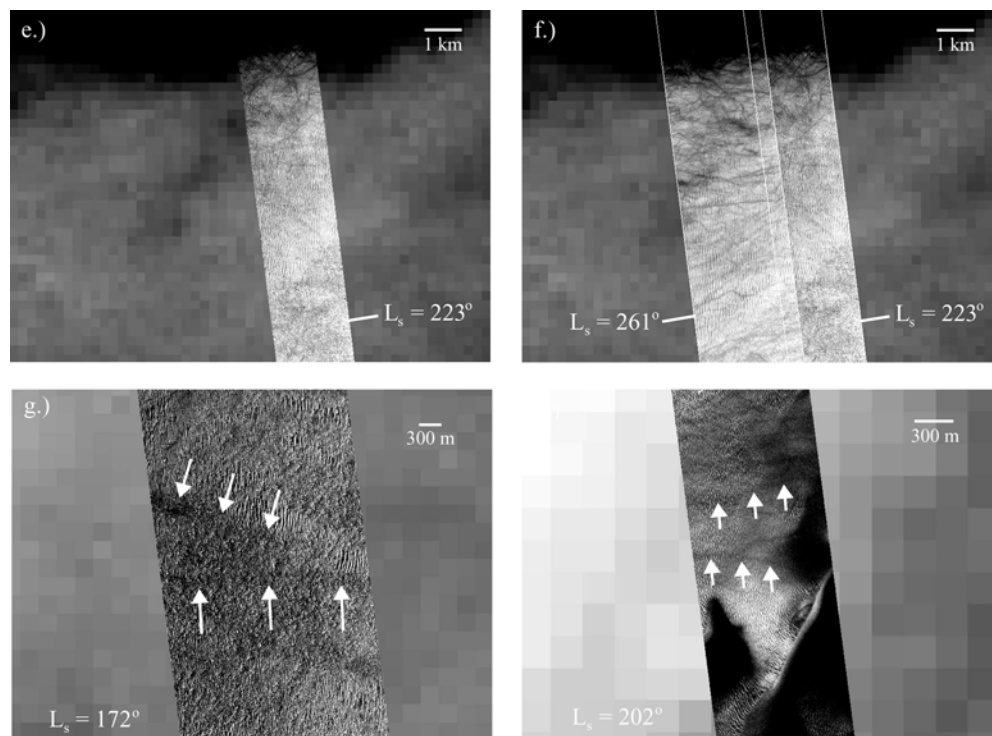
Fig. 3.5 (cont.) e.) and f.) are overlapping images from the late spring showing a growing number of dust devil tracks (MOC NA M0802629, M1001334). g.) (MOC NA M0303087) and h.) (MOC NA M0701445) are images showing potential dust devil tracks in the winter time, although the faintness of the tracks (images have been greatly stretched) may indicate that these tracks are remnant features from the previous summer season.

track marked by white arrows. It is oriented ENE–WSW, consistent with the modal peak in Fig. 3.4. The black arrow shows a patch of CO_2 ice on a shady slope that has disappeared by late spring, when the second frame was taken.

The second set of overlapping images is shown in Figs. 3.5e and 3.5f, which are located just south of the edge of the dark dunefield. In late spring, in Fig. 3.5e, the dust devil tracks are not very abundant and seem to be concentrated near the edge of the dunefield. Dust devils that form early in the season are probably more common on the dark dunes than on the rest of the crater floor because the low albedo of the dune sand should increase surface heating and encourage dust devil

formation. Later in the summer, in Fig. 3.5f, dust devils are much more common. Most of the tracks in the overlapping portion of the springtime image are still present in the summertime image, indicating that they are not often erased by strong summer winds. This suggests that, if winds are occasionally strong enough to saltate sand, there is no loose sand readily available that might kick up dust into suspension. The average orientation of dust devil tracks does not appear to change from one frame to the next, indicating no net seasonal shift in wind direction.

There are two examples of dust devil tracks from earlier in the season, shown in Figs. 3.5g and 3.5h (white arrows). In each case the image contrast was stretched a great deal to show these features. Both sets of tracks are oriented with the two dust devil winds. Because of the time of year at which these images were taken and the faintness of the features, we interpret these tracks as old features from the previous summer. They were likely covered by frost over the winter, and have been recently exposed. It may be that in early spring there has not yet been enough dust fallout to obscure them completely, and that a process such as this occurs more commonly throughout spring as the dust loading in the atmosphere steadily increases.

There is only one summertime image on the crater floor that does not contain any dust devil tracks. This is in the same area north and east of the dunefield in which the small bright duneforms appear rounded and eroded (see Fig. 3.3g). If this is a place of constant wind erosion, then there may be no thin layer of settled dust to be lifted by a passing dust devil. Either this is a place where dust is prohibited from settling, perhaps from strong winds, or it is quickly remobilized with a mechanism other than dust devils, such as saltation in local sand sheets. Another explanation may be that there is dust on the surface here, but that there is little contrast between it and the underlying surface. However, thermal inertia

calculations, discussed below in Section 6.4, are high enough that there can be very little dust on the surface in this area, supporting the proposal that this area does not accumulate fines. Not surprisingly, the effectiveness of wind action appears to vary spatially across the crater floor.

Dust devil tracks are useful probes of the Martian surface underlying the annual dust fallout. Dark tracks reveal the presence of relatively brighter dust, wind directions at noon during the summer, winds as a function of time throughout the summer as the number of tracks builds up, and surfaces containing darker materials underlying the dust. Only a few outcrops and an area northeast of the dark dunes do not have a darker surface underlying the dust deposits. The orientations of the tracks indicate that local winds in Proctor Crater have remained consistent for many years. Their fresh appearance every summer indicates that dust fallout annually obscures most of the tracks. Further studies of these tracks throughout the summer season can lead to estimates of dust accumulation rates and changes in apparent thermal and compositional properties of the underlying surface.

3.3.2 Frost Features. *Malin and Edgett* [2000b] studied the frosting and defrosting of dunes at both poles. They found that the dunes are generally the first features to develop frosted surfaces during autumn, and they are the last features to lose frost in the spring. They suggest that Martian dunes may trap volatiles, much as *Sharp* [1966] found that the Kelso Dunes of the Mojave Desert trap water. In addition, *Malin and Edgett* [2000b] found that defrosting tends to begin with small dark spots commonly located at the dune margins, which enlarge slowly and coalesce until the entire dune surface is defrosted. They proposed that dark sand beneath thin bright frost accumulations warms more quickly than in other areas, causing the frost to sublimate in patches. Little is known about the relationship

between frost and dune sand on Mars, but the MOC Narrow Angle images indicate that the interactions are complex and certainly worth further study.

Although Proctor Crater is located in the midlatitudes (47° S), rather than near the poles, the region is covered in seasonal CO_2 frost each winter. Thus the numerous images of the dunefield provide an opportunity to compare how these dunes frost and defrost relative to the polar dunes. Frost cover begins in mid northern fall, at approximately $L_s = 50°$, and remains in patches on the dunes until late winter at approximately $L_s = 165°$. Because Proctor Crater is located in the midlatitudes, the seasonal frost cover does not last as long as it does closer to the poles. Image coverage during the southern fall is too sparse to determine if the dunes acquire frost before the remainder of the Proctor Crater floor does, as is expected. However, poleward-facing slopes on the dunes are certainly the last surfaces to defrost in late winter, consistent with the observations of *Malin and Edgett* [2000b].

Figures 3.6a and 3.6b show overlapping images during the late winter from two consecutive years. Each image shows partially defrosted dunes within the Proctor Crater dunefield with dark spots similar to those found by *Malin and Edgett* [2000b]. Interpreting images with partial frost cover can be tricky, because features can appear bright from either frost albedo or incident sunlight. Determining whether an area is inherently bright or only apparently so from shading differences requires experience with viewing several MOC images, preferably over different seasons and under different lighting conditions. Figure 3.6c shows an interpretation of the features shown in Figure 3.6b, built from such a knowledge base. Dune crestlines refer to linear peaks of dunes. Slipfaces generally begin from these crestlines, but not all slopes that reach to the crest are necessarily slipfaces. Bright duneforms are located in the interdune flats and thus represent low-lying areas. Slope or slipface adjustments, as defined here,
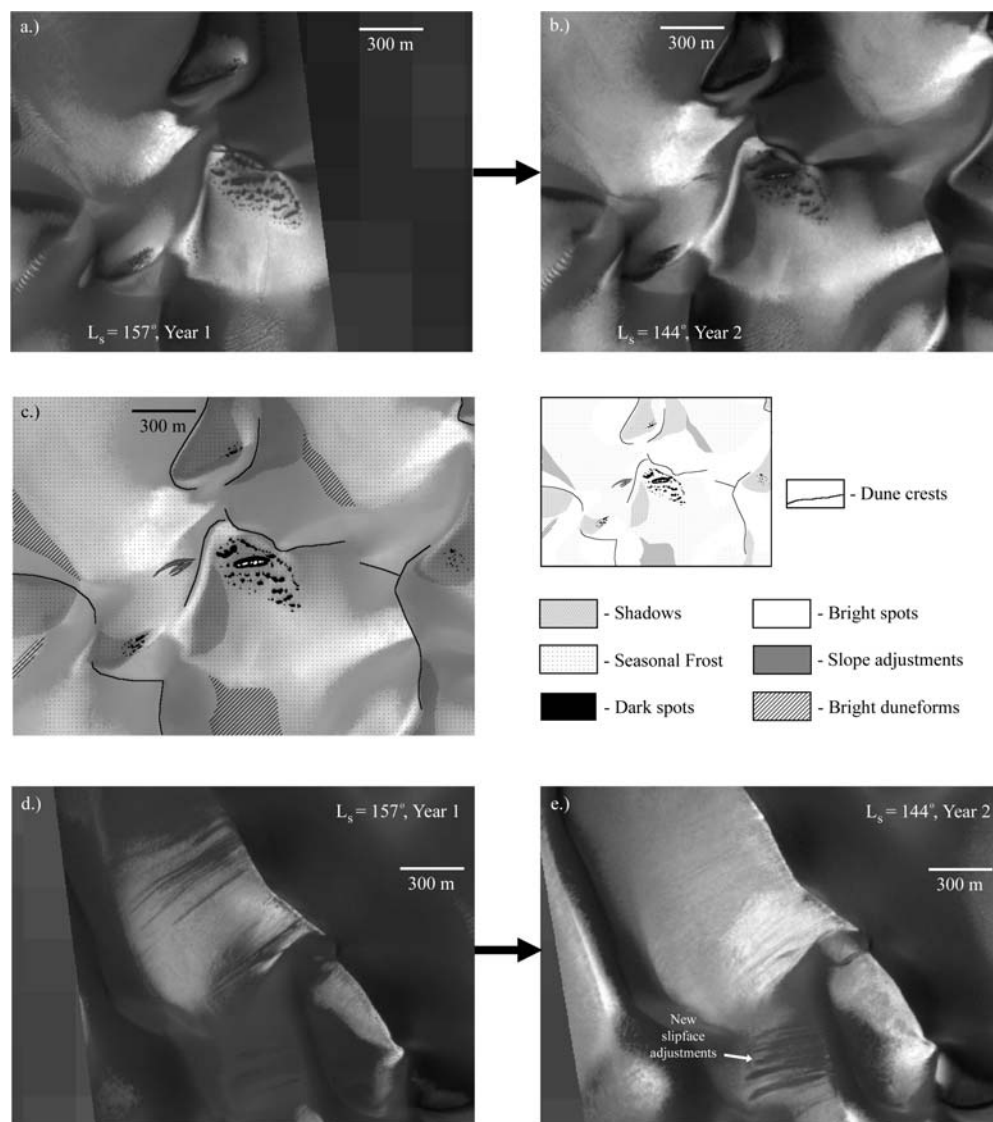
Fig. 3.6. Frost in the dark dunefield. Frames a.) and b.) show the same area nearly one Martian year apart. Defrosting spots occur in the same locations, suggesting that they are produced by some underlying persistent aspect of the dunes (MOC NA M0202711, E0301039). c.) A diagram of the features in b.). Images d.) and e.) show the same region nearly one year apart, with new slipface adjustments formed within the year (MOC NA M0202711, E0301039). Frames f.) , g.) and h.) form a sequence of images over the same area of the dunefield, each showing slope adjustments that persist for at least a year. f.) Late winter image of Year 1, where such adjustments appear to be superimposed on seasonal frost, giving the impression that they are fresh features (MOC NA M0202711).

Fig. 3.6. (cont.) Frames f.), g.) and h.) form a sequence of images over the same area of the dunefield, each showing slope adjustments that persist for at least a year. f.) Late winter image of Year 1, where such adjustments appear to be superimposed on seasonal frost, giving the impr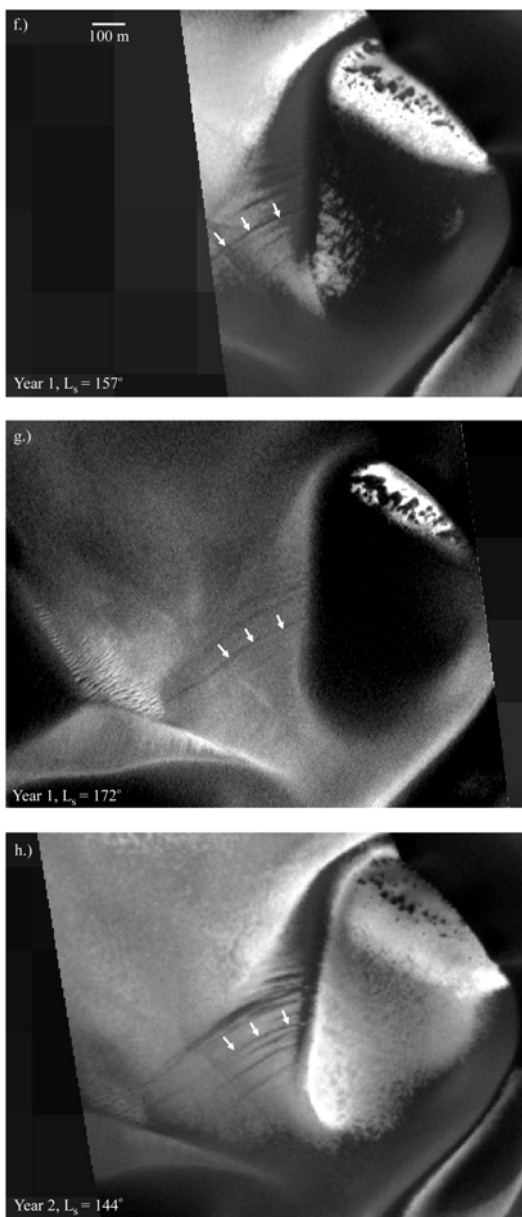ession that they are fresh features (MOC NA M0202711). g.) Shortly after the frost has disappeared from the slope, the same adjustment scars are still visible (MOC NA M0303088). h.) Nearly a year after the first frame, when the frost has reformed, the slope adjustment scars are still visible, giving the impression that they are recent movements over the seasonal frost. Rather, they must be somewhat older features that inhibit frost formation or allow frost to sublimate more easily (MOC NA E0301039).

are avalanches of sand that has been oversteepened by the wind at the brink of a dune. Such slope adjustments are generally oriented downhill and are good indicators of the local gradient. The patchy seasonal frost is located as drifts in low-lying areas, and on the southern and western sides of dunes. Shadows are located southeast of dune crests, created by a low winter afternoon sun to the northwest.

Like the polar dunes, the Proctor Crater dunes develop dark spots as they defrost. A new development of these features reported here is that they persist in location from year to year. The repetitiveness of dark spot locations indicates that their position is dependent on some relatively stable aspect of the dune surface. Unlike the dark spots on polar dunes, the dark spots on the Proctor Crater dunes are concentrated on steep slopes, rather than along the dune margins. In addition, these features rarely appear on hills facing any direction but towards the pole. The largest spots in Figs. 3.6a–3.6c contain bright cores, which have not been observed in polar dunes. The cores are brighter than frost on the surrounding slope, indicating that this material is not simply a remnant frost patch from the previous uniform cover. *Bridges et al.* [2001] found that dark spots located in small gullies on Mars, similar to the spots on the dunes, are aligned with the local dip and channel trend (*i.e.,* downhill along the channel). In contrast, the spots in the Proctor Crater dunes appear to be aligned either along the strike of the south-facing dune slope or parallel to the crest.

It is possible that the spots are associated with granule ripples that can form on dune slopes. However, in areas where there is summertime coverage of slopes that form dark spots while defrosting, there is no evidence for any features on the smooth dune slopes. Furthermore, there is no physical reason why granule ripples would preferentially form on pole-facing slopes, as the dark spots do. Another idea is that the dark spots are small avalanches over the seasonal frost cover,

although no known mechanism causes slope adjustments to form in the same locations in the middle of dune slopes year after year. Finally, it may be that the dark spots are concentrated along interfaces between exposed dune strata. Such strata on terrestrial dunes accumulate water. A similar process could occur on Mars with either H_2O or CO_2 ice, thus keeping the contacts between sand strata cooler than the dark dune sand itself. This could easily cause reprecipitation of sublimating frost, creating the bright cores of the dark spots, much like the mechanism proposed by *Malin and Edgett* [2000b] to explain bright frost halos around dark sublimation spots. Additionally, wind could blow frost from elsewhere into small cracks that are exposed by defrosting, such as the process described for polar "spiders" by *Piqueux et al.* [2002], although summertime images of dunes slopes show a surface devoid of any roughness that could trap windblown ice grains.

Because of the yearly persistence and the lack of associated topographic features, the most likely explanation for these aligned dark spots is preferential sublimation along exposed dune strata. However, it is not clear what process would cause a higher sublimation rate along dune strata, particularly if these strata tend to accumulate seasonal ice. The melting of snow lenses trapped in terrestrial dunes is known to cause unusual surface features, such as small sinkholes and tensional cracks [*Koster and Dijkmans,* 1988]. However, features created by the sublimation of trapped CO_2 frost may be very different from those created by the melting of H_2O snow lenses.

Since these spots mostly form on the shaded slopes and manage to persist much longer into the season than on other slopes, the frost may have enough time to undergo sintering caused by compaction and grain growth in a process modeled by *Eluszkiewicz* [1993]. Thus, preferential sublimation may occur from differential ice grain growth, in which transparent areas absorb more heat from insolation

and sublimate faster than opaque areas. This process may in turn be influenced by ice trapped in underlying exposed dune strata. For example, the weight of frost overlying an exposed icy layer between dune strata may compact some of the upper icy layer enough that it sinters into larger grains, which become more transparent to sunlight as they grow. As the frost slowly thins from sublimation, this relatively transparent layer becomes more and more exposed to daily heating until enough heat is collected to begin localized sublimation. There is no reported terrestrial analog for this process, or for defrosting spots on sandy surfaces such as these. This process is similar to that suggested by *Malin and Edgett* [2000b] and *Bridges et al.* [2001] to explain dark sublimation spots. In the case of the Proctor Crater dunes, sintering in the upper layer of ice trapped between dune strata explains the alignment of dark spots along the slope of the dune. The presence of ice lenses may also explain the bright cores, since the remaining ice between dune strata may be cold enough to cause reprecipitation of locally sublimating frost, once the initial wave of defrosting has occurred and swept outward from the center of the spots.

Edgett and Malin [2000] show slipface adjustments in Proctor Crater dunes and propose that they are fresh movements over seasonal frost. However, as they consider, and as discussed below, such slope adjustments may not be as fresh as they appear. Fortunately, there is new evidence confirming that the dunes in Proctor Crater are indeed active from year to year, although the season in which these movements occur is not constrained. Figures 3.6d and 3.6e show the same area roughly one year apart. Figure 3.6d is the same area shown in Figure 17 of *Edgett and Malin* [2000]. In the first frame a frost-covered slope shows superimposed dark tongues of sand that are typical of dune slipface adjustments from easterly winds. In the second frame, taken nearly one year later, seasonal frost has since sublimated away and reformed on the dunefield. The slipface features of the previous year are barely discernable beneath the recent year's

accumulation of CO_2 frost. However, new dark tongues of sand have formed farther south, overriding some older scars that are faintly visible in the first frame. In both cases the sand-moving winds come from the east. These dunes are without question active with fresh slipface scars forming each year. However, these movements do not appear to be very common, as not all of the slope adjustments of the previous year are buried by subsequent activity.

There is enough coverage over enough time to show that some slipface adjustment scars remain for at least a year, and that they therefore may superimposed on annual frost cover as suggested by *Edgett and Malin* [2000]. Figure 3.6f, g, and h show the same area at three different times, each showing the same set of slipface adjustments. Figure 3.6f was taken during the time of partial frost cover, in late winter. Arrows point to a prominent dark slope adjustment lobe that appears to have formed over the frost. Figure 3.6g shows the same area later that year, when most of the frost has sublimated away. In this frame, most of the bright surfaces are sunlit slopes, whereas in Fig. 3.6f most of the bright surfaces are frosted slopes. Even though the frost is gone, the dark stripes from slipface adjustments are still visible. The following winter, in Figure 3.6h, the same dark slope adjustments are still visible, although a new larger and darker scar has formed in the intervening year. Clearly, although these features appear to be superimposed on seasonal frost, they are not. Some aspect of the nature of these scars inhibits frost from forming, and/or allows frost to sublimate more easily than on the surrounding slopes. Slipface adjustments loosen the surface material, and it may be that these less densely packed surfaces expose more surface area to the air and thus allow frost to sublimate more quickly than on a more densely packed surface.

The assessment of frost features on the Proctor Crater dunes reveals more about the nature of the dunes than it does about the frost that covers them. In

particular, the defrosting surfaces of dunes indicate two aspects of the dunes: that they are active in the current wind regime, but only barely so, and that there may be lenses of ice trapped within the dunes, causing the formation of dark defrosting spots.

3.4 Bright Duneforms

MOC Narrow Angle images have revealed the almost ubiquitous presence of small, generally bright aeolian features over much of the Martian surface [*Malin and Edgett,* 2001]. Morphologically, these features are similar to terrestrial granule ripples, and thus they have generally been given the title "granule ripples" or "ripple-like bedforms" [*Malin and Edgett,* 2001; *Zimbelman and Wilson,* 2002; *Williams et al.,* 2002]. The difficulty with the presence of granule ripples on Mars is the well-known correlation of ripple wavelength with the size of the grains that comprise them [*Sharp,* 1963; *Greeley and Iversen,* 1985]. For example, *Sharp* [1963] found granule ripples in the Coachella Valley, California, with wavelengths up to 3 m and surface grain sizes in the range of 2–5 mm with a few grains ranging up to 10 mm in size. The bright duneforms on Mars are an order of magnitude larger than the granule ripples of the Coachella Valley. Present day winds on Mars that are strong enough to saltate sand-sized grains, much less granules, are rarely if ever measured by lander experiments [*Hess et al.,* 1977; *Schofield et al.,* 1997] or predicted by atmospheric model simulations [*Greeley et al.,* 1993; *Fenton and Richardson,* 2001b; see also Paper 2]. If granule ripples are formed by the saltation of granules or even larger grains, then their existence must be explained given the current wind regime. It may be that they were formed in an ancient wind regime in which winds were stronger than they are today. If this is the case then the bright duneforms are indeed old, because model simulations of the past few million years show that winds do not dramatically increase in intensity simply by varying Mars' eccentricity, obliquity, or passage of perihelion [*Fenton and Richardson,* 2001b]. An alternative explanation may be that granule ripples form by

the rolling of large grains rather than by saltation, as has been proposed for terrestrial granule ripples, thus lowering the wind stress required to set these particles into motion [*Sharp,* 1963; *Williams et al.,* 2002]. In order to understand how these features formed it is important to take a close look at their morphology, stratigraphic relation to other features, and state of degradation.

The locations and orientations of bright bedforms within Proctor Crater have been identified and mapped (see Fig. 3.7a). White boxes outline the locations of Narrow Angle images. Like dust devil tracks, the bright bedforms are generally only visible in Narrow Angle images, and so inferring the distribution of bright bedforms is an interpretation dependent on the spatial coverage of the MOC NA frames. The bright duneforms cover most of the floor of Proctor Crater, including the western and central pits. As described by *Malin and Edgett* [2001], they are more common in low-lying areas such as small craters and local troughs. This is true on a larger scale as well, because these features are less common on the nearby intercrater plains than they are on the floor of Proctor Crater, which can itself be regarded as a low-lying area with respect to the surrounding highlands (see Fig 3.1b). The bright bedforms appear to be absent along the northernmost and southernmost rim of the crater floor, although coverage is too poor to determine if this is a trend that spans the entire outer edge of the crater floor.

To determine the average orientation of the bright bedforms, the along-crest direction of 961 bedforms was measured. The resulting rose diagram is shown in Figure 3.7b. Like the dust devils, these linear features appear symmetrical at this scale, with no obvious upwind or downwind slopes, and thus there is a directional ambiguity of 180°. All directions are therefore constrained to greater than 270° or less than 90°. There are two modal directions that appear in the wind rose: a primary one at 330–350° and a secondary one at 5°. If these bright duneforms are
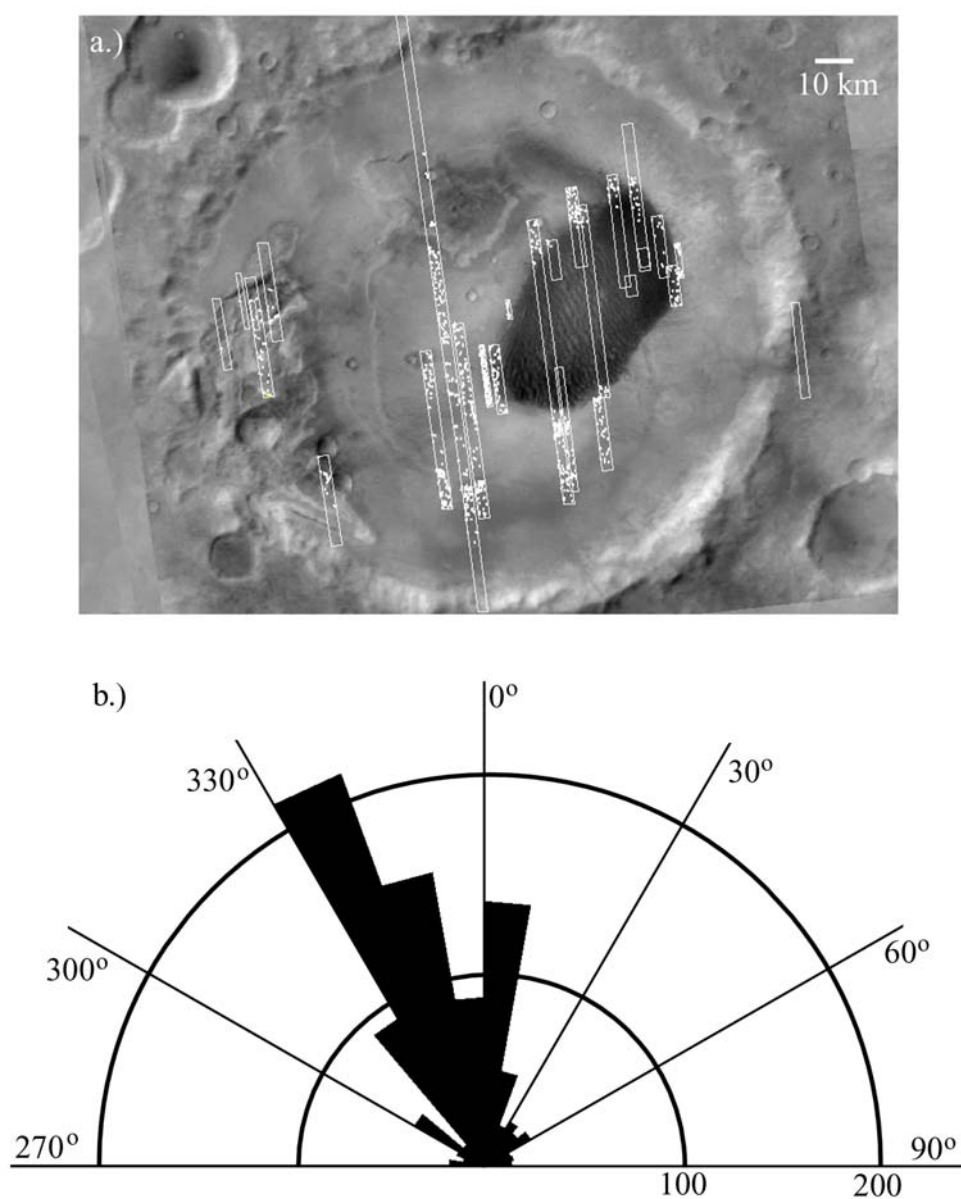
Fig. 3.7. a.) MOC Wide Angle mosaic of Proctor Crater. Boxes outline the location of Narrow Angle images. White dots locate the bright duneforms on the floor of Proctor Crater, which are generally only visible at Narrow Angle resolutions. b.) Rose diagram of bright duneform orientations. If these features are transverse the winds that form them are orthogonal to these directions. An orientation of 0° indicates a north-south alignment, while orientations of 90° or 270° indicate an east-west alignment. Because of an upwind versus downwind measurement ambiguity, all orientations are restricted to an orientation of 90°–270°. Note two concentrations of orientations at 330–350° and 0–30°.

oriented transverse to the winds that most recently shaped them, as would be the case if they are granule ripples, then they reflect winds oriented ENE–WSW and ESE–WNW, respectively. The first of these matches the dust devil track orientation, and both directions correspond to measured dune slipface orientations (discussed in Section 4.2). Although the dust devil tracks are known to be contemporary, the bright duneforms may be ancient in comparison (see discussion below). Thus the fact that the wind orientations that formed them are similar to current wind directions suggests that circulation patterns have changed little since they were created. *Fenton and Richardson* [2001b] showed that over the past several million years, surface wind stresses and directions on Mars have remained very stable. If these features are indeed granule ripples that formed under wind stresses strong enough to saltate granules, then it must have happened long ago enough under conditions that cannot be predicted by current atmospheric models, but recently enough that wind patterns have not changed since their formation. Alternative explanations must be considered, such as the rolling traction motion described by *Williams et al.* [2002] that allows the bright duneforms to be contemporary, or the possibility that these bedforms are not granule ripples but rather that they are small, cemented dunes.

The bright bedforms on the floor of Proctor Crater display a wide variety of morphologies. Several examples are shown in Figure 3.8. Figure 3.8a shows an area southwest of the main dunefield in which the bright duneforms appear to be either eroding away or being buried. Arrows point to an example of a crest that appears intermittently. The appearance of this bedform crest could indicate that it has been either degraded by erosion or buried in low places, an ambiguity that is resolved by considering the density of boulders in the area. Boulders should preferentially disappear under any mantle that might also bury the bright duneforms, but this is not the case in Fig. 3.8a. Rather, the boulders become more prevalent in areas where the dunes appear less crisp, indicating that the
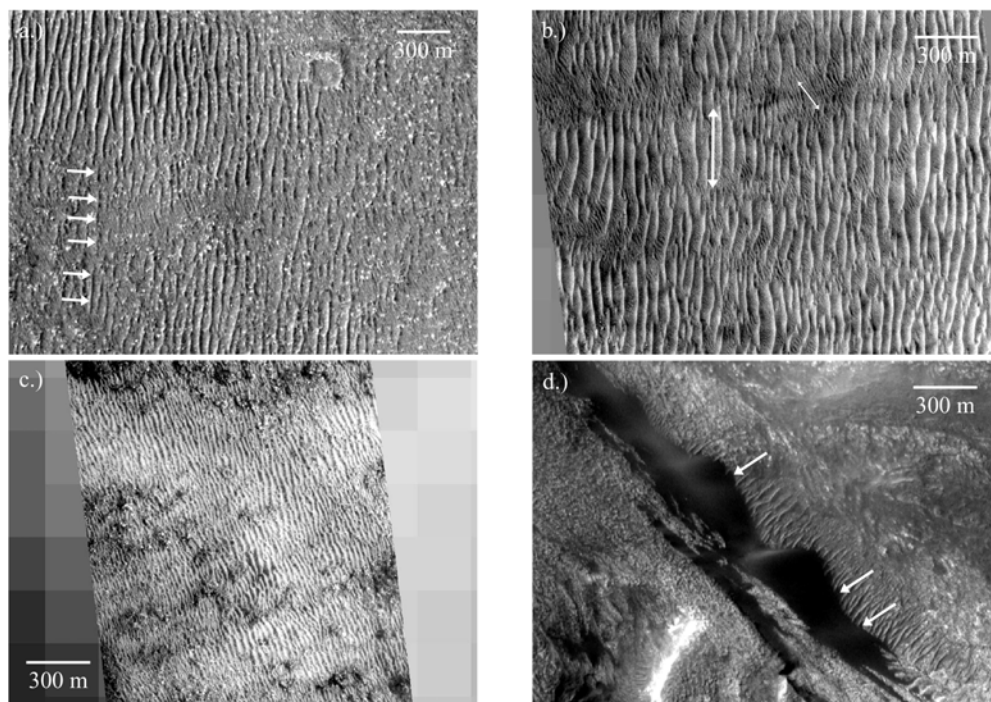
Fig. 3.8. Bright duneforms on the Proctor Crater floor. a.) Degraded crests of bright duneforms, with arrows delineating one example (MOC NA M0301614). b.) Two sets of bright duneforms, differing in wavelength and orientation (MOC NA M0802629). c.) Rounded crests of bright duneforms east of the dark dunefield, possibly indicating gradual abrasion or deflation (MOC NA M1002249). d.) Dark falling dunes overriding smaller bright duneforms (MOC NA M0300338).

process influencing the bright duneforms is erosion, not burial. It is unclear what process causes the erosion of the bright duneforms, but the fact that not all regions of the Proctor Crater floor show this degradation demonstrates that this process is local rather than regional.

Figure 3.8b shows an area south of the main dunefield in which two sets of bright duneforms can be seen (indicated by large and small arrows). Figure 3.8a also shows two sets of duneforms, although they are less obvious. Note that both sets of bedforms in Fig. 3.8b have sharper crests than those in Fig. 3.8a. Each set of bedforms has a distinct wavelength and orientation. These two sets of duneforms were produced at different times under different wind conditions. The smaller set
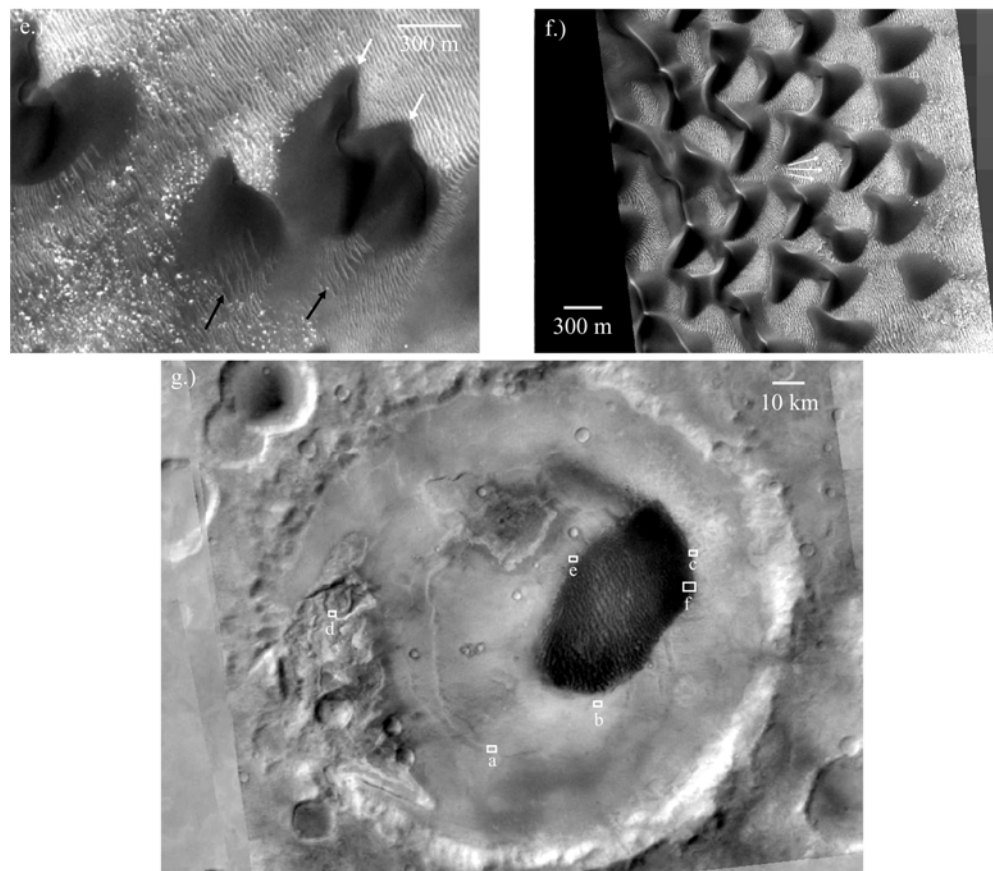
Fig. 3.8 (cont.) e.) Dark barchans overriding bright duneforms. As the barchans pass by they erode away the bright duneforms, but small ripple-like features reform in the wake of the barchans (MOC NA M1001334). f.) In the interior of the dark dunefield, bright duneforms reflect local winds influenced by the large dark dunes. This is not generally the case at the edge of the dunefield (MOC NA M1900307). g.) Context for frames a through f.

of duneforms must postdate the larger, because they crosscut these larger, more degraded bedforms. The smaller bedforms were likely formed from material eroding off the larger bedforms. In addition, while the larger bedforms were created by winds coming from either the east or west, the smaller bedforms were produced from winds from either the southwest or the northeast. This may represent a change in dominant wind directions with time. Alternatively, if the bright duneforms are indeed granule ripples then the difference in characteristic

bedform size indicates either a change in grain size or a change in wind strengths. These smaller, newer bedforms may be influenced by weaker and more persistent winds from one direction, while the larger bedforms may have been created by much stronger wind gusts that were less frequent, but that were strong enough to move the larger grains that form the larger bedforms.

Figure 3.8c shows bright duneforms just off the eastern edge of the dark dunefield. These features appear to be much more rounded (*i.e.,* eroded) than the sharp-crested features of Fig. 3.8b. This rounding is an erosional process distinct from that shown in Fig. 3.8a. It may be caused by wind deflation or abrasion, either of which could preferentially erode crests, leaving behind rounded remnants. The rounded crests also suggest some amount of cohesion in these bright bedforms in that some part of their structure has remained resistant to the process that has eroded them. *Malin and Edgett* [2001] found stabilized dark dunes in the Herschel Basin that also display wind erosion in what may be a process similar to that acting on the bright dunes east of the dark dunefield in Proctor Crater.

Previous work by *Malin and Edgett* [2001] has demonstrated that the large dark sand dunes stratigraphically overlie the small bright bedforms where they are found together. In Proctor Crater there is a similar relationship wherever dark dunes and bright bedforms coincide. Figure 3.8d shows dark falling dunes in a depression in the western pit overriding bright duneforms. Arrows point to areas where the dark dunes, migrating northwestward, have piled dark sand against the upwind side of bright duneforms. This demonstrates not only that the dark dunes lie stratigraphically above the bright duneforms, but also that they have been active more recently than the bright duneforms. Figure 3.8e shows a similar relationship between bright duneforms on the northwestern edge of the main dunefield. Here, barchans traveling to the northeast ride over the smaller, bright

features. White arrows point to places where dark sand can be seen burying bright duneforms. In the wake of the dark dunes (*i.e.,* upwind of the dunes), the bright features are no longer present, indicating that the passage of the dark barchans disturbs the bright duneforms and erodes them. Similar erosion in the wake of dunes occurs on the eastern side of the dark dunefield, demonstrating that at some point dark sand existed to both the east and southwest of the current dunefield perimeter. In Figure 3.8e, a few small darker ripple-like duneforms have reformed on the upwind side of some of the barchans (see dark arrows), suggesting that the process that forms the small bedforms is still active when the proper materials are present. The fact that dark dunes in one part of the crater floor erode bright duneforms as they migrate over them, but in another area have little effect, indicates that there is a spatial variation in either the amount of cohesion of the bright duneforms or the strengths of the winds that saltate dark sand and abrade the bright duneforms.

Within the main dark dunefield, the relationship between dark dunes and bright bedforms is more complex. Figure 3.8f shows both types of features near the eastern edge of the dunefield. On the right, dark dunes pass over bright duneforms without influencing their orientations. Farther into the dunefield, on the left, the large dark dunes clearly affect the orientations of the small bright duneforms. *Malin and Edgett* [2001] describe the refraction of bright bedforms around topographic obstacles. The same pattern appears to be in effect here, even illustrating Huyguen's Principle by creating hemispherical waves in the wake of two closely spaced dark dunes (see arrows). It seems that at the edge of the dunefield, bright bedforms are unaffected, older and possibly more stabilized than the dark sand. However, farther into the dunefield the bright bedforms are clearly affected by windflow around the dark dunes, indicating that the dunes and bright bedforms are coeval. It is likely that inside the dunefield, wind gusts accelerate when channeled between dark dunes, causing winds that are strong

enough to reactivate the bright bedforms. This suggests that the bright duneforms, while stable relative to the dark dunes, are not so cemented that they cannot be reactivated by strong winds.

The bright duneforms are an ambiguity in several ways. It is not certain whether they are partially cemented dunes or granule ripples, or whether they were formed by saltating or creeping grains. Although they lie stratigraphically beneath the dark sand dunes, indicating that they are older, their morphology is clearly affected by the presence of the dark dunes, suggesting that in some places they have been remobilized since the accumulation of the dark dunefield. Varying states of degradation indicate that either the bright duneforms were not cemented to the same degree in all places, or that erosional processes have not acted uniformly across the crater floor.

Although many aspects of the bright duneforms are unresolved, it is possible to speculate on the origin of these features. The widespread presence of these duneforms throughout the crater floor, their apparent difficulty of mobilization, as well as the lack of transport pathways of bright material into the crater, indicate that these features were probably produced from local material. The numerous boulders and degraded craters on the floor of Proctor Crater indicate that a large amount of material has been stripped off the surface, some of which accumulated into these bright bedforms. In contrast, the dark dunefield is localized in the center of the crater floor, with indications of a transport pathway from the southwest. Because some of the bright duneforms are eroded by the passage of the dark dunes, the bright duneforms must have accumulated and become relatively immobile before the dark sand first entered Proctor Crater.

4. The Dark Dunes of Proctor Crater

4.1 MOC Narrow Angle images

Close examination of MOC Narrow Angle images of the dark dunefield in Proctor Crater has led to a number of surprising discoveries regarding the aeolian environment on the surface of Mars. Figure 3.9a shows the dunefield with all available MOC Narrow Angle images superimposed on a MOC Wide Angle mosaic. At the scale of the Wide Angle mosaic, the dunes display their characteristic northwest-to-southeast trend, which has led to the interpretation that these dunes are transverse to either a southwesterly wind [*Cutts and Smith,* 1973] or a northeasterly wind [*Ward et al.,* 1985].

Closer inspection of the dunes leads to a new interpretation of dune morphology. Figure 3.9b shows widely spaced dunes at the eastern edge of the dunefield. The edges of dunefields are useful locations to study dune morphology, because here the sand deposits tend to be thinner than in the center of the dunefield [*Porter,* 1986], often leading to barchanoid dunes [*Wasson and Hyde,* 1983] with smaller and simpler slipfaces that are easier to interpret. The smaller dunes are about 300 m across and, as determined from MOLA elevations, they are ~50 m high. Based on their overall crescentic shape, these dunes appear to be barchans created by ENE winds (*e.g.,* wide arrows). In fact these dunes also have slipfaces oriented to the NNE, indicating another dune-influencing wind from the SSW (*e.g.,* thin arrow). Thus, even at the edge of the dunefield where a thin sand cover limits dune morphology, the situation is not as simple as originally thought. It seems that both previous estimates of directionally opposed dune-forming wind orientations were correct [*Cutts and Smith,* 1973; *Ward et al.,* 1985].

A sample of the interior of the dunefield is shown in Figure 3.9c. The large dunes have a spacing of up to 2 km and heights determined by MOLA elevations of up to 300 m. These dunes are not transverse, but rather they have the
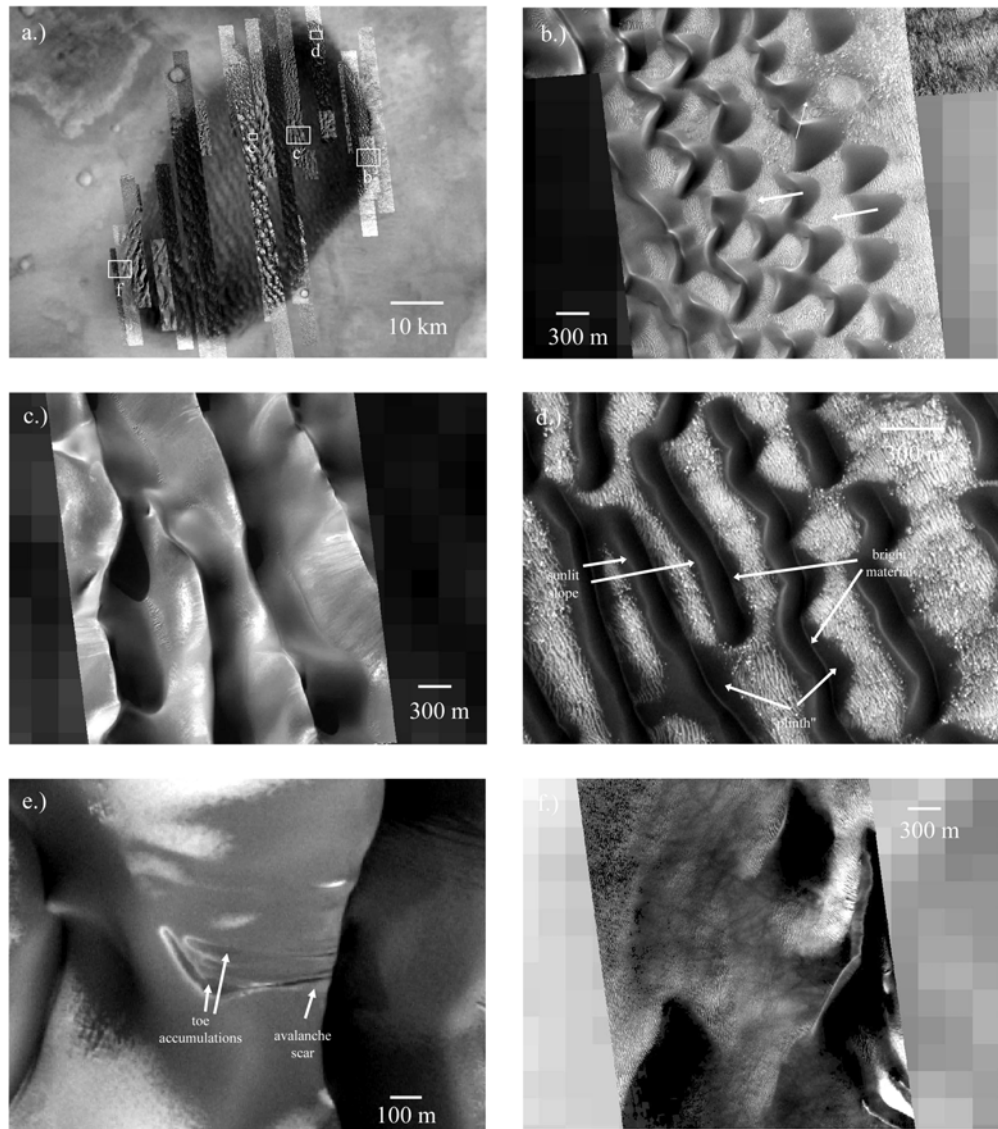
Fig. 3.9. The dark dunes of Proctor Crater. a.) Context for frames b through f. b.) Barchans at the eastern edge of the dunefield containing two differently oriented slipfaces (see arrows) (MOC NA M1900307). c.) Large dark sand ridges (in this case covered in frost) with an appearance similar to reversing transverse dunes, because neither side is obviously a slipface. Note the lack of superimposed secondary dunes (MOC NA M2301221). d.) Dunes near the eastern edge of the dunefield with accumulations of bright sand on their eastern slopes (MOC NA M0702777). e.) Unusual slope adjustment resembling a typical landslide, indicating some amount of dune induration (MOC NA E0301039). f.) Transverse dunes dominate the northwest edge of the dunefield. This example is partially defrosted (MOC NA M1501278).

appearance of reversing transverse dunes and star dunes, as inferred by *Lancaster and Greeley* [1987]. Reversing dunes are produced by two winds oriented roughly 180° apart, leading to a slipface that reverses direction depending on whichever wind is dominant at the time of observation. The constant slipface reversal generally leads to steep inclines on both the stoss and lee slopes (*e.g.,* the reversing crests of the Kelso Dunes, California [*Sharp,* 1966]). In the case of the Proctor Crater dunes, it is difficult to determine which slipface is active in these images. Star dunes are produced by more than two dune-influencing winds of differing orientations, leading to at least two overlapping transverse slipfaces that create a star-like form in plan view. The dunes in Figure 3.9c appear most like reversing transverse dunes (*e.g.,* the large ridges are symmetrical, indicating that slipfaces form on either side of the crest), implying that at least two wind directions affect the morphology of the dunes.

Perhaps more important even than the new morphological dune classification is the fact that there are no secondary dune structures on the slopes of these features. On Earth, large dunes (> ~500 m) nearly always have smaller, superimposed dunes, either of the same type (*i.e.,* small barchans on a large barchan), or of a different type (*i.e.,* small star dunes on a large linear dune) [*Lancaster,* 1988]. By the classification of *Breed and Grow* [1979], the former system is termed a "compound" dune, and the latter is termed a "complex" dune. Dunes with no superimposed dune structures, such as those in Proctor Crater, are called "simple." The transition from simple dunes to compound and complex dunes is not well understood. The difference has been attributed to changes in climatic wind strengths [*Kocurek et al.,* 1991], a shift in bedform type akin to that between ripples and dunes [*Wilson,* 1972], and variations in transport rates on the larger dunes, as though dune slopes grow to approximate a small desert floor that accumulates their own small dunes in turn [*Lancaster,* 1985]. Regardless of what causes the shift between simple and compound/complex dunes, this transition is

not seen on Mars, even at the 1–2 km scale of the Proctor Crater dunes. It may be that the scale at which this transition occurs on Mars is much larger than that on the Earth. It is tempting to dismiss this lack of superimposed dunes to a simple difference in atmospheric conditions on Mars and Earth, but previous studies comparing dune length, width, and spacing have shown that Martian dune dimensions in general correlate well with those of Earth dunes [*Breed et al.,* 1979]. Many of the terrestrial dunefields used in the study by *Breed et al.* [1979] consisted of compound and complex dunes that correspond well to the simple Martian dunes, suggesting that secondary bedforms likely have little effect on the overall structure of large primary dunes. There is no obvious reason why large Martian dunes should fail to produce secondary dunes. *Breed et al.* [1979] note the lack of secondary dunes from images at Viking resolutions, proposing that any secondary features that might have once existed have since eroded away. However, recent slipface adjustments (as discussed in Section 3.4) demonstrate that the Proctor Crater dunes are still active, and so secondary features, by the standards of terrestrial dunes, should form under the current wind regime. This observation may bring into question all currently understood theories of bedform climbing. Alternatively, it may simply be that conditions that would produce secondary dunes on terrestrial structures do not exist on Mars at the observed scales.

The interpretation of images of any surface involves discriminating the cause of brightness variations. These are most often created by changes in shading (*e.g.,* topography) and by inherent albedo patterns (*e.g.,* patches of ice on a dark surface). In some cases the interpretation requires careful consideration. Note that in the image analysis in this work, the terms "bright" and "dark" refer to relative brightness differences, and that no attempt is made to measure absolute brightnesses. Figure 3.9d shows a number of dark dunes at the northeastern edge of the dunefield. This image was taken during the summertime, when no frost cover was present. Like all of the narrow angle images in this area, the sun

azimuth angle is NNW–NW. From this perspective, the sun should reflect strongly off all slopes facing roughly north and west. The west-southwest facing slopes of the dark dunes are thus bright because of reflected sunlight. The east-northeast facing dune slopes, however, have both a dark and a bright line. The dark stripe is likely a shady slope, most likely a slipface, oriented away from the sun. The bright stripes on the ENE slopes are less easy to interpret. They seem to lie on broad plinths of dark sand that underlie the top portion of the dunes. In places near the slipfaces, the plinths become thin, exposing the underlying surface beneath the dark dunes. Even along these places where the plinth is gone and the top part of the dune rests on the bright duneforms that comprise this layer of the crater floor, the bright stripe is still present. These bright stripes are interpreted as accumulations of bright material. They only appear on dunes near the eastern edge of the dunefield. It is possible that this bright material is accumulated dust. However, bright dust is easily kicked into suspension from the impact of saltating sand, which is easily cleaned off the majority of the dark dunes, and would also strip away this bright layer if it were composed of dust. It is more likely that the bright stripe is an accumulation of (relatively) bright sand that has been blown onto the ENE facing slipfaces. The source of the bright sand on the Proctor Crater dunes may be the tops of the bright duneforms rounded from erosion shown in Figure 3.3g. In a similar study of the White Rock structure, *Ruff et al.* [2001] also propose that lighter material concentrated at the tops of dark ripples comes from the nearby eroding bright massifs that comprise White Rock. If this is the case, this bright stripe of material may be evidence that the bright duneforms are composed of sand rather than granules, because the bright material has saltated up the dune to accumulate at the base of a slipface. There is a more detailed discussion of these bright stripes and how they related to seasonally shifting wind directions in Paper 2.

There are variations in the morphology of slipface adjustments on dunes in the center of the dunefield. In Figure 3.6f though 3.6h, the persisting dark lobes of material have no apparent topography. Most likely they are typical of slipface adjustments in loose sand, in that slender lobes of sand propagate downhill, only slightly disturbing the surface and leaving only a thin layer of loosened sand behind. Figure 3.9e shows a very different type of slipface adjustment. This feature has an appearance similar to a terrestrial landslide. Sublimating frost clings to the edges of the lobes on the lower part of the slope. Near the crest of the dune there is a scar indicating where material has been removed. At the bottom of the slope (*i.e.,* at the toe of the landslide) there is an accumulation of sand that formed from material excavated from the scar uphill. Avalanche scars such as the example shown in Fig. 3.9e are not stable in unconsolidated sand because they cannot retain their sharp edges, and thus they are not generally found on active sand dunes. The presence of an avalanche scar in the Proctor Crater dunes indicates some amount of sand cohesion. Because the more typical slipface adjustments are more common in the dunefield, such cohesion is not likely to be typical in the Proctor Crater dunes. It may be that trapped volatiles freeze the dune, allowing landslide-like structures to form and maintain their shape. However, this feature is also visible in an image from the previous winter, indicating that its structure survived a volatile-free summer. It is possible that parts of the dunefield are effectively stabilized from further activity by some cementation process.

The northwestern edge of the dunefield (see Fig. 3.9a) contains a series of dune structures oriented obliquely to the NW–SE trend of the bulk of the dunefield. Closer inspection (Fig. 3.9f) shows that *Cutts and Smith* [1973] correctly interpreted these features as large transverse dunes with slipfaces indicating winds from the southeast. These slipfaces correspond to yet another wind direction influencing dune morphology. Residual frost coats a few areas on the upwind

sides of these dunes, and dust devil tracks cover irregularly shaped sand sheets that fill in and cover the underlying small bright duneforms.

The MOC Narrow Angle images have provided a new view of the Proctor Crater dunes. In some cases, they have confirmed the work of previous studies, as with the case of dune orientations. In other cases, the higher resolution provides new information on dune morphology and activity, requiring modifications to the previous understanding of dune formation.

4.2 Slipface orientations

One of the main goals of this work is to understand the relationship between the aeolian features in Proctor Crater and the atmosphere in its current climatic state. Dune slipfaces are created by slope adjustments to oversteepening (*i.e.,* landslides) created in part by an influx of saltating sand to the brink of the dune slipface from upwind. Grain fall from suspended sand may also contribute to the slipface surface. Transverse dunes have slipfaces that dip downwind, and longitudinal dunes often have slipfaces that are oriented at an angle to their crests but that dip downwind of the last wind to influence them. Even oblique dunes, which are produced in a bi-directional wind regime that forces the dunes to move in a direction different from predominating winds, have slipfaces oriented downwind from the winds that shape them [*Hunter et al.,* 1983]. Barchan dunes are the main exception to this rule in that they have crescentic slipfaces, the central axis of which is oriented downwind, although this axis is simple to identify. Thus, slipfaces are a reliable marker of wind direction in that they almost always face downwind. In this work, slipfaces were identified by their crescent-shaped slipface brinks if the dunes are barchans (*i.e.,* Fig. 3.9b), and by long sharp slipface brinks on steep slipfaces that reach from the brink to the crater floor if they are transverse dunes (*i.e.,* Fig. 3.5h). The large reversing crests are not considered slipface brinks because the slopes on either side are not obviously recent slipfaces

and therefore may not directly reflect wind directions (*i.e.,* Fig. 3.9c). Only the clearest cases are considered slipfaces. To provide the best "ground truth" possible for comparison with the mesoscale model experiments (discussed in Paper 2), the orientations of as many slipfaces as possible were measured. Measurements were made by hand, and directions were marked only for obvious slipfaces and where the orientation was clear. Care was taken to avoid marking dune crests rather than slipface brinks, which are not necessarily co-located.

Figure 3.10a shows the dunefield with all slipface markings (lines are parallel to the wind directions that produce each slipface). We found that three main wind directions influence dune morphology. Figures 3.10b and 3.10c show specific examples of slipfaces exhibiting each of the three orientations. Figure 3.11 shows wind roses of each of the three main slipface directions and the mean wind orientations that produce them. Almost all of the measured slipface brinks were crisp, suggesting that they have not undergone erosion since they were last modified. Terrestrial dunes that experience more than one sand-moving wind tend to develop rounded brinks and subdued slipfaces under modification from oblique winds [*Sharp*, 1966]. This rounding process is not so obvious in the Proctor Crater dunefield, suggesting that these dunes may be partially cemented. In Antarctic dunes, snowfall buried by subsequent slipface activity has been observed to allow oversteepened cornices of sand cemented by snow to develop on lee slopes [*Calkin and Rutford,* 1974]. Similar lenses of snow have remained in terrestrial dunes throughout the summer season, such as those of Wyoming [*Steidtmann,* 1973] and the Antarctic dunes [*Calkin and Rutford,* 1974], and for a good portion of spring, Alaskan dunes [*Koster and Dijkmans,* 1988]. Like the sides of the landslide scar shown in Fig. 3.9e, these sharp brinks in the Proctor Crater dunes may indicate the presence of seasonal CO_2 frost trapped within the dunes. Although it is unlikely that the CO_2 frost would remain throughout the summer, it may persist long enough to allow old slipface brinks to retain their crispness.

The first slipface orientation, shown in yellow (see Fig. 3.10), is pervasive throughout the dunefield, producing barchanoid dunes near the edges and contributing to the large reversing dunes that dominate the central portion of the dunefield. Because they are so pervasive, these slipfaces are referred to as the primary slipfaces. The average orientation of 354 measured primary slipfaces (see Fig. 3.11a) indicates formative winds from $239° \pm 18°$ (mean $\pm$ standard deviation), or WSW. (In this system, $0°$ indicates winds from the north). The spread in slipface orientations is caused by a gradual shift from WSW in the western and central portions of the dunefield to SW on the eastern edge of the dunefield (compare arrows in Figs. 3.10b and 3.10c). These slipfaces are consistent with the southwesterly wind regime proposed by *Cutts and Smith* [1973]. They also match the trend of most dust devil tracks (see Figs. 3.3a and 3.4), most bright duneforms (see Fig. 3.7), and a number of small dark sand streaks extending off the southeast edge of the dunefield (see Fig 3.1a).

A secondary wind, shown in turquoise in Figures 3.10a and 3.10b, has an average wind orientation from 150 measurements of $110° \pm 18°$ (see Fig. 3.11b), or from the ESE. This secondary wind is found in all but the easternmost portions of the dunefield. This wind produces the transverse dunes on the northwest edge of the dunefield, shown in Figure 3.9f. It is also partly responsible for creating the large reversing dunes found in the center of the dunefield, in conjunction with the primary WSW winds. This ESE wind also produces the large dark sand streak that extends to the west-northwest from the northernmost tip of the dunefield (see Fig. 3.1a). Finally, it matches the orientations of the secondary set of bright duneforms that cover the crater floor.

The third wind orientation found is shown in magenta in Figures 3.10a and 3.10c. Unlike the primary and secondary winds, it appears to affect only the eastern portion of the dunefield, although here this wind is dominant. Based on 154
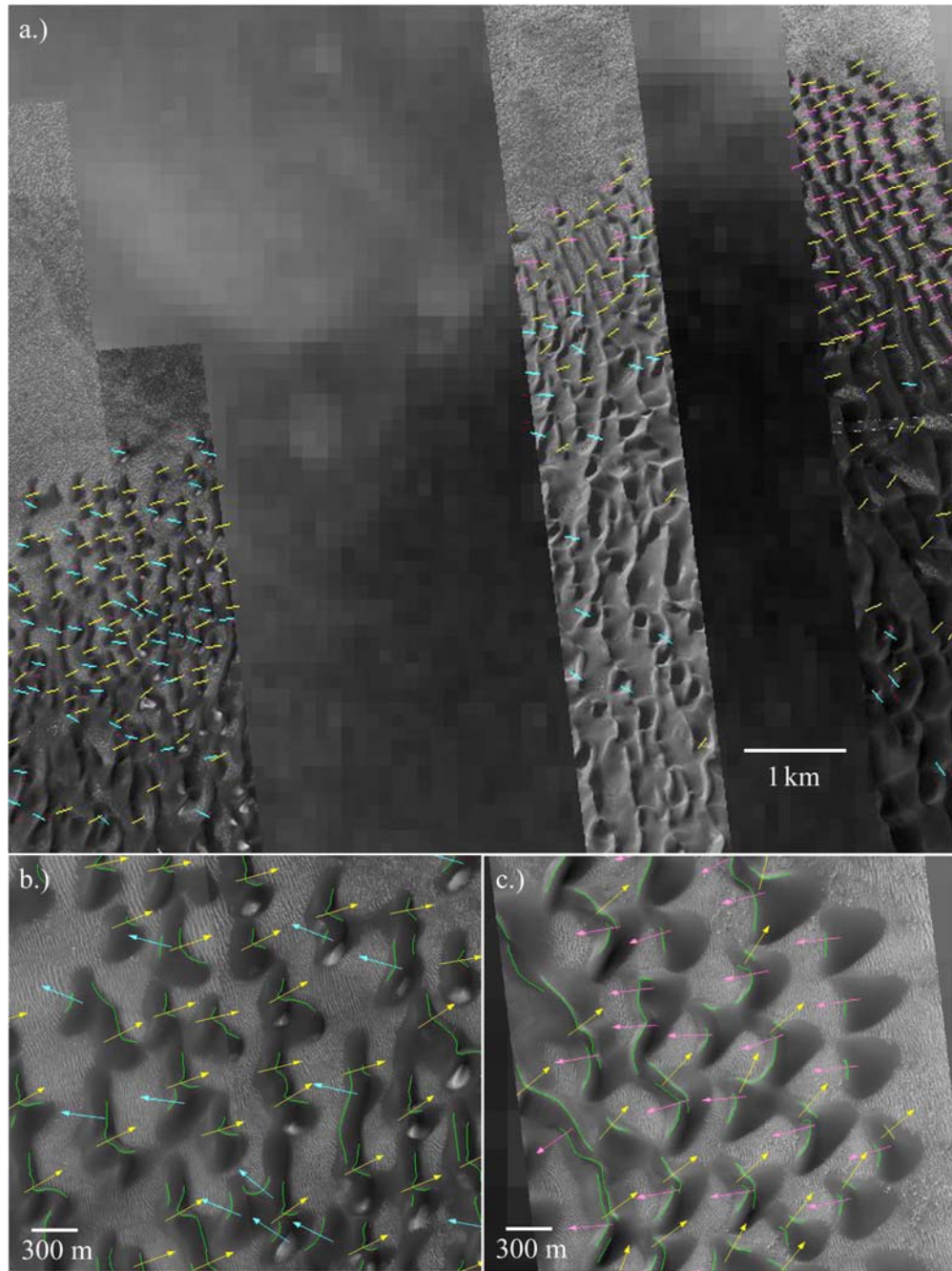
Fig. 3.10. a.) The northern part of the dark dunefield with markers on measured slipfaces. Colors correspond to wind direction: Primary winds (yellow) are from the WSW, secondary winds (blue) are from the ESE, and tertiary winds (magenta) are from the ENE. Frames b.) and c.) show examples of the three different slipface orientations.
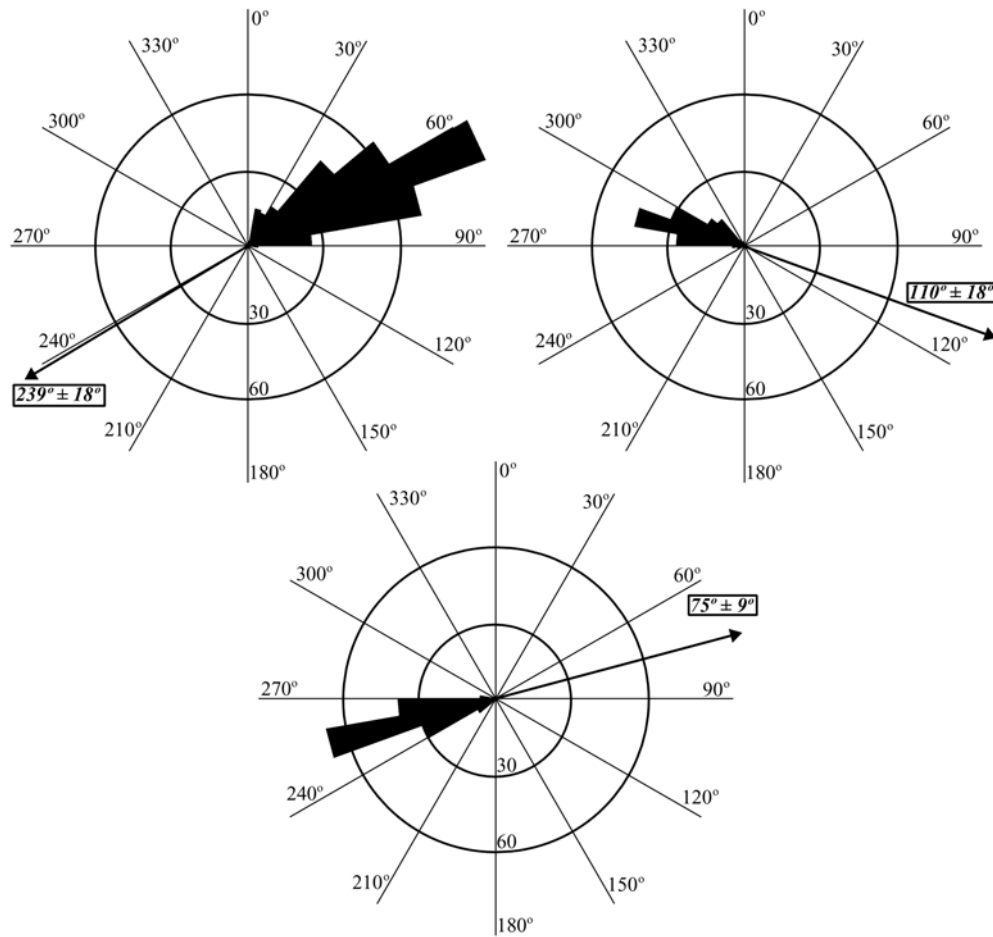
Fig. 3.11. Rose diagrams of the three dune slipface orientations shown in Figure 3.10. Boxed numbers and thick arrows indicate the mean and standard deviation wind direction of the primary, secondary, and tertiary winds. In this system, 0° represents winds from the north.

measurements, this tertiary wind has an orientation of 75° ± 9°, or ENE (see Fig. 3.11c), consistent with the dune orientations mapped by *Ward et al.* [1985]. Both the secondary and the tertiary winds are oriented obliquely to almost 180° with respect to the primary winds, leading to the observed mixture of reversing transverse dunes and star dunes at the center of the dunefield. The tertiary wind is oriented roughly 180° from the primary wind, which may mean that dust devil tracks and bright duneforms that appear to align with the primary wind in fact

correspond to this wind. However, this third wind only appears on the eastern portion of the dunefield, and thus it is likely only present over the northern and eastern portion of the crater floor. North and east of the dunefield, dust devil tracks are conspicuously absent and bright duneforms are either rounded from erosion or absent. Thus, there are no surface features other than dune slipfaces and a small area of rounded bright duneforms that reveal this wind in the MOC NA images.

The dunes as seen today correspond well to the orientations of not only bright duneforms, which are older and less mobile than the dark dunes, but also dust devils, which are reformed and erased on an annual basis and thus are much younger than the dunes. It appears that the wind regime that built the dunefield is still active today. Given the three opposing winds, the dunes are clearly located in an area where winds converge. This is expected of reversing transverse and star dunes. *Christensen* [1983] proposed that the intracrater dunes in the southern highlands are trapped because the winds are strong enough to saltate sand downhill into the crater, but not strong enough to saltate sand uphill out of the crater. Here, the measurement of wind directions shows that the dunefield is located where winds are balanced, leading to net sand deposition. If the sand were truly trapped by topography alone then the dunes would be located in the lowest places on the crater floor, the western and central pits (see Fig. 3.1b), but this is not the case. Outside the crater walls the dominant wind must have been from the west-southwest, in order to transport material into the crater and leave behind falling dunes as the remnants of an ancient transport path. Inside the crater, however, the winds must be influenced by the crater walls, producing a convergent airflow that traps the sand quite effectively. This suggests that all of the intracrater dunefields in the southern highlands of Mars are features trapped, not by topography alone, but by convergent local winds that are influenced by topography.

4.3 Dunefield Volume, Structure, and EST (Equivalent Sand Thickness)

The volume of the Proctor Crater dunefield is a useful parameter for comparison to other dunefields on Earth and Mars. *Wasson and Hyde* [1983] define the equivalent sand thickness (EST) of a dunefield as "the thickness of a continuous sheet of sand which results from the hypothetical spreading out of dunes over a specified area." They used this parameter as an estimate of net sand supply to a dunefield to show that dunes of differing morphology form in areas where sand is accumulating or migrating. If the volume of the dunefield is known, the EST can be calculated by dividing the volume by the area covered by the dunefield. Below is a discussion of volume and EST estimates using two different techniques, both of which use MOLA elevations.

The first method uses tools built into ArcView to directly estimate the volume of a three-dimensional figure. A "triangulated irregular network" (TIN), or a three-dimensional construct of the dunefield, was created using MOLA elevations. Using this topographic model, the amount of dune sand was calculated using a volume defined to be above the local crater floor (at a height of 541 m) and within a perimeter defined by the edge of the dark dunes as observed in MOC Wide Angle and Narrow Angle images. The resulting volume is 140 km^3. The estimated planimetric surface area defined by the perimeter at the edge of the dunefield is 1728 km^2. One difficulty with using the TIN to estimate volume is that although most of the large dunes are resolved along each MOLA track, the distance between tracks is usually too large to fully construct a proper model of the dunefield (*i.e.,* the dunes are aliased). The volume calculation only accounts for the volume beneath the modeled TIN, and it is subject to inaccuracies caused by the aliasing.

The second method of determining the dunefield volume uses each MOLA track that crosses the dunefield, but only considers along-track estimates of dune

height. Many of the dunes are well resolved along each MOLA track, allowing for an accurate determination of sand area beneath each track, or an integration of the area below the curve for each track. Once this value is determined, the average height of sand for each track can be calculated by dividing the integrated area by the length of that MOLA track across the dunefield. This leads to an estimate of the equivalent sand thickness (EST) for each track. Forty-eight MOLA tracks are distributed uniformly across the dunefield, and thus the mean EST from all of the tracks provides a reasonable estimate of the average EST of the entire dunefield. This mean dunefield EST value multiplied by an estimate of the surface area beneath the dunes leads to a sand volume estimate. Using the planimetric surface area of 1728 km^2 calculated in ArcView, the estimated volume of the dunefield is 180 km^3. This value is larger than that calculated by the built-in script in ArcView. The second method is considered to be more reliable because it relies only on the along-track MOLA distances in which most of the dunes are resolved, rather than on a three-dimensional construct in which cross-track surfaces are calculated using aliased data.

The first volume estimate method described above leads to an EST of 80 m, and the second leads to an EST of 105 m. Both estimates are very high values, larger than those for most dunefields on the Earth. It is consistent with a convergent wind regime in which the sand transport into the dunefield is greater than that out of the dunefield. *Wasson and Hyde* [1983] found that star dunes form in areas with large EST values and a high variability of wind direction. The reversing and star dunes of Proctor Crater are certainly located in an area of convergent and variable winds, as evidenced by the three different slipface orientations described above. The northern polar sand dunes have a mean EST of only 1.8 m, consistent with the barchanoid and transverse dunes that are observed in these ergs [*Lancaster and Greeley,* 1990]. It seems that while the dunefields of Mars can be

directly compared to those of Earth both morphologically and dynamically, the variations among dunefields on Mars is at least as great as that on Earth.

Figures 3.12a and 3.12b show MOLA reflectivities and elevations, respectively, for a traverse across the dark dunefield in Proctor Crater. This is a nighttime groundtrack, thus avoiding any complications caused by reflected sunlight. Each MOLA footprint is 170 m wide, and the along-track shot spacing is 300 m [*Smith et al.,* 2001]. The location of the traverse is shown in a MOC Wide Angle mosaic in Figure 3.12d and in the 400 m resolution shaded relief DEM in Figure 3.12e. Although most of the track crosses the dark dunefield, only the large dunes in the southern two-thirds of the track are fully resolved. The northern third of the groundtrack crosses dunes that are smaller than the spacing of the MOLA shots. Although the larger dunes are barely resolved, a number of observations can be made based on MOLA data alone. First, the largest dunes are superimposed on a mound of sand that reaches up to 50 m thick. The large dunes themselves range from 100 m to 250 m high, or phrased another way, 50 m to 200 m on the 50 m high sand mound. In places where net deposition of sand occurs, sand seas accumulate. If the deposition outpaces the rate of migration, then eventually bedforms will migrate over one another, causing dunefields to accumulate strata of sand beneath the current overriding dunes [*Rubin and Hunter,* 1982]. The presence of the mound supports the conclusion that the dunes of Proctor Crater are and have been located in an area of net deposition since the dunefield began accumulating. Considering that the wind regime is convergent, and appears to have been convergent for the history of the dunefield, this result is not surprising.

One way of determining the location of the underlying sand mound within the dunefield is to use MOC NA images. Boulders are strewn over the entire area surrounding and underlying the dunefield, but only appear where the sand is thin enough to reveal their presence. The area in which MOC NA images do not
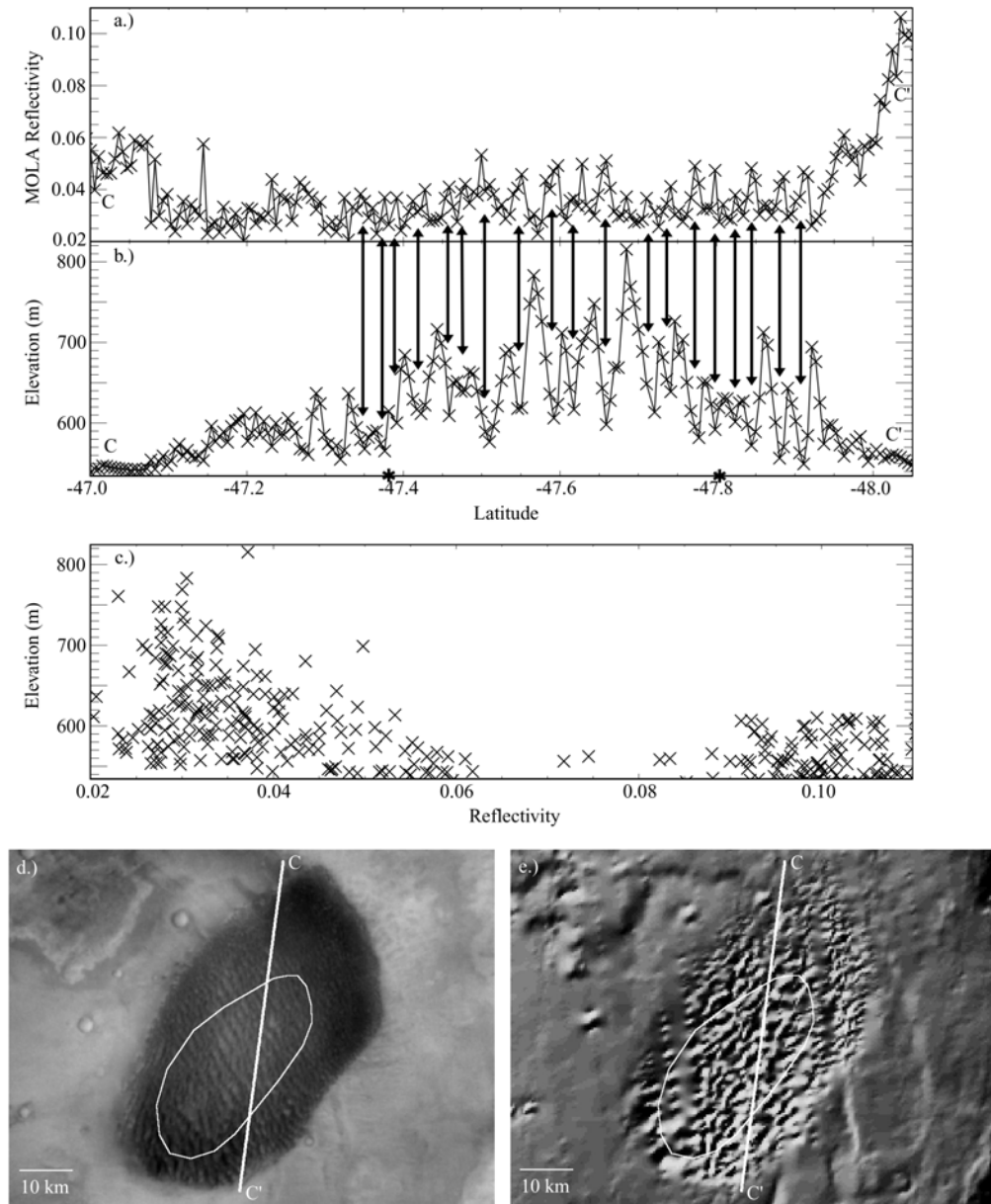
Fig. 3.12. a.) MOLA reflectivities and b.) MOLA elevations for traverse CC' (shown in d.). Black arrows between a.) and b.) connect the low-lying areas between dunes, all of which correspond to higher MOLA reflectivities. Stars along the latitude axis indicate the edges of the 50 m high sand mound beneath the dunes. c.) Scatter plot of MOLA elevations vs. reflectivity showing that only the low elevations are bright (*i.e.,* are not purely dark sand). d.) MOC Wide Angle image of the dunefield. e.) Shaded relief based on a 400 m resolution MOLA DEM. In both d.) and e.), the traverse CC' and an outline of the sand mound is shown.

show any boulders is outlined in Figures 3.12d and 3.12e. Boulders visible in MOC NA frames in Proctor Crater are 5–20 m wide, and presumably as high, so where the boulders disappear the sand cover must be at least 5 m thick. The boulders are barely resolved, and so it is difficult to tell from inspection whether they are partially buried or fully exposed. Because of the incomplete coverage of NA images over the dunefield, the border of the sand deposit is highly uncertain. Stars have been marked on Fig. 3.12b where the border of the sand deposit intersects with the MOLA track. These locations match fairly well where the sand deposit begins to thin out in the MOLA track. The bulk of the sand accumulation is in the central and western portions of the dunefield. This suggests that in the eastern and northern portions, where the dunes are smaller (and poorly resolved by MOLA as a result), either the wind regime leads to less net deposition than in the rest of the dunefield, or that the northern and eastern portions are simply younger and have not had the time to accumulate as much underlying sediment.

A second observation from Figure 3.12b is that the large dunes resolved by MOLA are fairly symmetrical. In general, transverse dunes have a long shallowly-angled stoss (upwind) and a short, steep lee (downwind) slope. The fact that this is not the case on the large ridges in the dark dunefield indicates that these dunes cannot be simple transverse ridges. A symmetrical cross section is more consistent with reversing transverse dunes, as suggested by MOC NA images, or with longitudinal dunes.

Another observation made using the MOLA track is that MOLA reflectivity correlates inversely with elevation. That is, the dune peaks are dark and the troughs between dunes are bright. This is well illustrated in a scatter plot of elevation versus reflectivity in Fig. 12c, in which high elevations always have low reflectivities but some low areas have relatively high reflectivities. This correlation of bright material in interdune areas is not surprising given the appearance of

bright duneforms in these areas. However, arrows in Figs. 3.12a and 3.12b indicate that this relationship appears to hold true for every dune and trough that is resolved by MOLA, even over the 50 m accumulation of sand in the center of the dunefield where bright duneforms are nonexistent. Given this inhomogeneity and the multidirectional wind regime, the central deposit of sand is not likely to be a stratigraphically simple unit. In most cases on terrestrial dunes, grains decrease in size from the base of a dune to its crest [*Lancaster,* 1995], and so this change in reflectivity may reflect a shift in average grain size. If this is the case then there may be two populations of sand: one that is finer grained and dark, and one that is coarser and relatively bright. This violates the classic interpretation of Martian aeolian grains in that dark particles are considered to be sand-sized while the bright grains are considered to be finer dust-sized particles. However, interdunes contain sediments that are much more poorly sorted than adjacent dunes [*Lancaster,* 1995], and so the brighter interdunes may merely reflect a higher concentration of bright dust that has not bee stripped by saltation. Like many terrestrial dunefields, the interdune areas in the Proctor Crater dunefield may serve as a depositional location for fines.

4.4 Comparison with the Kelso Dunes, California, USA

The Kelso Dunes are a well-studied set of dunes located in the Mojave Desert of California. They are situated in a valley surrounded by three mountain ranges. A multidirectional wind regime balances the flow of sand, causing the sand to accumulate into tall reversing transverse sand ridges [*Sharp,* 1966]. *Lancaster* [1993] estimated that the Equivalent Sand Thickness (EST) might reach 46 m over these large ridges, placing them in the range of star and transverse dunes as calculated by *Wasson and Hyde* [1983]. The dunefield is much smaller than that of Proctor Crater, with an estimated volume of 1 km^3 and covering an area of 100 km^2 [*Lancaster,* 1993], but morphologically the two sand seas are similar.

Figure 3.13 shows spacecraft data from the Kelso Dunes, presented in a similar format as Figure 3.12. The traverse in Fig. 3.13a was constructed from the DEM, which has been represented as a shaded relief map in Fig. 3.13c. The shaded relief map comes from a recently released 30 m resolution DEM from the Shuttle Radar Topography Mission (SRTM) [*Farr and Kobrick,* 2000]. The SRTM was conducted aboard the Space Shuttle Endeavor in February, 2000, collecting the highest quality topographic data of the Earth to date between the latitudes 60° N and 56° S. Although the data over many sandy areas cannot be correlated, leading to gaps in the data, the Kelso Dunes are largely well correlated. Two data gaps (black spots) are visible on either side of the traverse near the point D'; most of the rest of the dunefield has no such data losses.

Figure 3.13b shows a 15 m resolution VNIR (visible to near infrared) image of the Kelso Dunes from the Advanced Spaceborne Thermal Emission and Reflection Radiometer (ASTER). This image is a grayscale version of a three color composite from the three VNIR channels of ASTER. Some of the streaks running from northwest to southeast are clouds and their respective shadows, but careful inspection reveals a bright sand sheet stretching northwest from the dunefield, slowly feeding sand to the Kelso Dunes. Three prominent dune ridges are evident in the dunefield, both in this image and in the SRTM DEM (Fig. 3.13c).

The traverse across the Kelso Dunes in Fig. 3.13a is shown at a much higher spatial resolution than that across the Proctor Dunes in Fig. 3.12a. Nevertheless, information similar to that obtained for the Proctor Dunes can be measured for comparison. The Kelso Dunes have been pushed up against the north face of the Granite Mountains, the mountain range visible in the bottoms of Figs. 3.13b and 13c. To reach the dunefield, the incoming sand has climbed uphill onto an alluvial fan emanating from the Granite Mountains [*Sharp,* 1966]. This uphill
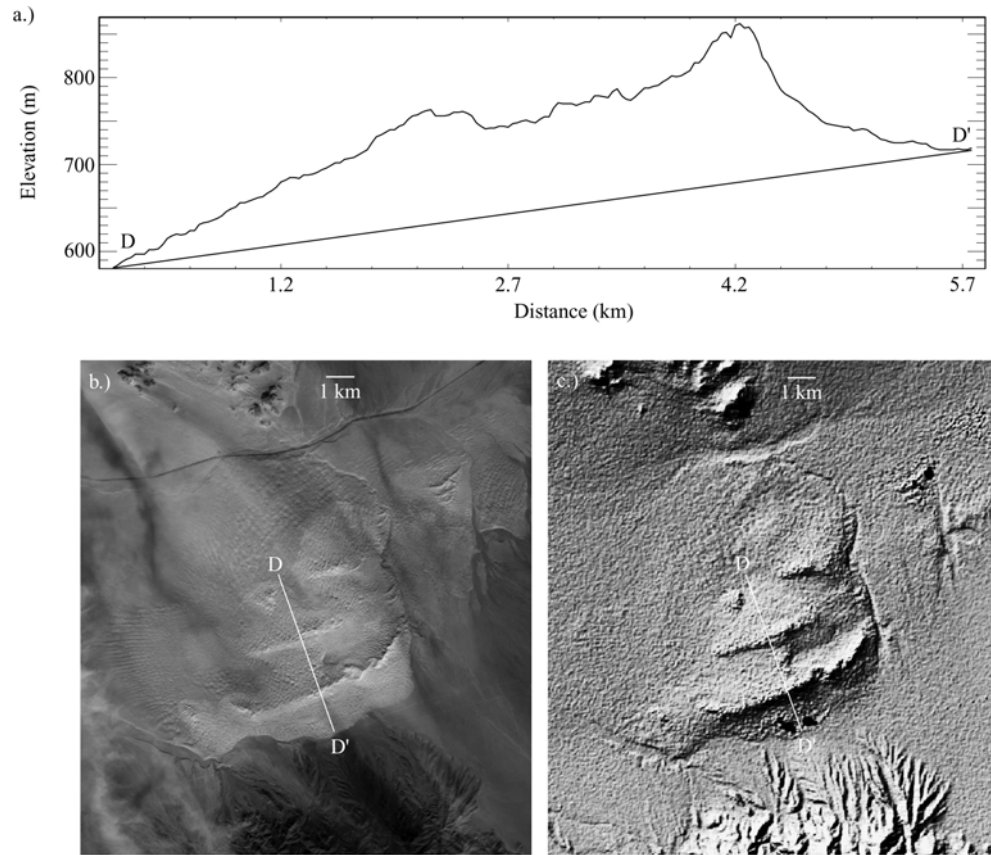
Fig. 3.13. The Kelso Dunes of the Mojave Desert. a.) SRTM elevations of traverse DD' across the Kelso Dunes. b.) ASTER image of the Kelso Dunes at a resolution of 15 m/pix. c.) Shaded relief at a resolution of 30 m/pix based on the SRTM DEM. The location of traverse DD' is shown in both b.) and c.).

slope is approximated as a straight line beneath the dunes in Fig. 3.13a, although the underlying surface is most likely slightly concave. The two peaks that the profile crosses are 130 m and 180 m above the approximated alluvial fan surface. Like the Proctor Crater Dunes, the Kelso dunes are superimposed on an accumulation of sand, in this case 100 m deep. In comparison, the Kelso dunefield is composed of smaller dunes superimposed on a deeper mound of sand relative to those in Proctor Crater. The Kelso dunes may reside in a more highly depositional environment than the Proctor Crater dunes, given that the

sand mound at Kelso is twice as deep as that in Proctor Crater. The wind regime and local topography in Proctor Crater likely allows for more lateral migration of sand, although the net result is still a deep sand heap where winds converge.

5. Composition

Dunes tend to have a composition distinct from that of their surroundings; thus, composition is a useful tool in studying sand dunes and locating sand sheets and sand sources. On the Earth, thermal infrared multispectral scanner (TIMS) and Landsat thematic mapper multispectral images have been used for a number of purposes: to identify changes in composition within dunefields [*Blount et al.,* 1990], to discover previously unrecognized or misidentified sand sources [*Ramsey et al.,* 1999], and to provide a more accurate estimate of mineral concentrations at the surface [*Bandfield et al.,* 2002].

On Mars, spectra obtained from both ground-based and spacecraft interferometers have been used to identify surface mineralogy. In particular, TES has provided high-resolution spectra in the thermal infrared at a surface resolution of 3 by 6 km, which has been used to determine the correlation of rock compositions with geological units on the surface. The most detailed work with TES data involves the deconvolution of spectra using several endmembers, including both surface and atmospheric components [*Bandfield et al.* 2000; *Smith et al.* 2000]. In their work on global surface compositions, *Bandfield et al.* [2000] identified two spectral signatures that comprise a large percentage of the martian surface. The first component, labeled Type 1, has a shape similar to that of terrestrial Deccan Traps flood basalts that are composed predominantly of plagioclase and clinopyroxene. This is the same endmember identified in initial aerobraking TES data from Cimmeria Terra by *Christensen et al.* [2000a]. The second component identified by *Bandfield et al.* [2000], labeled Type 2, matches spectra from basaltic andesites to andesites made of plagioclase, glass, and

pyroxene. In general, the low albedo surfaces of Mars are composed of spectral Types 1 or 2, or some mixture of the two. Areas with a mixed spectral signature may indicate either a composition intermediate between basalt and andesite or a physical mixture of the basaltic and andesitic components [*Bandfield et al.,* 2000].

A reassessment of the deconvolution of TES spectra indicates that the Type 2 surface component may be indicative of weathered basalt rather than andesite [*Wyatt and McSween,* 2002]. *Wyatt and McSween* [2002] reasoned that because sheet silicates such as clays have spectra similar to high-silica glass, surface Type 2 may not be andesitic, but instead may be aqueously altered basalt. They performed a deconvolution of TES spectra using a library of minerals that omitted the high-silica glass found by *Bandfield et al.* [2000] to compose part of surface Type 2. Their deconvolutions provided reasonable fits to the spectra, indicating that their hypothesis cannot be ruled out. Each conclusion regarding surface Type 2 has contrasting but important implications for the geological history of Mars. Because at this point either conclusion may be correct, surface Type 2 will be referred to as such in this work rather than as andesite or weathered basalt.

Further spectral studies using TES data have identified surface compositions other than igneous rocks. *Christensen et al.* [2000c] found the distinct signature of hematite in Sinus Meridiani. This mineral is considered to be coarsely crystalline based on the spectral shape observed by TES. It is associated with layered deposits and may indicate the former presence of near-surface water. *Clark et al.* [2002] found outcrops of olivine, indicating that at least in some regions on the surface, aqueous weathering has not occurred. *Bandfield and Smith* [2002] have used spectra from multiple emission angles to better separate atmospheric and surface components in TES data. This has produced the first mineral identifications of bright regions. They found that the bright region spectra match well with fine particulate silicate minerals. In particular, the bright regions have

spectra consistent with intermediate to high-calcium plagioclase feldspar and minerals with either bound or adsorbed water, indicating that the surfaces here have not been completely altered by chemical weathering.

Using TES data analyzed with the techniques described above and further data from HST, work has progressed on identifying the composition of Martian dune sand. Early work using Viking Orbiter camera filters led to the idea that dark dune sands were composed of iron oxides, such as goethite [*Thomas and Veverka,* 1986]. Basaltic sand has been found in Cimmeria Terra in the southern highlands [*Christensen et al.,* 2000a] and in Nilosyrtis Mensae in the northern lowlands [*Rogers et al.,* 2000]. Intracrater sand in Arabia Terra has been interpreted as having a basaltic core surrounded by an andesitic arc on the downwind side, suggesting a compositional sorting of sand based on particle size [*Wyatt et al.,* 2001]. The large northern polar erg has been studied with both Hubble Space Telescope (HST) near-infrared data and TES spectra. The HST has detected the signature of pyroxene, indicating the presence of mafic rocks [*Bell et al.,* 1996]. Analyses of TES data have shown that plagioclase feldspar and sheet silicates and/or high-Si glass are also present [*Noe Dobrea and Bell,* 2001; *Bandfield,* 2002], leading to the conclusion that the polar dunes are andesitic [*Bandfield,* 2002].

In this work, the deconvolution method described in *Bandfield et al.* [2000] and *Smith et al.* [2000] has been applied to TES spectra to determine the composition of the Proctor Crater dune sand and the surrounding crater floor. Using the same software written for the global analysis, J. Bandfield (pers. comm.) provided deconvolutions of TES spectra from summertime groundtracks over Proctor Crater. A total of eight endmembers were used in this analysis: four atmospheric components and four surface components. The atmospheric spectral endmembers included dust at both high and low dust opacity, and water ice at two particle size distributions. The surface endmembers included the surface

Types 1 and 2 from *Bandfield et al.* [2000], hematite [*Christensen et al.* 2000c], and a blackbody spectrum to account for differences in spectral contrast.

The concentration of surface Type 2 (andesite/weathered basalt) is strongly influenced by the presence of atmospheric dust. The spectral signatures of andesite and dust are similar enough that under non-ideal conditions, the surface component and the atmospheric component are not properly separated. Thus it is important to consider only the clearest spectra, to minimize contamination by dust. Because Proctor Crater is located in a known dust-raising area, the air is dusty in the summer when the signal is strongest and most reliable. However, full spatial coverage of the study area, and therefore the use of as many viable orbital tracks as possible, is desirable in order to seek out sand deposits and transport pathways. Therefore data from a single orbit, that were obtained over a warm surface with a clear atmosphere, is discussed first to provide a basis for comparison with the rest of the data. The discussion then extends to all orbits crossing the study area.

Figure 3.14a shows original and modeled spectra averaged from eight TES pixels centered on the dark dunefield in Proctor Crater. The TES pixels were chosen from a warm summertime orbit ($L_s = 282.6°$) with a relatively dust-free atmosphere (ock or orbit 5498, see Fig. 3.14b). The original spectrum measured by TES, in magenta, shows the strong 667 cm^{-1} (15 µm) absorption due to CO_2 gas, a broad absorption between 800 and 1200 cm^{-1} (8–12 µm), and a relatively shallow absorption with small, sharp spectral features short of 500 cm^{-1} (>20 µm) due mostly to water vapor. The model produced by the linear least squares fit of the endmembers described above is shown in blue. The modeled spectrum closely matches the original spectrum, indicating that the fit is good. The spectral RMS error for the fit is 0.002, a low value for this dataset [*Bandfield et al.,* 2000]. The dust opacity for this orbit is 0.12, and the ice opacity is 0.0. Figure 3.14a also
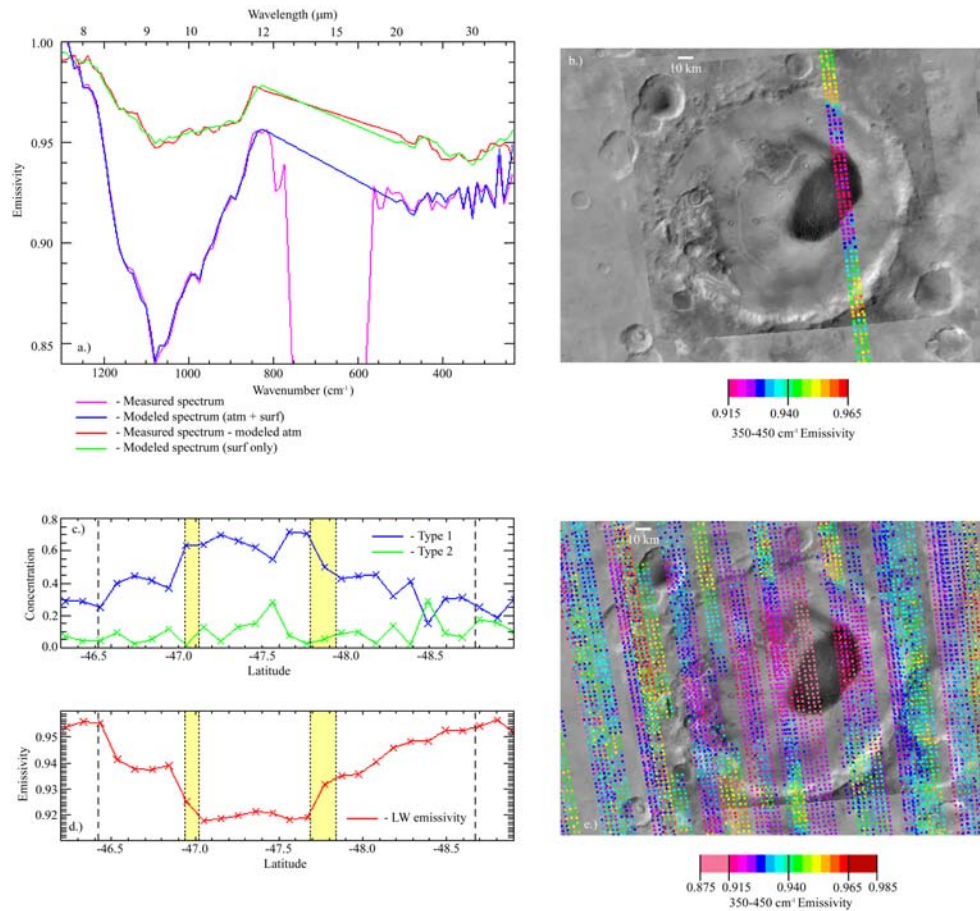
Fig. 3.14. Composition and thermal inertia from TES. a.) Results from the deconvolution of TES spectra over the dark dunes. The dune spectra are consistent with basalt spectra. b.) Plot of long wavelength emissivity for a nondusty traverse across the dark dunes. c.) Concentrations of spectral endmembers Type 1 (basalt) and Type 2 (andesite or weathered basalt) across the traverse shown in b.). d.) Long wavelength emissivity for the traverse across the dark dunes shown in b.). In both c.) and d.), dashed lines mark the inner edge of the crater rim, and yellow shaded regions mark the obliquely-oriented edge of the dark dunefield. e.) Long wavelength emissivity for all summertime groundtracks over Proctor Crater. Variations from orbit to orbit are caused by changes in atmospheric dust content.

shows the original spectrum with the modeled atmospheric components removed (red) and the modeled surface components only (green). Both of these spectra closely resemble surface Type 1 from *Bandfield et al.* [2000], providing a qualitative
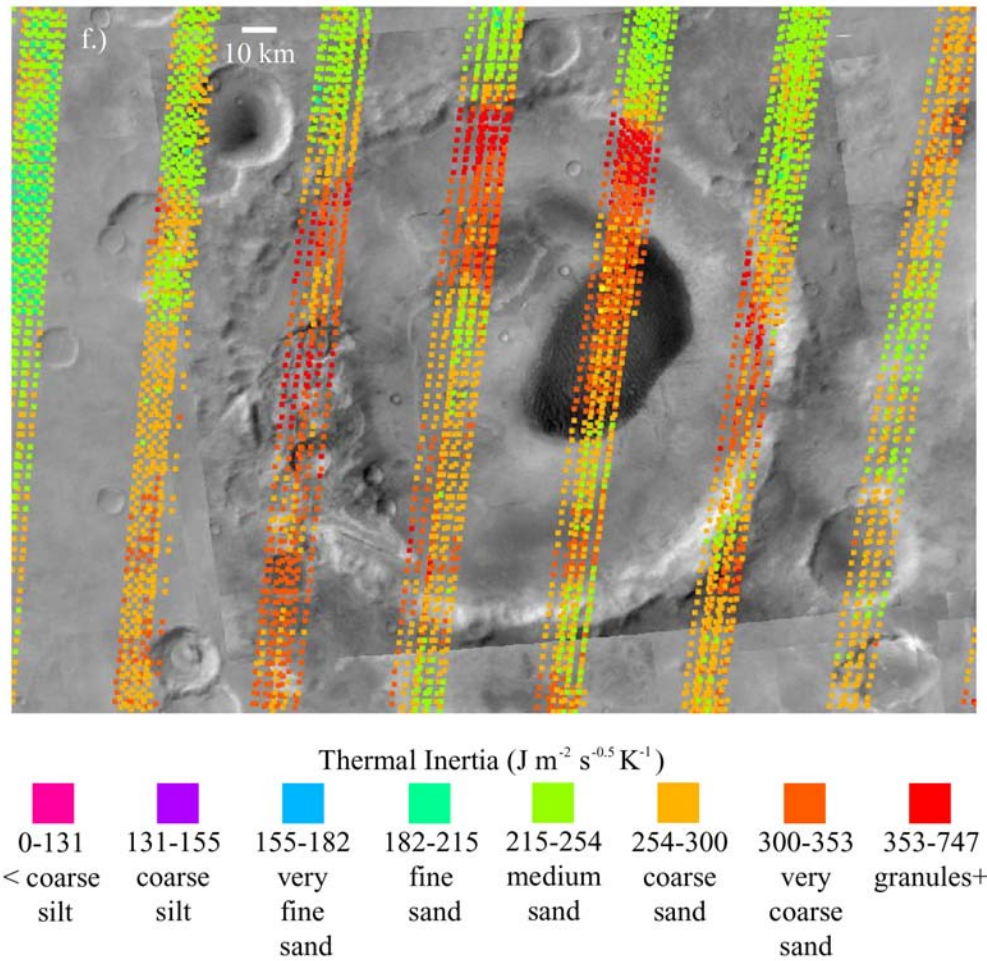
Fig. 3.14 (cont.) f.) Thermal inertia of summertime groundtracks over Proctor Crater, binned by effective grain size. The dark dunes have a thermal inertia consistent with coarse to very coarse sand.

identification of basaltic sand. Concentrations from the endmember fit are 66.1% for the Type 1 component (basalt) and 7.5% for the Type 2 component (andesite/weathered basalt). The concentrations represent the amount of spectral contrast relative to the other endmembers used in the deconvolution. The spectral contrast present in the Proctor Crater dune spectra is consistent with that of terrestrial basalt sands [*Christensen et al.* 2000a; *Bandfield et al.* 2000; *Bandfield* 2002].

Figure 3.14b shows the location of the TES orbit for ock 5498. Concentrations for surface Types 1 and 2 along this track are plotted in Figure 3.14c. The concentrations have been averaged into bins of six pixels to account for any differences in the calibration of the six detectors on TES. Dashed lines mark the edges of Proctor Crater in Figure 3.14c, and the edges of the combined dunefield and the dark sand streak on its north edge are marked by dotted lines. Because the TES groundtrack crosses both the dunefield and the dark sand streak at an oblique angle, there is an area of transition in Figure 3.14c from the crater floor to the sand deposits, marked as the light yellow area between dotted lines. The concentration of surface Type 1 (basalt) increases over the dunes and the large dark streak, although it appears to be present in lower quantity along the rest of the track across the floor of Proctor Crater. Surface Type 2 (andesite/weathered basalt) generally remains at or below the detection limit of ~0.15, indicating that it may not be present at all, although there are a few spots where the concentration climbs to 0.3, suggestive of a small local accumulation or outcrop. Unlike the basalt component, the surface Type 2 profile has no trend along the TES track, indicating that if any such material is present, it does not correspond with the location of the dark dunefield or any other surface structure.

Another measurement of use is a simple band index from original TES spectra in a useful wavelength range. *Bandfield* [2000] shows that band indices of spectral Types 1 and 2 are simply calculated and compare well to maps produced from the linear deconvolution method. Band indices are affected by changes in elevation and atmospheric interference, and they provide only a qualitative estimate of composition. However, because the calculation for the band index is not subject to sensitive discrimination between different endmembers, unlike the compositions derived from deconvolution, the resulting values are less variable from point to point. *Bandfield et al.* [2000] discuss an absorption in Type 1 (basalt) spectra from ~200 to 500 cm^{-1}. Although this feature is present in both surface

Types 1 and 2, the low concentrations of surface Type 2 along the single clear track (see Fig. 3.14c) indicate that little if any of this endmember is present in Proctor Crater. In addition, dust accumulations have very low spectral contrast throughout the TES spectral range, which would elevate the emissivity in this wavelength range. Therefore low emissivities in this band index are used as an indicator of surface Type 1 (basalt) only, and high emissivities are used as an indicator of dust. The band index used here to distinguish this feature is the average emissivity of uncorrected spectra between 350 and 450 cm^{-1}. It is this parameter that is mapped in Figure 3.14b and plotted in Figure 3.14d. The long wavelength emissivity mirrors the basalt track in Figure 3.14c, lending weight to the argument that this band index is diagnostic for basalt in this area. In Figure 3.14b the dunefield is well marked by low emissivity (*i.e.,* stronger absorptions). On either side of the dunefield there are moderately low emissivities (in violet and blue), indicating an intermediate amount of basalt in the middle and northern part of the crater floor.

Figure 3.14e shows the long wavelength emissivity for all daytime, nadir-looking TES pixels with a surface temperature above 250 K. This figure is shown with an extended version of the scale used in Fig. 3.14b. There is a great deal of variation in the long wavelength band index in this data set. Within each orbit, each of which is three pixels wide, there is little variation in dust opacity, so along-track variations in emissivity reflect actual changes in surface composition. However, differences in emissivity from orbit to orbit show the effects of uncorrected atmospheric parameters, especially atmospheric dust. The changes in emissivity from one orbit to another make interpretation difficult, however features persisting from one track to the next are considered real even if their relative emissivities are different.

As with the single orbit shown in Figure 3.14b, the strongest signals in Figure 3.14e are those over the dunefield and the dark streak of sand emerging northwestward from the northernmost tip of the dunefield. There is a general concentration of basalt west of the dunefield and in the bottoms of both the western and the central pits, reflected by fairly low emissivities (blue and violet). The low-lying floors of the pits undoubtedly retain some amount of basalt sand that passes through the area, causing the low emissivities there (*i.e.,* see Fig. 3.3e), although the concentrations may also be indicative of exposed outcrops of basalt in the basin fill. Outside the crater walls, the emissivity rises, indicating the presence of finer, brighter particles. The transition from low to high emissivity is rather sharp along the northern rim of the crater floor, suggestive of a contact between floor materials and intercrater and rim materials. The transition across the northwestern and southern parts of the crater floor is not as well defined, suggesting that more dust has accumulated along this border. This area may be more sheltered from wind relative to the rest of the crater floor, where either fewer dust devils pass by or winds are not strong enough to saltate sand that would scour away seasonal dust fallout. Alternatively, the poorly defined change in emissivity may be caused by surface features that preferentially retain dust, for example, by a surface texture that impedes the effect of the wind. This lack of spectral contrast is most likely caused by accumulated dust, and affected more by local meteorology than by surface morphology.

Much of the area surrounding the dunefield, especially to its west, has a fairly low emissivity, indicating a moderate level of basalt on the crater floor. Bright duneforms are absent northeast of the dark dunefield but present south of the dunefield, and this lack of correlation with composition indicates that they are not likely responsible for these moderately low emissivities. Boulders are present almost everywhere on the crater floor outside the dunefield, including areas of both high and low emissivity, so they also are not responsible for the variation in

emissivity. The lower emissivities around the dunefield likely indicate the lack of accumulated dust, and they may indicate the presence of basalt in the materials comprising the crater floor. Thus the crater floor materials are potentially some combination of basalt grains plus fines that have become indurated over time.

Proctor Crater is located in the southern midlatitudes, a zone in which the surface transitions from a strongly basaltic signature to the north, to a Type 2 surface to the south [*Bandfield*, 2002]. *Bandfield* [2002] also points out that TES spectra only sample surficial, particulate materials and that this latitudinal compositional transition does not appear to have distinctive boundaries. The zonal shift may well be caused by a regional sorting of sand grains by the wind, potentially from midlatitude westerlies that produce the primary slipfaces in the Proctor Crater dunefield. Compositional sorting of sand by the wind has been studied in terrestrial basaltic dunes by *Bandfield et al.* [2002] and, as discussed above, proposed in dunefields on Mars by *Wyatt et al.,* [2000]. The lack of evidence for sand of surface Type 2 in Proctor Crater implies that, if there is any such material in this particular region of the compositional transition, it is most likely obscured by dust deposits. However, basalt sand dominates the dunefield and much of the floor of Proctor Crater, indicating that basaltic sand has accumulated on the crater floor and remained exposed at the surface.

Transport pathways for basaltic sand outside Proctor Crater, if they ever existed, have been since buried, eroded away, or both. In this situation, compositional information is not very useful in locating sand sources or transport pathways, save for providing the information that they are not easily discernable at the surface. While it is possible that the western pit is the source of the basalt sand that now comprises the dunefield, the presence of dark falling dunes on east-facing cliffs within the western pit (*i.e.,* see Fig. 3.3e) suggests that the sand originated to the west of the western pit, and thus most likely from beyond the

western rim of Proctor Crater. Several other craters in Noachis Terra also have large dunefields, and not all of these have pits that could have supplied such a quantity of dark sand. Since transport pathways in the vicinity of Proctor Crater are not apparent, it may be necessary to search for them on a larger scale.

Although the compositional data are difficult to interpret, broad conclusions may be made from investigating this data set. The dark sand in Proctor Crater is without doubt basaltic. Other regions on the crater floor appear to have some amount of basalt, but it is unclear whether this is from the presence of sand that has been transported into the crater or from basaltic outcrops from the layered materials. The bright duneforms do not have a composition distinct from their environment, suggesting that they are composed of easily available local materials, and that there may be no compositional selection based on grain size. There appears to be a difference in wind regimes between the northern rim and the rest of the crater, in which the rest of the crater contains more accumulated dust, indicating less erosive winds. The true value of compositional analysis comes through the comparison to other data sets, in which some of these ambiguities may be resolved.

6. Thermal Inertia

6.1 Background

Thermal inertia is a measure of a material's thermal response to the diurnal heating cycle. Loose, fine-grained sediments lose heat rapidly after sunset, leading to low thermal inertia values. Increasingly consolidated sediments and coarser-grained materials (*i.e.,* sand, gravel, boulders, and bedrock) lead to successively weaker diurnal temperature extrema from higher heat retention and therefore they produce progressively higher thermal inertia values. In ideal situations where all other factors are accounted for, thermal inertia can be used to estimate the

average grain size of a particulate surface material. Typical values of thermal inertia for various grain sizes are listed in Table 3.1.

Table 3.1. Thermal Inertia and Effective Grain Size[a]

Name	Phi	Diameter	Thermal Inertia ($J\ m^{-2}\ s^{-0.5}\ K^{-1}$)
Pebbles	-4 to -2	4–16 mm	417–580
Granules	-2 to -1	2–4 mm	353–417
Very coarse sand	-1 to 0	1–2 mm	300–353
Coarse sand	0 to 1	0.5–1 mm	254–300
Medium sand	1 to 2	250–500 μm	215–254
Fine sand	2 to 3	125–250 μm	182–215
Very fine sand	3 to 4	63–125 μm	155–182
Coarse silt	4 to 5	31–63 μm	131–155
Medium silt	5 to 6	16–31 μm	112–131
Fine silt	6 to 7	8–16 μm	95–112
Very fine silt	7 to 8	4–8 μm	80–95
Clay	8+	<4 μm	<80

[a] Using the relation from *Presley and Christensen* [1997a] with a surface atmospheric pressure of 5 mbar.

The thermal inertia of Martian dunes has been studied in detail since the first thermal models were produced for Mars. In particular, the dunefields of the Helluspontus area in Noachis Terra have been used as a basis for comparison between different models. In all of the thermal studies described below, thermal inertia was calculated using a single measured surface temperature that was matched to a predicted temperature from a thermal model that involved thermal inertia and other various parameters such as albedo, season, and dust opacity. Methods differ mostly in how the atmosphere influences predicted and measured surface temperatures.

Christensen [1983] made the first thorough study of the thermal inertia of dark intracrater materials with Viking IRTM data, using a thermal model developed by *Kieffer et al.* [1977]. This model calculates thermal inertia based on estimated surface temperature variations for a particular albedo, local time, latitude, and season. *Christensen* [1983] calculated a modal value of 397 $J\ m^{-2}\ s^{-0.5}\ K^{-1}$ for the dark intracrater deposits, and using the relationship from *Kieffer et al.* [1973] converted

this value to an effective grain size of 0.9 mm. Although this value is large for dune sand, *Christensen* [1983] correctly concluded that the intracrater features are accumulations of dark aeolian material, which is easily trapped in topographic lows such as craters. Using an updated conversion relation by *Presley and Christensen* [1997a], the same thermal inertia at an atmospheric pressure of 5 mbar corresponds to a grain size of 3.3 mm, a larger value than originally calculated and in the range of granules (2–4 mm).

Edgett and Christensen [1991] also used the thermal model of *Kieffer et al.* [1977] to calculate thermal inertia with Viking IRTM data, although they modified the result with a correction for the effect of atmospheric dust on surface temperatures [*Haberle and Jakosky,* 1991]. For the Hellespontus dunes, *Edgett and Christensen* [1991] calculated a thermal inertia of 322 ± 33 J m^{-2} s$^{-0.5}$ K^{-1} for a clear atmosphere and 301 ± 33 J m^{-2} s$^{-0.5}$ K^{-1} for a dusty atmosphere, leading to an average dune sand grain size of roughly 500 ± 100 µm (medium to coarse sand) using the relation from *Kieffer et al.* [1973]. Using the updated relation by *Presley and Christensen* [1997a], these thermal inertias correspond to 1.02 and 1.36 mm, respectively, and both are in the range of very coarse sand (1–2 mm).

Edgett and Christensen [1994] compared the thermal inertias of Proctor Crater dune sand produced by three different techniques: the method of *Kieffer et al.* [1977] alone, and the *Kieffer et al.* [1977] method modified by two different atmospheric corrections modeled by *Haberle and Jakosky* [1991] and *Paige et al.* [1994]. In a dusty atmosphere with a visible opacity of 0.4, the Proctor Crater dunes have a thermal inertia of 340 J m^{-2} s$^{-0.5}$ K^{-1} using the *Kieffer et al.* [1977] model, 230 J m^{-2} s$^{-0.5}$ K^{-1} when adjusted by the *Haberle and Jakosky* [1991] correction, and 120 J m^{-2} s$^{-0.5}$ K^{-1} when adjusted using a correction from *Paige et al.* [1994]. Although the different methods produce grain size estimates ranging from silt to coarse sand, *Edgett and Christensen* [1994] conclude that the dunes are most likely

composed of sand-sized grains based on physical and compositional considerations.

Herkenhoff and Vasavada [1999] made the most recent estimates of thermal inertia of the Proctor Crater dunes for comparison with the sand of the northern polar erg. They used the thermal model developed by *Paige et al.* [1994] on IRTM data. In this case, they used an atmospheric correction with optical properties for dust developed for IRTM data by *Clancy and Lee* [1991]. All previous thermal inertia calculations involved optical properties developed for the Viking Lander 1 site [*Pollack et al.,* 1979], which produced overestimated surface albedos. *Herkenhoff and Vasavada* [1999] argue that using the method of *Paige et al.* [1994] with updated dust optical properties most appropriately accounts for atmospheric effects on IRTM data, because this was the first model to include both a realistic treatment of the effect of the atmosphere on surface temperatures and the effect of the atmosphere on measured IRTM surface radiances. *Herkenhoff and Vasavada* [1999] calculate a thermal inertia range of 245–280 J m^{-2} s$^{-0.5}$ K^{-1} for the Proctor Crater dunes. Using the relation of *Presley and Christensen* [1997a], this corresponds to a particle size range of 430–755 μm (medium to coarse sand) at an atmospheric pressure of 5 mbar.

To study the thermal properties of the floor of Proctor Crater, we have used thermal inertia values calculated from TES thermal bolometer measurements [*Jakosky et al.,* 2000; *Mellon et al.,* 2000]. They matched single nighttime (2 AM) temperature measurements from TES to a large lookup table of temperatures produced by a thermal model. The lookup table includes several parameters required for the model calculations, such as albedo, dust opacity, time of day, season, surface pressure, latitude, and thermal inertia. The thermal dust optical depth is assumed to be 0.1, scaled to the mean pressure level at 6.1 mbar. *Jakosky et al.* [2000] and *Mellon et al.* [2000] use a thermal model based on that of *Haberle*

and Jakosky [1991], with additional considerations of seasonal and latitudinal variations. Although the thermal inertia values used here were calculated using brightness temperatures from the TES bolometer rather than from a single spectral band (as was previously done with the 20 μm channel of the IRTM data set), *Jakosky et al.* [2000] showed that the difference between the two surface temperature measurements had little effect on thermal inertias in the range of 50 to 300 J m^{-2} s$^{-0.5}$ K^{-1}.

In this work, thermal inertia measurements were converted into particle size estimates using the empirical relation determined by *Presley and Christensen* [1997a]. This calculation employed a surface atmospheric pressure of 5 mbar, a typical value for summer nights at the latitude of Proctor Crater according to the model results from the work discussed in Paper 2. In order to choose the most reliable values, we used only thermal inertias measured during southern summer (L_s = 240°–360°), with emission angles less than 10°, and with the best data quality ratings (values of 0 or 1).

It must be emphasized that the particle sizes discussed here do not necessarily represent actual particle sizes, but rather the *effective* particle sizes for unconsolidated particulate materials in each TES pixel. One challenge in interpreting thermal inertia measurements is that each TES pixel represents a thermal response from a 3 km by 6 km area on the surface, which could easily contain any combination of dust, outcrops, boulders, sand, and consolidated materials, each with its unique thermal signature. A further complication is that consolidated fine material produces the same thermal effect as larger but unconsolidated particles. Thus thermal inertia maps are most valuable for studying either places containing unconsolidated fine materials, which produce the lowest and least ambiguous values, or areas where the particle size range of the surface has been previously constrained.

Dunefields are one of the few geological structures in which the degree of consolidation and range of particle sizes is predictable. By definition, active sand dunes are composed of unconsolidated sand grains, relieving the thermal ambiguity introduced by consolidated materials. In addition, sand dunes consist almost entirely of particles in a narrow size range that are lifted into saltation by the wind, thereby doing away with another complication of thermal inertia caused by poorly sorted materials. Thus, dunes are among the most ideal features to study using thermal inertia. It is for these reasons that dunes have been consistently targeted as a control for new thermal inertia calculations of Mars.

Nevertheless, once grain sizes are estimated from thermal inertia, it can be quite a challenge to relate these grain sizes of dune sands to such geological processes as transport, deflation, and accumulation. On Earth, the grain size most easily lifted by the wind is in the range of very fine sand, or ~75 µm [*Iversen and White,* 1982]. However, most terrestrial dunefields are composed of fine to medium sand (160–330 µm), two to four times this optimum grain size [*Lancaster,* 1995]. Given that Earth has the only well-studied analogs for Martian aeolian processes, this disparity must be clarified before interpretations can be made of Martian dune sand.

Experimental work done on the abrasive action of subareal saltation on Earth indicates that sand grains undergo an average loss of about 10 per cent of their mass in transit, which tails off asymptotically upon grain rounding [*Kuenen,* 1960b]. Furthermore, smaller grains (less than 100 to 150 µm) experience much less abrasion than larger grains, indicating that sand grains simply never wear down to the optimally moved size of 75 µm [*Kuenen,* 1960a]. *Kuenen* [1960b] attributes this lack of abrasion to the lower momentum sustained by smaller particles during saltation, thus inhibiting these grains from chipping on impact. Further measurements of field samples show that silt and smaller-sized grains

(<63 μm) are produced by the chipping of sand-sized grains during saltation, explaining an apparent dearth of particles in the range between 50 and 250 μm (very fine to fine sand) [*Rogers et al.,* 1963]. Thus, although terrestrial dunes are composed of sand-sized particles that are capable of transport under saltation, it might appear that the nature of the transport process itself inhibits grains from being reduced to the optimal grain size for saltation. One might conclude that this reflects the distribution of the original grain population that supplies terrestrial sand, for if the original sand source contained particles of 75 μm then these grains would almost certainly saltate downwind to become incorporated in terrestrial dunefields.

However, there is observational evidence that the situation on Earth is more complex. In a study of the petrology of dune sand of the Ka'u Desert on the island of Hawaii, *Gooding* [1982] demonstrated a genetic relationship between the dunes and volcanic ash beds located upwind. Although the source material had a broad grain size distribution, including grains at the optimum size of ~75 μm, the dune sands clustered at ~330 μm. Clearly the source material does not necessarily reflect the grain size distributions found downwind. In addition, some other process must be found to explain why the optimally saltated grains are not found downwind in dunes, which are depositional features composed wholly of saltated grains.

On Mars, the situation for aeolian grains is less constrained. The most easily saltated sands have a diameter of ~115 μm [*Iversen and White,* 1982]. Experimental work on the abrasion of basalt grains under Martian atmospheric conditions indicates that lithic fragments, such as those composing the Proctor Crater dunefield, can easily survive saltation long enough to accumulate into dunes [*Greeley and Kraft,* 2001]. In that experiment, *Greeley and Kraft* [2001] found that basalt grains with an average diameter of ~540 μm abrade quickly at first, then

asymptotically approach a diameter of ~470 µm. The quick drop in size is attributed to sharp edges that easily chip off, effectively rounding the grains. This loss in size of ~70 µm amounts to a mass loss of about 35 per cent, indicating that, like on the Earth, saltation on Mars is an ineffective process for abrading sand grains into successively smaller particles. If the original sand source contained sand grains at the optimally moved size of 115 µm, one might expect that they would preferentially saltate downwind and collect in sand dunes. The situation for Mars may well be more extreme than that for Earth, because Martian winds above the threshold stress for saltation are so rarely observed at lander sites [*Hess et al.,* 1977; *Schofield et al.,* 1997] or produced by atmospheric models [*Greeley et al.,* 1993; *Fenton and Richardson,* 2001b]. If winds on Mars tend to just barely exceed the saltation threshold, then one might expect that only sand near the optimum size of 115 µm will be transported downwind.

The situation of observed versus predicted particle sizes is resolved by investigating the conditions required for particle suspension. If the terminal velocity of a particle (U_F) is equal to or less than the lowest threshold friction speed for which that particle can saltate (u_*), then that particle will rise into suspension when the wind blows strong enough (*i.e.,* $U_F/u_* < 1$) [*Iversen et al.,* 1976]. This threshold occurs at a particle size of 52 µm on Earth. *Edgett and Christensen* [1991] calculated a range of particle sizes for which "modified saltation" would occur ($0.7 < U_F/u_* < 2.5$). "Modified saltation" may be considered a transition between saltation and suspension in which saltation path lengths are so long they may almost be considered infinite. On Earth, dune sand is consistently coarser than the grains in the "modified saltation" range of 50–80 µm. This suggests that dunes grow only from those sand grains that are transported by pure saltation, and not at all by grains moving in "modified saltation." While it may require a lower wind to saltate 75 µm grains than any

other size on Earth, these particles are too easily carried into "modified saltation" and thus rarely form dunes.

On Mars, a lower gravity, lower atmospheric drag, and stronger required threshold friction velocities for saltation combine to create very long saltation path lengths [*Iversen et al.,* 1976]. The resulting particle size for which $U_F/u_* = 1$ is 210 µm. The "modified saltation" range of *Edgett and Christensen* [1991] is 200–250 µm. They conclude, as did *Greeley and Iversen* [1985], that Martian dunes should therefore be composed of sand grains coarser than those of terrestrial dunes.

Because of the downwind isolation of a particular grain size in dunes, it is a challenge to determine the size distribution of the source material of the dunes. What may be concluded from the grain size measurements is that whatever range of particle sizes are observed in a dunefield must also be present in the source material.

6.2 Thermal Inertia of Proctor Crater Dunes, Broad View

6.2.1 Results. TES thermal inertias over Proctor Crater are shown in Figure 3.14f. Colors are chosen to represent standard divisions in the Wentworth (phi) scale. The dark dunefield displays a distinctive and fairly uniform thermal inertia relative to the surrounding terrain. The mean and standard deviation thermal inertia is 305 ± 22 J m^{-2} s$^{-0.5}$ K^{-1}. Using the relation of *Presley and Christensen* [1997a] with a surface atmospheric pressure of 5 mbar, the thermal inertia converts to grain sizes of 1.1 ± 0.3 mm, in the range of coarse sand (see Table 3.1). This thermal inertia is fairly consistent, if on the high end of, previous thermal inertia estimates of the dune sand. However, this size estimate suggests the dunes are composed of sand with grain sizes ten times the most easily moved grain size for Mars of ~115 µm [*Iversen and White,* 1982], and several times the

estimated upper limit of the "modified saltation" range defined by *Edgett and Christensen* [1991]. This apparent inconsistency must be examined in detail in order to explain how measurements relate to actual conditions on the surface of Mars.

First, uncorrected atmospheric effects must be considered. In their model, *Mellon et al.* [2000] include thermal radiation from a dusty, CO_2 atmosphere and latent heat from seasonal condensation of CO_2. However, they assume that the atmospheric dust optical depth remains at a constant value of 0.1, normalized to a 6.1 mbar pressure level. During the southern summer, in which the relevant TES data in Proctor Crater were obtained, the dust opacity easily climbs higher than this value, leading to a potential overestimate in thermal inertia values and therefore in effective particle sizes. At the elevation of the dunefield, ~700 m above the datum, the dust opacity scales to 0.094. *Liu et al.* [2002] have calculated thermal infrared dust opacities using TES spectra, and so it is possible to investigate the effect of atmospheric dust on thermal inertia calculations from *Mellon et al.* [2000]. *Liu et al.* [2002] calculated 9 μm dust optical depths for TES data for comparison with Viking and Mariner 9 data. Figure 3.15a shows 9 μm dust opacities provided by J. Liu (pers. comm.) over the floor of Proctor Crater during the summer season in which thermal inertia values are available. The optical depths slowly drop throughout the summer season, only reaching values near 0.094 at the end of the summer. Six nighttime tracks of TES crossed the dunefield during this season. Their respective thermal inertias are shown in Figure 3.15b. Of the six tracks, ocks (*i.e.,* orbits) 4425 and 5079 only cross the northernmost part of the dunefield. The remaining four traverse the entire dunefield, as shown in Fig. 3.14f. Like the dust opacities in Fig. 3.15a, the thermal inertia values drop as the summer season progresses, reflecting the influence of uncorrected atmospheric dust on surface temperatures. The track with the closest correspondence to dust opacities near 0.094 is the last one, ock 5406. Thus the

thermal inertias from the last track are considered the most accurate of the six. The average thermal inertia of ock 5406 over the dunefield is 277 ± 17 J m^{-2} s$^{-0.5}$ K^{-1}, leading to a grain size estimate of 740 ± 170 μm. This is in the range of coarse sand (500–1000 μm), which is more consistent with previous work and less surprising than the original estimate of 1.1 ± 0.3 mm.
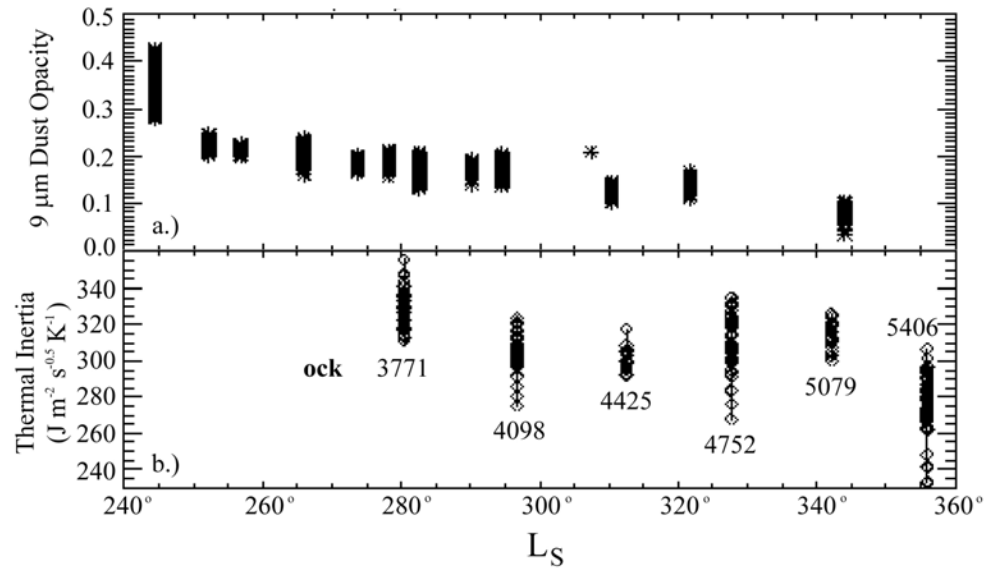

Fig. 3.15. a.) Thermal infrared dust optical depths as a function of season inside Proctor Crater. Note the slow decay as fall approaches. b.) Measured thermal inertias from over the dark dunefield as a function of season. Note how the highest thermal inertias roughly correlate with higher dust opacity.

A second simplification of most previous thermal inertia calculations, including that of *Mellon et al.* [2000], is that they do not account for the effect of slope on surface temperatures. However, dunefields are by definition comprised of slopes of varying degrees and azimuths. Depending on the orientation of the average slope within a TES pixel, the effective surface may be either more or less heated by the sun during the day. Slopes facing away from the sun (southward) will receive less direct sunlight for a shorter time during the day than will sunward-facing (northward) slopes. In addition, the excess surface area created by

topography will lead to more radiative cooling at night than is accounted for by the current assumption of a flat, horizontal surface. The effect of daytime heating will vary depending on the geometry of the dunefield; the effect of nighttime cooling is to slightly lower the measured thermal inertia. At the scale of TES pixels this effect is difficult to estimate, but daytime heating is considered in detail in the following section.

Another possible error may come through the conversion from thermal inertia to effective particle size. The relation of *Presley and Christensen* [1997a] involves surface air pressure, for which we selected a constant value of 5 mbar, chosen from typical summertime values predicted in Proctor Crater by the Mars Mesoscale Model 5 (described in Paper 2). It may be that the model predictions are incorrect, or that the assumed constant value is unrealistic. However, the dependence of thermal inertia on air pressure is not strong. If the air pressure were lower by as much as 1 mbar, which is unlikely, then *Presley and Christensen* [1997a] predict an average grain size of 820 μm corresponding to the measured thermal inertia of 277 J m^{-2} s$^{-0.5}$ K^{-1}. At an air pressure as much as 1 mbar higher, the equivalent grain size is 640 μm. In either case, the estimated particle sizes are still in the range of coarse sand. Thus an incorrect air pressure does not greatly change the estimated particle size.

The packing *Presley and Christensen* [1997a] used in their samples is described as "medium dense," like that of loose sediments on a surface, and not unlike that expected for dune sand. Thus grain packing differences between Martian dunes and their samples do not seem to be an issue. *Presley and Christensen* [1997b] discuss the effect of bulk density on thermal inertia. In their samples, they used spherical glass beads that pack more tightly than angular grains of the same size distribution. A lower bulk density from more poorly packed grains, likely more representative of real dune sand than their glass spheres, produces a lower

thermal conductivity and therefore a lower thermal inertia estimate than spherical particles. Thus the measurement of 740 ± 170 µm sized spherical grains may also be explained by even larger angular grains with a lower bulk density, although the transport of larger grains into the dunefield would be difficult to explain.

Presley and Christensen [1997b] discuss the effect of particle size sorting on thermal inertia. Preliminary studies may indicate that thermal inertia measurements reflect only the largest particles in a sample. If this is indeed the case, then it may well be that the majority of the dune sand is smaller than the observed coarse sand fraction estimated from the thermal inertia measurement. Further work is necessary to determine if this effect is real.

6.2.2 Interpretation. A further challenge of the thermal inertia measurement is in its interpretation. *Edgett and Christensen* [1994] point out that the surface grains of dunes may be coarser than the average grains of the dune volume because ripples composed of larger grains tend to form on the surface of dunes. Additionally, it is possible that the thermal inertia measurement of 277 ± 17 J m^{-2} s$^{-0.5}$ K^{-1} actually indicates that the dunes are composed of grains, smaller than the estimated size of 740 ± 170 µm, that are partially cemented. This is consistent with two observations made in MOC Narrow Angle images, in which unexpectedly sharp slipfaces and landslide scars on the dunes may indicate some amount of induration (see discussion in Sections 4.1 and 4.2). However, the lack of seasonal dust accumulations on the dunes would seem to indicate that the dunes are regularly cleaned of any dust deposits, and therefore that they are active. Perhaps a thin top layer of uncemented sand is present and sweeps the dunes clean, while not providing enough of a thermal signal to block an underlying cemented layer of grains.

Alternatively, the dune sand may truly be in the range of 740 ± 170 μm, or coarse sand. If this is the case, then interpretations can be made on the nature of the source material. Because of the downwind isolation of a particular grain size in dunes, it is a challenge to determine the size distribution of the source material of the dunes. The only information provided by the grain size distribution of dune sand is that the range of particle sizes that are observed in a dunefield must also be present in the original source, and thus a number of source materials must be considered.

Experimental work intended as a study of the lunar surface showed that roughly five per cent of the impact ejecta from a basalt surface is composed of grains in the range of coarse sand (500–1000 μm) [*Gault et al.,* 1963]. Actual lunar soil samples, created by impacts and subsequent bombardment ranged in mean particle sizes from 380 μm down to 32 μm [*Lindsay,* 1976]. He proposes that soil grains decrease in size with age as continual impacts pulverize the surface material into increasingly smaller and well-sorted particles. Recent calculations of impact gardening on Mars indicate that since the Noachian era several tens of meters of regolith should have been produced by the constant bombardment of small impactors [*Hartmann et al.,* 2001]. However, only the least exposed surfaces would have created particles in the size range of the coarse sand grains in the Proctor Crater dunes, because according to the reasoning of *Lindsay* [1976], surfaces exposed to more bombardment would accumulate successively finer soils less likely to contain the coarse sand now present in the Proctor Crater dunefield. However, before reaching this steady-state of soil fining, such surfaces may have been buried and later re-exposed, exposing the preserved sand-sized grains to the wind and allowing them to become a sand source for the dunes. Thus, although unlikely, impact gardening cannot be completely ruled out as a source of Martian dune sand.

Measurements of volcanic ash from phreatomagmatic eruptions of the Kilauea volcano show a broad distribution of particle sizes [*Gooding,* 1982], indicating that this is one possible source of coarse sand. *Edgett and Lancaster* [1993] have proposed that Martian dune sand could be created by the fluvial erosion of lava flows or by the aeolian reworking of pyroclastic materials. *Malin and Edgett* [2000a] consider volcanic material as an unlikely source for the extensive layered deposits on Mars because the lack of Martian plate tectonics inhibits widespread explosive volcanism. However, phreatomagmatic eruptions, such as those of the Kilauea volcano that produced thick ash beds, clearly do occur on volcanoes without the need for global processes such as plate tectonics. Instead of changes in magmatic composition caused by subduction, it is ground water that is responsible for the explosive eruptions. Recent studies of MOC Narrow Angle images have revealed structures morphologically similar to rootless cones, volcanic structures found in Iceland that are produced by the explosive interaction of lava with ground water [*Lanagan et al.,* 2001]. Such eruptions produce beds of glassy ash and scoria that could easily be a source of the coarse basaltic grains in the Proctor Crater dunes. Phreatomagmatic eruptions may in fact be prevalent on Mars, although the extent of the material they have produced is at this time unquantifiable. Thus volcaniclastic material cannot be ruled out as a source of basalt sand on Mars.

Meteoritic material may also be considered as a potential source of dune sand. *Flynn and McKay* [1990] calculated that given the mass influx of meteorites to Mars and their chance of surviving entry into the atmosphere without being melted or vaporized, the meteoritic component of 60–1200 μm particles in the Martian soil is expected to be between 2 and 29% by mass. However, the basaltic composition of the Proctor Crater dunes is inconsistent with meteoritic material. Furthermore, it is likely that any sand-sized meteoritic particles in the Martian soils are too fragile to withstand sustained saltation (see Fig. 3 of *Flynn and McKay* [1990]), and thus fragment into smaller grains before they reach the large dunefields. If this is

the case then the fact that the dark dunefields are composed almost entirely of basalt indicates that the sand grains were transported farther from their source material than any meteoric material could survive under saltation.

Of the three source materials considered (impact ejecta, volcaniclastic grains, and meteoric material), only meteoric material may be ruled out based on compositional differences. Alternate grain sources, such as dust aggregates [*Greeley,* 1979], may be ruled out on a compositional basis. It is possible that dune material may have multiple sources, particularly if it has traveled a great distance from its source. It is possible that a sand transport path may cross various sources, each of which adds to the saltating material as it progresses downwind. Thus the most likely source, volcaniclastic grains, and the potential secondary source, impact ejecta, may both be responsible for various accumulations of basaltic sand on Mars, although to what extent each process plays a role in Martian aeolian history remains to be determined.

6.3 Thermal Inertia of Proctor Crater Dunes, Spatial View

6.3.1 Results. We have discussed the mean thermal inertia of the Proctor Crater dunes and how it may relate to the provenance and transport of the dune sand. However, close inspection of particle sizes across a dunefield can reveal a pattern that has implications for the history of the dunefield itself. On Earth, the finest sand grains are those most easily moved by the wind. Thus the coarser grains generally remain behind as the finer grains are transported downwind, often leading to a subtle trend across a dunefield [*e.g., Lancaster,* 1995]. The Proctor Crater dunefield on Mars shows a tantalizing trend in thermal inertia that may be indicative of a progression in particle size.

Figure 3.16a shows thermal inertia versus latitude for the six nighttime passes over the dunefield for which bolometric thermal inertias are available (shown
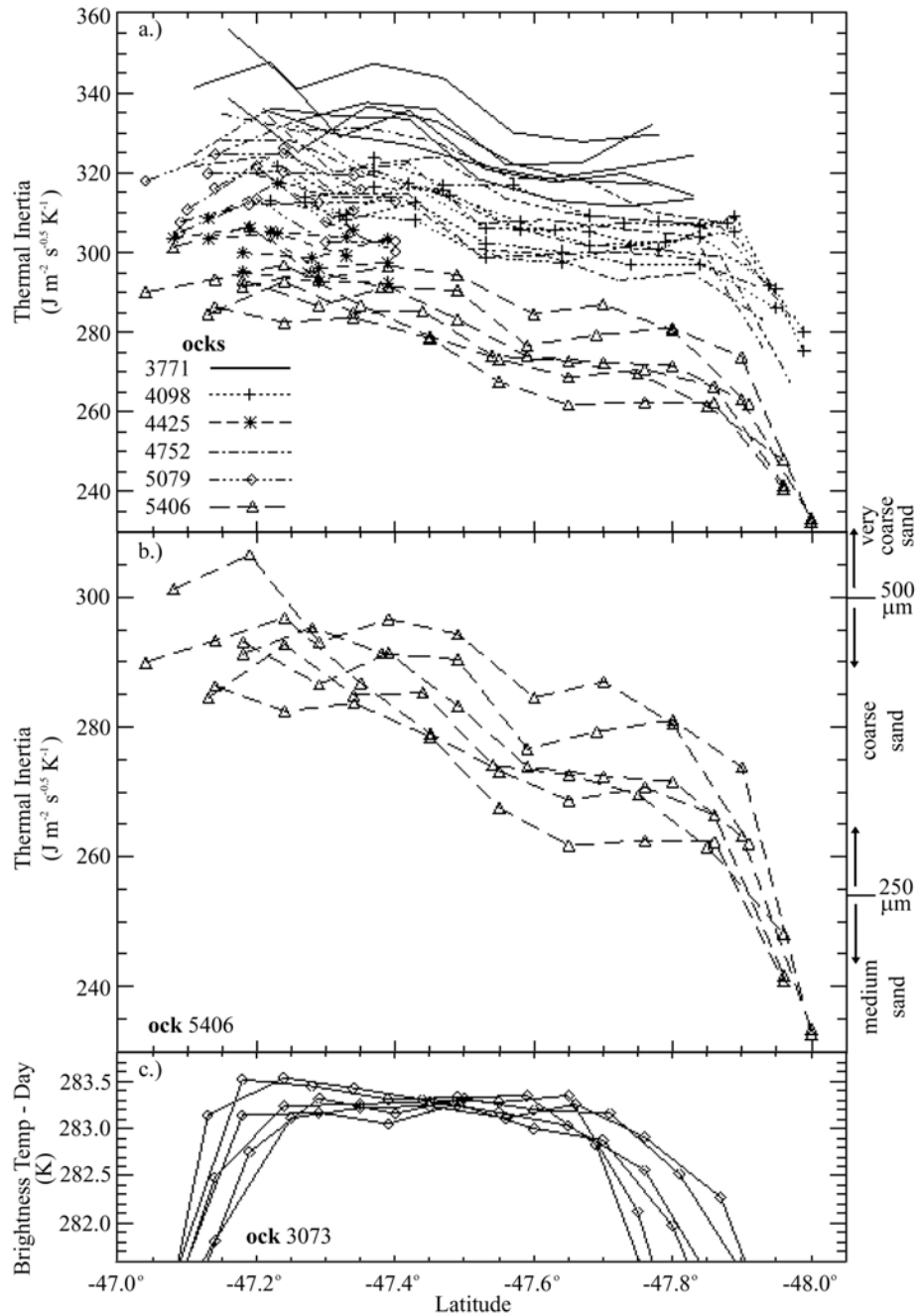
Fig. 3.16. Trends in thermal inertia across the dunefield. a.) All summertime thermal inertia measurements for each of six orbits (see Fig. 3.15b) and each of six detectors. Note the general downward trend to the south. b.) Thermal inertias from ock 5406 only. Ock 5406 is considered to have dust opacities closest to those used in the thermal inertia calculation, and thus ock 5406 has the most accurate thermal inertia values. c.) Daytime brightness temperatures from ock 3073.
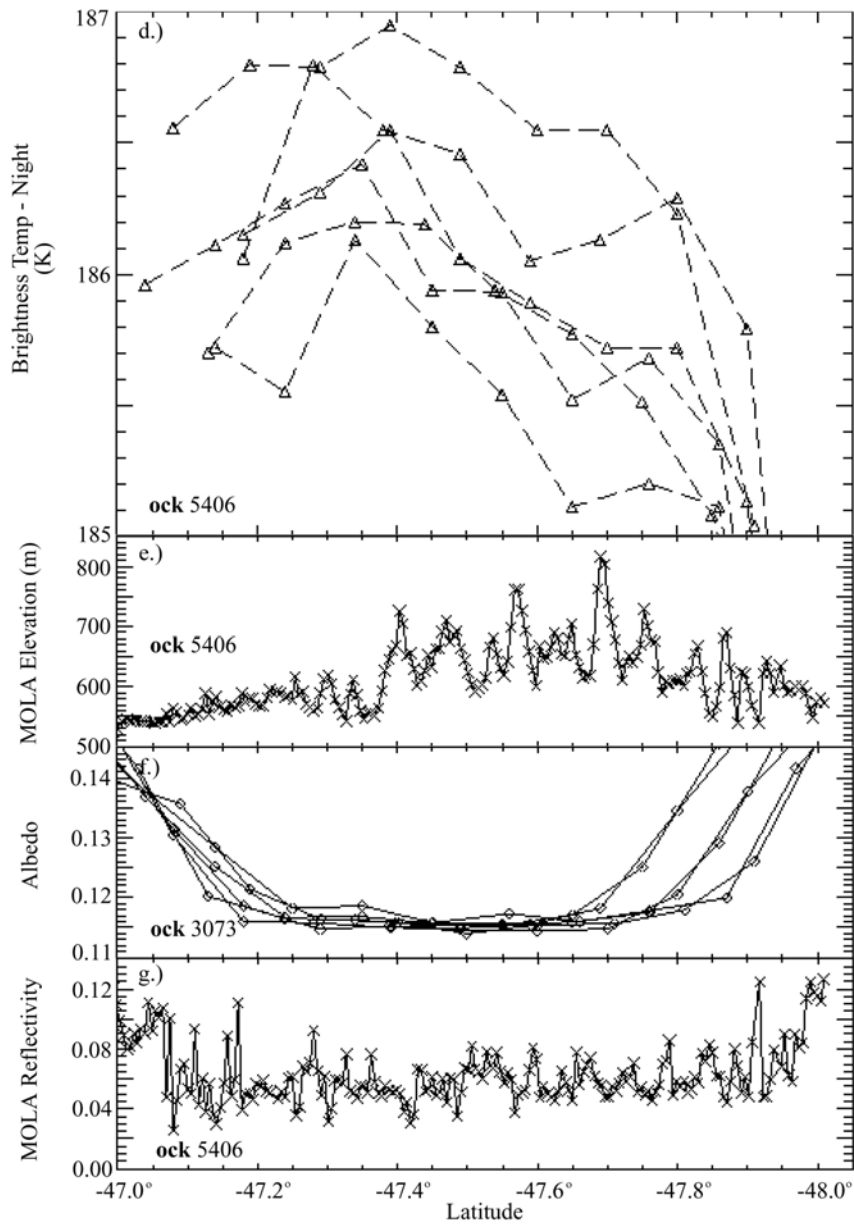
Fig. 3.16 (cont.) d.) Nighttime brightness temperatures from ock 5406. e.) MOLA elevations from ock 5406. f.) TES albedos from ock 3073. g.) MOLA reflectivities from ock 5406. Note that the downward trend in thermal inertia in frames a and b do not correlate with any measured parameter other than nighttime brightness temperature, from which the thermal inertias are calculated.

spatially in Fig. 3.14f). For each orbit, each of the six detectors is plotted separately to reduce any confusion caused by calibrational inconsistencies from one detector to another. Two of the passes only cover the northernmost edge of the dunefield. The TES tracks cross the dunefield at an oblique angle, causing differences in the latitude of the dunefield edges. In addition, the tracks vary in length because they cross the dunefield at different longitudes.

Figure 3.16a demonstrates that there is a wide spread in calculated thermal inertia values over the dunes, varying from ~233 to ~355 $J\,m^{-2}\,s^{-0.5}\,K^{-1}$. This effect is alsoshown in Fig. 3.15b. The variation from orbit to orbit is far greater than that between detectors within a single orbit. As discussed in the previous section, the dominant cause of these variations is in differences in atmospheric dust opacity from one orbit to another. As before, we consider the measurements of ock 5406 to provide the thermal inertias most representative of actual surface properties. These values are replotted on a different scale in Fig. 3.16b.

The thermal inertias of ock 5406 show a clear downward trend from north to south across the dunefield, ending in a steep drop at the southernmost edge. The plot also shows effective particle sizes estimated using the empirical relation from *Presley and Christensen* [1997a], assuming a surface atmospheric pressure of 5 mbar. If this trend is real, rather than an artifact of the data or data processing, then it may indicate a change in effective particle size or cementation across the dunefield. However, first it must be shown that this trend is a real effect on the Martian surface.

The trend in thermal inertia may be caused by a shift in daytime temperature across the dunefield. As discussed in the previous section, irregularities in the geometry of the dunefield could lead to differential daytime heating. One pass over the dunefield is shown in Fig. 3.16c. This orbit is the one spatially closest to

the nighttime orbits, but it crosses the dunefield farther east and at a different angle, leading to a shorter and more northerly track across the dunes than is shown in the nighttime tracks. The daytime temperature clearly peaks over the dunes, which have a low albedo and thus absorb a higher percentage of incident solar energy. At the edge of the dunefield the temperatures fall off to reflect the brighter surface of the crater floor. However in the center of the track, from latitude 47.3° S to 47.7° S, the daytime temperatures show little variation. Thus at the scale of TES, there are no observable effects on the surface temperature from any features on the surface.

Nighttime temperatures, on which the thermal inertia values are based, do show a change across the dunefield. Figure 3.16d shows measurements from ock 5406, which clearly shows the downward trend in temperatures to the south. Note that the southernmost measurements are cut off in this plot to emphasize the trend along the remainder of the track. Thus the shift in thermal inertia originated in the surface temperatures in the original measurements from the bolometer. In addition, the southward shift in thermal inertia appears in all tracks crossing the dunes with an L_s range spanning the southern summer (see Fig. 3.16a). This repeatability indicates that the shift is not caused by uncorrected atmospheric effects or a calibration problem in TES, but rather that it is a real phenomenon on the Martian surface.

It is possible that physical factors other than particle size or degree of cementation are affecting the surface temperatures and thus the thermal inertias across the dunefield. Figure 3.16e shows MOLA elevations across ock 5406. Because *Mellon et al.* [2000] correct for elevation using a 1° by 1° MOLA map, the majority of the dunefield is assumed to be at a single elevation in thermal inertia calculations. However, the central and southern region of the dunefield is actually about 150 m higher than the northern end of the dunefield. A lapse rate of

-2.5 K/km [*Zurek et al.,* 1992] indicates a mean decrease in air temperature of 0.4 K with an increase in height of 150 m, a value similar to the drop seen in each detector in Fig. 3.16d. Thus it might appear that the gradient in thermal inertias is simply due to a change in altitude. However the sensible heat flux from the surface to the atmosphere on Mars is so small (*e.g., Sutton et al.,* [1978]), particularly at night, that surface temperatures should not be expected to reflect the ambient air temperature. Therefore the change in air temperature with elevation will not affect thermal inertia calculations.

Thermal inertia is also directly affected by changes in air pressure, and thus with elevation [*Presley and Christensen,* 1997a]. However, the 150 m of elevation change leads to a drop in surface pressure of 1.4%, or 0.07 mbar. A change in air pressure this small has little effect on calculated thermal inertias, and therefore does not explain the change in thermal inertia across the dunefield.

It is also possible that a change in surface albedo could cause differences in daytime surface heating and thus create the observed downward trend in thermal inertias. For example, a relative increase in brighter interdune areas towards the southern end of the dunefield could lead to lower daytime temperatures, which would in turn lead to the slightly lower nighttime surface temperatures measured by TES. Figures 3.16f and 3.16g show surface reflectivity from the broadband visible TES bolometer and from MOLA at 1.064 μm, respectively. The TES track in Fig. 3.16f shows measurements from the same orbit in which daytime surface temperatures were measured (Fig. 3.16c). In the TES track the dunefield appears as a consistently dark area with a visible albedo ranging from 0.115 to 0.12. There is no trend across the dunefield that corresponds to the nighttime surface temperatures. Likewise, MOLA reflectivity, taken from the nighttime pass corresponding to ock 5406 in Fig. 3.16b, shows a uniform low value across the dunefield, save for a few bright interdune spots. The frequency of bright

interdune spots remains low and constant, except at the edges of the dunefield where the spots become larger and more common. It is clear from both TES and MOLA reflectivities that the drift in thermal inertia is not influenced by a spatial variation in albedo across the dunefield. Even if there were some effect from albedo, it should be reflected in daytime surface temperatures, and no such trend appears in Fig. 3.16c.

6.3.2 Interpretation. Thus far, effects from dust opacity, atmospheric temperatures, changes in air pressure with altitude, daytime surface temperatures, and both TES and MOLA albedo have been ruled out as influencing the trend of thermal inertias across the Proctor Crater dunefield. Therefore the trend in thermal inertia, directly reflected in nighttime surface temperatures, does reflect differential cooling rates of surface materials within the dunes. A number of situations could lead to the observed trend.

First, there may be bright interdunes that are unresolved at the scale of both TES and MOLA. These areas may be composed of material that is more indurated and thus effectively has a higher thermal inertia than loose sand. The northern part of the dunefield (between -47.0° and -47.4° S) has smaller dunes that are largely unresolved in MOLA profiles (see Fig. 3.16e). This area of the dunefield is not superimposed on the broad 50 m thick layer of sand discussed in Section 4.3, and it may well have a higher percentage of indurated interdune areas. However, south of latitude -47.4° S, where the dunes are superimposed on the layer of sand and where interdune areas are nonexistent, the gradient in thermal inertia continues. In any event, the surface of the crater floor just outside the dunefield has lower thermal inertias relative to the dunefield (see Fig. 3.14f). Since the interdunes are small exposures of the same lower thermal inertia surface surrounding the dunefield, then a higher frequency of interdune areas should

decrease the average thermal inertia of a TES pixel, rather than increasing it as is observed.

Second, the degree of dune cementation may vary across the crater. This could be the case if one side of the dunefield experienced more frequent winds above the saltation stress threshold relative to the other side. However, the entire dunefield seems to be swept clean of bright fines that might otherwise collect on more cemented and thus less active dunes. Furthermore, there is no obvious change in dune morphology across the dunefield that reflects any change in cementation (*i.e.,* erosional slumps or sandblasting on solidified dunes). Therefore a change in cementation across the dunes seems unlikely.

Finally, the thermal inertia gradient may be caused by a steady decrease in grain size to the south. If this is the case then this trend has implications for the history of the dunefield. Because any such implications on Mars are almost entirely unknown at this time, studies of terrestrial dunefields will be used as a basis for comparison. In terrestrial sand seas where there is a single upwind sand source and a dominant prevailing wind direction, the sand tends to become both finer and better sorted downwind, reflecting the transportability of smaller grains [*e.g., Lancaster*, 1989]. The Proctor Crater dunes have a single sand source, from the west-southwest, but the wind regime reflected in slipfaces indicates convergent wind orientations. Based on terrestrial studies, one would expect the coarsest grains to be located in the western and southern parts of the dunefield, but instead thermal inertias suggest a general fining of grains to the south. It may be that the east-southeasterly and east-northeasterly winds have recently been more dominant, causing the finer grains to move back towards the west and south. MOC Narrow Angle images show recent slope adjustments indicative of winds from the east-northeast (shown in Fig. 3.6f through 3.6h, and discussed in Section 4.1). If these slope adjustments show more than just a seasonal trend that

is erased by reversing winds each year, then these winds may have sent the finer grains downwind. It is unclear how readily a shift in prevailing winds could affect the grain size distribution across an entire dunefield, but only the top layer of sand is represented in a thermal inertia calculation and thus only this layer need be affected.

Other possibilities explaining a trend in grain size must be considered. In the dunes of the northern Sahara, it has been found that the grain size and dune size are directly correlated [*Wilson,* 1973]. However, measurements from several other dunefields have shown that this relation does not generally hold true [*e.g., Wasson and Hyde,* 1983]. If this translates to Martian conditions, then there is no correspondence between the increasing dune size in the southern part of the dunefield and the finer estimated grain size in that area. In any case, *Wilson* [1973] proposed a positive correlation between dune size and grain size, opposite of the effect indicated in the Proctor Crater dunes. Thus the effective grain size across the Proctor dunes likely has little bearing on the pattern of dune size and spacing.

6.4 Thermal Inertia of the Proctor Crater Floor

The remainder of the Proctor Crater floor shows an interesting patchwork of varying thermal inertias. Surrounding the dark dunefield and covering a great deal of the floor of Proctor Crater are smaller, brighter duneforms (see Figures 3.7 and 8, Section 3.4). Where these features predominate, the average thermal inertia appears to be that of medium to coarse sand. In addition, the areas where these bright duneforms are most plentiful correspond to the lowest thermal inertias measured on the floor of Proctor Crater (compare Figures 3.7a and 3.14f). High-resolution images of these areas shows boulders that could raise the average thermal inertia and dust devil tracks revealing the presence of bright dust accumulations that would lower the average thermal inertia of these areas. The complications caused by these other features makes thermal inertia

interpretations of the small bright duneforms difficult. The bright duneforms are most likely either small, cemented dunes composed of sand-sized particles or the granule ripples proposed by *Malin and Edgett* [2001], *Zimbelman and Wilson* [2002], and *Williams et al.* [2002]. This is supported by two observations. First, these smaller duneforms are relatively immobile with respect to the large, dark dunes (see Section 3.4). Smaller dunes contain less material than larger dunes and, all other factors being equal, should move faster as a result. Second, some of the bright duneforms are highly eroded (see Figures 3.8a and 3.8c), leaving behind rounded or fragmented remnants that are suggestive of some amount of induration. However, their indurated or granular nature is not demonstrated in thermal inertia measurements.

Because the bright duneforms are probably not composed of medium to coarse sand, other factors must be considered that would lead to this thermal inertia result. It may be that a layer of seasonal dust fallout partially obscures the surface of the bright duneforms, thereby effectively lowering their thermal inertia. Such a dust layer would be intermediate in the *Pelkey et al.* [2001] terms "thermally thick" and "thermally thin." If this dust layer is present then the correspondence of bright duneforms with the lowest thermal inertia measurements in Proctor Crater suggests that the bright duneforms preferentially retain accumulated dust relative to the surrounding terrain, perhaps by sheltering dust in the cracks between granules or pebbles. A good test for the preferential accumulation of dust would be to seek progressive seasonal shifts in thermal inertia with increasing concentrations of dust devil tracks. TES and MOC data are too sparse for such a study, but the THEMIS data set could provide such information.

The compositional analysis discussed in Section 5.1 indicates that many bright duneforms are located in areas with a moderate basalt signature. This implies that the material forming the bright duneforms is partially composed of basalt. This

compositional signature is surprising given that it is in an area we have interpreted as partially thermally obscured by dust accumulations. However, dust devil tracks are prevalent over the bright duneforms, exposing parts of the underlying bright duneforms. It is likely that these swaths of uncovered material contribute to the basaltic signature in these areas.

The northern region of the crater floor has a high thermal inertia, indicative of a gravelly or well-consolidated surface. The northern rim of Proctor Crater experiences strong drainage air flows during the night during part of the year (see Paper 2). It may well be that these areas are scoured clean of loose sediments, as suggested by *Christensen* [1983], exposing a rocky or consolidated surface. Indeed the bright duneforms in this area, nearly ubiquitous across the rest of the crater floor, appear to be highly eroded or absent (see Figs. 3.7a and 3.8c, Section 3.4). The moderate basaltic signature in this area, shown in Fig. 3.14e, indicates that this scoured surface contains some amount of basalt.

Outside the crater rim to the north, the thermal inertia sharply drops to a value consistent with medium sand. This sharp contact indicates a fundamental change either in the surface or in the wind regime at the edge of the crater. Based on atmospheric modeling (see Paper 2), strong nighttime spring and summer winds should carry any loose sediments across this contact from the intercrater plains to the crater floor, and yet there appears to be no thermally distinct evidence for such transport. Perhaps the most plausible explanation for the sudden change in effective particle size is a change in surface roughness inside the crater. If winds sweeping down the crater rim abruptly encounter a smoother, flatter surface with a lower roughness height, then loose particles will be much more easily lifted into saltation, in turn kicking any dust into suspension, and leaving behind a scoured surface of immobile material that will have a relatively high thermal inertia. These

strong drainage flows will also serve to keep new dust from settling onto the surface.

The southern edge of the crater floor grades into the rim and intercrater plains, much as the long wavelength emissivity does in this area. This area has a weaker basalt signature than on the rest of the crater floor (see Fig. 3.14e) and no bright duneforms (see Fig. 3.7). It is probably a terrain like that on the northern edge of the crater floor, only this area does not experience strong nighttime drainage winds that would scour the surface clean. Thus some amount of dust can settle out on the surface here, partially obscuring the higher thermal inertia of the indurated sediments and almost completely obscuring their basaltic signature.

The floor of the large western pit, like the northern part of the crater floor, also has a fairly high thermal inertia. There are known dark sand accumulations, bright duneforms, and abundant boulders in the pit (see Fig. 3.3e), but overall the area seems to be swept clean of fines, much like the northern area of the crater floor. This implies that the western pit floor is composed of consolidated materials, like that on the northern crater floor. The central pit has a slightly lower thermal inertia, suggestive of more accumulated fines. Much of the exposed materials in the western pit are the layered sediments comprising its walls and local relief. The terrain exposed in the western and central pits and along the north edge of the crater floor are most likely the same sedimentary unit, indicating that the ~450 m of basin fill in Proctor Crater is composed of indurated material. Given the relief and steep slopes evident in Figure 3.3e, this result is hardly surprising. Combined with the basaltic signature in the pits discussed in Section 5.1 and shown in Fig. 3.14e, the correlation of composition with high thermal inertias are more evidence for the presence of basalt in the layered sediments within Proctor Crater.

The high thermal inertias of the pits and northern crater floor coupled with their moderate basalt signature may have implications for the origin of the sedimentary deposits filling Proctor Crater. *Malin and Edgett* [2000a] proposed that sedimentary deposits such as these were produced by one of two processes: either they collected as lake sediments in low-lying basins, or they were transported by the wind through suspension to their current location. If the sedimentary layers in Proctor Crater were deposited as lakebeds then some amount of the basaltic material would have been aqueously altered. *Wyatt and McSween* [2002] reinterpreted the "andesitic" surface Type 2 of *Bandfield et al.* [2000] as low-temperature aqueously altered basalts. However, very little of Surface Type 2 is found on the crater floor (see Fig. 3.14c). Rather, the areas on the crater floor and in the pits interpreted as swept clean of fines have a signature that indicates some amount of unaltered basalt. The evidence suggests that the layered material in Proctor Crater was deposited by aeolian processes, the second of the two hypotheses proposed by *Malin and Edgett* [2000a].

7. Conclusions and Geomorphic Sequence

This study has led to an understanding of the sedimentary history of the interior of Proctor Crater. Each of the different data sets incorporated into the GIS has provided a unique set of information about the surface of the Proctor Crater floor. Here the conclusions are summarized in chronologic form, so that results from each data set are integrated into a single consistent history.

Proctor Crater was formed during the period of heavy bombardment. It is 150 km in diameter, in the size range of peak ring basins. Wall slumping is expected in a crater this size, although currently no such features are visible.

After the crater was formed, up to 450 m of layered sediments filled the crater basin. These deposits have a thermal inertia consistent with indurated material

and a partially basaltic composition. Much of the material is hard enough to produce boulders upon impact, but friable enough to be eroded by the wind. The basaltic component of the surface composition indicates that the layers are probably not lake sediments, which would produce aqueously altered minerals. Rather, the sediments are probably produced by accumulated fallout of aeolian material, possibly volcaniclastic. Some volcanic flows may be interfingered with the aeolian deposits, although evidence for them is difficult to establish in the images. This influx of material was part of a global-scale deposition of layered sediments reported by *Malin and Edgett* [2000a], who proposed that these deposits were formed by either subaerial or subaqueous processes. The results in this work support deposition by subaerial processes.

There is a 50 m high ridge concentric to the crater rim at half the crater diameter. This "concentric ridge" is proposed to be one of three constructs: 1.) It may be an outcrop of resistant sedimentary layers. If so then the sedimentary material in Proctor Crater consists of contiguous layers that were deposited uniformly across the entire crater floor. Like the strata of *Malin and Edgett* [2000a], these layers dip so that they follow the crater walls, probably as a result of basin subsidence from the immense weight of 450 m of sediments. Furthermore, at least 50 m of material has been differentially eroded from the surface of the crater floor in order to leave these erosional remnant ridges. Aeolian erosion is the most probable source of deflation. 2.) The concentric ridge may simply be the remnant top of the peak ring that was formed during the impact that created Proctor Crater. 3.) In places the concentric ring has a morphology similar to wrinkle ridges. Such features have been formed in craters, either along the floor as part of a larger system, or along the crater rim in a material that previously buried the crater. If it is a wrinkle ridge, then it most likely formed from thrust faults along shallow décollement surfaces in the layered sediments within the crater. Compression could have been forced by a number of processes, such as

subsidence of basin fill, or by a regionally uniform removal of ground water or cooling of ponded lava. It is difficult to conclude from morphology alone which of these processes contributed to the formation of the concentric rings.

After the sediments were emplaced, further small impacts bombarded the Proctor Crater floor, producing small craters with associated boulder fields. Today these craters are in varying states of erosion, some of which are barely discernable. Ubiquitous boulder fields with no apparent source crater hint at a large quantity of long-erased craters, indicating that a great deal of the fine sediment on the crater floor has been stripped away by the wind.

Two large pits have been eroded out of the sedimentary layers filling the floor of Proctor Crater. The larger of the two, the western pit, covers approximately one tenth of the crater floor and reaches to a depth of one kilometer. The pits were likely eroded by aeolian abrasion and deflation, although there may have been weakening from below, for instance from underground water, that contributed to the erosion of these features. Large craters on the western side of the Protor Crater floor may also have initiated the weathering process that produced the western pit, although this seems unlikely because no such craters are present near the central pit.

Layers exposed in the walls of the western pit provide evidence for the former accumulation of sediments. Steep slopes in the walls and thermal inertias consistent with consolidated material indicate that the sediments are highly indurated. Indeed, the presence of boulders produced by impact onto the surface of these strata indicates that highly consolidated material and possibly clasts are present. The composition of the floor of the western pit is basaltic. Although falling dunes of dark sand are present, they do not dominate the interior of the

pit, and therefore this compositional signature is probably indicative of basaltic material in the ~450 m of sedimentary layers.

After and perhaps during the erosion of the pits, small bright bedforms appeared throughout the crater floor. These features are superimposed on pits and craters, and thus postdate them. They are much more common on the Proctor Crater floor than the surrounding intercrater plains. The bright bedforms are most likely formed from locally eroding basin fill, and thus represent the lag deposit of material that is not raised into suspension and blown out of the crater. A moderate basaltic signature supports the suggestion that the eroding sedimentary layers are at least partially basaltic.

These duneforms may be either small dunes composed of bright sand, or ripples composed of larger grains. Thermal inertias of these features are consistent with medium sand, but their eroded nature and lack of movement with respect to much larger, dark dunes suggests that if they are dunes then they must be at least partially cemented. It is possible that dust fallout, made obvious from the plentiful dust devil tracks that form every summer season, obscures the true thermal response of the material comprising the bright duneforms. It is also possible, that, if these features are granule ripples, they are composed of a mixture of fine and coarse materials that can produce a thermal inertia consistent with medium sand.

Some of the bright duneforms have rounded crests and eroded structures, indicating that in places they may have become cemented. However, in the interior of the dark dunefield, the orientations of these bedforms are strongly influenced by the presence of the large dunes. In addition, they reform after a dark dune has passed by, as the dark dune slowly destroys the older bright duneforms it encroaches on. Thus the processes and materials that produce

bright duneforms are still active today. These recently influenced or newly created bedforms are less likely to be cemented than their older, eroded counterparts. However, these young bright bedforms also move more slowly than the large dark dunes, like the older bright bedforms, which is not expected if any of the bright bedforms are dunes as well. Therefore, the bright duneforms are probably granule ripples rather than dunes.

Some time after the bright bedforms were established on the Proctor Crater floor, dark basaltic sand entered the crater from the southwest. Several other craters in Noachis Terra also contain large dunefields of dark sand, which were probably emplaced concurrently with the sand in Proctor Crater. The provenance of this sand is unknown. It cannot be derived from the south polar layered deposits, which have been shown to be composed of accumulated fines deposited from suspension [*Murray et al.,* 2001]. Regardless of the source of sand, its presence in craters in the southern highlands indicates that a large quantity of basalt sand was released in a single event, and that it was subsequently redistributed by the wind into dunes now trapped on crater floors.

A transport pathway, now largely defunct save for a few remaining falling dunes, carried sand towards the center of Proctor Crater by the primary winds from the WSW. Upon intersection with ESE and ENE winds, the incoming dark sand halted in a region defined by zero net transport and began to accumulate into large dunes. By the time the sand supply was cut off or depleted, a 50 m thick mound of sand in the center of the dunefield had been established, with large dunes superimposed on top. This deposit indicates a long history of sand accumulation, and it is likely to contain interfingered dust deposits. The dunefield location has probably not changed much since the dunes first accumulated, although slight deviations to the north and east have occurred as the dune-

forming winds varied in strength relative to one another. The large dunes take the form of reversing and star dunes, consistent with a converging wind regime.

A new observation regarding these dunes is that they do not contain smaller superimposed secondary dunes as terrestrial dunes of this size do (*i.e.,* they are simple dunes). This effect is not caused by the erosion of previously formed secondary dunes, because the dunes are still active and should be continuously forming smaller dunes. However, slipface avalanches appear to flow down the entire slipface of either side of the large dune ridges. The reason for this difference between Martian and terrestrial dunes may be related to different atmospheric conditions between the two planets, or by some influence of trapped volatiles on Martian dune morphology.

Parts of the dark dunes are clearly active today. Slipface adjustments that change in position from year to year are present, indicating that continual avalanching occurs. Because the dunes are influenced by winds from opposing directions, they do not migrate in any direction, but instead they probably fluctuate around a mean position, with the variations depending on the relative strengths of the winds in a particular year. In a few places, slope adjustments take the form of small narrow landslides that are not erased by subsequent slope activity. The fact that these avalanche scars retain their form indicates that the underlying sand in these locations is at least somewhat indurated.

The dark dunefield has an average thermal inertia of 277 ± 17 J m^{-2} s$^{-0.5}$ K^{-1}, leading to a grain size estimate of 740 ± 170 μm. This size is in the range of coarse sand, consistent with that expected and previously measured for this dunefield. As a result, three possible sand sources are considered: impact ejecta, meteoritic material, and volcaniclastic grains. Although with time impact gardening creates smaller particles than are present in the dunefield, such surfaces

may be buried before such a steady-state condition is reached, thus preserving sand-sized grains that may later be exposed by weathering. Thus impact ejecta, although unlikely, is a possible source of basaltic dune sand. Compositional arguments rule out meteoric material and aqueously altered sand. The remaining obvious source of sand is volcanic ash, which easily forms in the grain size and compositional range observed, and therefore this material is considered to be the most likely source of sand grains for the Proctor Crater dunefield.

The dunefield displays a uniform and repeatable decrease in thermal inertia from north to south that is interpreted to be a real physical phenomenon. It is not caused by a shift in percentage of interdune flats or by any observable change in dune cementation. It may reflect a change in grain size, indicating a decrease in grain size to the south. However, the primary wind blows from the WSW, and logically this wind should preferentially blow finer particles northward. Nevertheless, the wind regime is complex, and an expected particle size distribution is therefore difficult to predict. Only a higher spatial resolution data set, and perhaps *in situ* measurements, will resolve whether or not it is grain size changes that cause this shift in thermal inertia.

The observed wind pattern of all the aeolian features indicates that three main winds influence the floor of Proctor Crater. Dune slipfaces indicate three formative winds. The primary wind blows from the WSW, and this is the wind originally responsible for transporting sand into the crater. Slipfaces oriented to this wind occur throughout the dark dunefield. Both bright bedforms and dust devil tracks are aligned with this wind, indicating that this wind has blown since before the dark sand arrived and that it still blows today. Dust devil tracks are produced by spring and summer early afternoon winds, but these winds are most likely too light to produce movement on the dune slipfaces. A secondary wind blows from the ESE. This wind is represented by slipfaces throughout all but the

easternmost portions of the dunefield. A subset of the bedforms is oriented to this wind, indicating that these winds, like the primary winds, must blow strong enough to produce granule ripples. A tertiary wind blows from the ENE, but corresponding slipfaces in the dunes only occur in the eastern portion of the dunefield. Some sand movements in the center of the dunefield may be formed by this wind, although the dune slopes here are not obviously slipfaces. Dust devils tracks are not aligned with this wind, but some of the bright duneforms may be.

One region of the crater, to the northeast of the dark dunefield, is unique in several respects. The single MOC Narrow Angle image of this area shows a surface devoid of boulders and bright duneforms, which is an unusual characteristic of the Proctor Crater floor. It is also the location of the only summertime image that does not contain dust devil tracks. This region has a thermal inertia typical of indurated materials and a composition with a moderate basalt signature. This area is probably a windy zone, such that dust deposits, bright duneforms, and even boulders do not remain. The boulders, which are created from impact into the sedimentary deposits filling the crater, may withstand ejection upon impact but erode away under the persistent action of the wind. This area may be subject to strong slope winds, perhaps even the same tertiary winds from the ENE that influence the eastern portion of the dunefield. Only atmospheric modeling, discussed in Paper 2, confirms the existence of such winds.

The remainder of the geomorphic sequence of Proctor Crater includes seasonal features such as frost and dust accumulations. Dark dust devil tracks develop during the spring and summer, indicating that prior to this season some amount of dust has accumulated on the surface since the previous summer season. In the springtime tracks are most prevalent over dark sand, where the surface warms

enough to produce dust devils. As the summer approaches the tracks expand to include most of the rest of the crater floor. Dust devil tracks change little during the summer season, indicating that few are erased over the summer, and thus little sand is present beyond the edge of the dark dunefield that might otherwise saltate under strong winds and erase the tracks by removing nearby dust.

Frost forms on dunes at $L_s = 50°$ (mid fall) and sublimates away completely by $L_s = 165°$ (late winter). The sun-facing slopes quickly lose their frost as spring approaches, but the pole-facing slopes retain frost for a much longer time. On these south-facing slopes the frosts form dark spots as they slowly sublimate away. These spots persist in location from year to year, and they form lineations that may parallel exposed bedding structures from within the dunes. The largest sublimation spots have bright cores, which may simply be reaccumulated ice. Sintering potentially leads to increased transparency along bedding plains, which is one possible explanation for the coherent spacing of the dark spots.

The sedimentary history of Proctor Crater is one of a complex interaction of accumulating and eroding sediments. This history began with the eventual accumulation of ~450 m of potentially aeolian material that has subsequently been indurated, impacted, eroded, and reworked into bright duneforms. The sand in the dark dunefield is but the most recent set of sediments to enter the crater. All aeolian features indicate a very stable wind regime throughout the observable aeolian history, which is reflected both in old and stabilized bright duneforms and in recent seasonal dust and frost accumulations. Thus from its earliest history onward, the story of Proctor Crater has been one dominated by aeolian processes.

8. Acknowledgments.